A Numerical Study of Syngas Laminar Premixed Flames: Effects of Lewis Number and Flame Stretch

by

CESARE D'IPPOLITO
Laurea, Politecnico di Torino, Turin, Italy, 2015

THESIS

Submitted in partial fulfillment of the requirements
for the degree of Master of Science in Mechanical Engineering
in the Graduate College of the
University of Illinois at Chicago, 2015

Chicago, Illinois

Defense Committee:

Suresh K. Aggarwal, Chair and Advisor
Kenneth Brezinsky
Marco Carlo Masoero, Politecnico di Torino

To Fire

And Wonder.

ACKNOWLEDGMENTS

First and foremost, I would like to express my sincere gratitude to Prof. Suresh K. Aggarwal for helping and guiding me in the development of this thesis. Besides his genius, the tireless and enthusiastic commitment to research and transmission of knowledge have been the source of great admiration and inspiration.

Furthermore, I am particularly thankful to my co-advisors at Politecnico di Torino, Daniela Misul and Marco C. Masoero, who gave me the chance to develop this research work at UIC. I also thank Dr. Viswanath R. Katta for his assistance in the multidimensional CFD simulations.

Another thanks goes to my colleagues in the Flow and Combustion Simulation Laboratory: Xiao Fu and Daniele Bongiovanni for their willingness to help; Prithviraj Sabnis, Saurabh Sharma, and Abhijeet-Sanjay Badhe for the good times we had working together, always learning one from each other. Many thanks also to Francesco, my everyday friend and mate in Chicago.

My utmost gratitude and affection to my family: my father, Carlo, my mother, Antonella, and my brother, Paolo; thank you from the deepest of my heart for your support and your endless love, in the highs and in the lows of life. Thank you to Vittoria, my grandma.

Thank you to my friends and to the special people of my life, particularly Elisa.

The last acknowledgement is to myself for the hard-working days, the passion in what I do, and for never giving up in tough times.

CD

TABLE OF CONTENTS

CHAPTER		PAGE
1	**INTRODUCTION**	1
1.1	Motivations of Combustion Study	1
1.2	Syngas	2
1.3	Numerical Methods for Flame Calculations	3
2	**1D CFD CODE - CHEMKIN**	4
2.1	General introduction	4
2.2	CHEMKIN Overview	4
2.3	Employed CHEMKIN Library Codes	5
2.4	Chemical Reaction Mechanism	5
2.4.1	San Diego Mechanism	5
2.5	CHEMKIN Equilibrium Calculations	6
2.5.1	Minimization of Gibb's Free Energy	8
2.5.2	CHEMKIN Equilibrium Simulations Results	9
3	**2D CFD CODE - UNICORN**	13
3.1	General Introduction	13
3.2	UNICORN Overview	13
3.3	UNICORN Computational Model	14
3.4	Setting up a Numerical Simulation with UNICORN	15
4	**SYNGAS LAMINAR PREMIXED FLAMES**	17
4.1	Laminar Premixed Flames Fundamentals	17
4.2	Laminar Flame Speed	18
4.2.1	CHEMKIN Laminar Flame Speed Calculation	19
4.2.1.1	1D Flame Equations	20
4.2.1.2	Mixture-Averaged Transport Properties	21
4.2.1.3	Multicomponent Transport Properties	23
4.2.1.4	Boundary Conditions	24
4.2.1.5	Finite-Difference Approximations	25
4.2.2	Effects of Nitrogen Dilution	28
4.2.3	CHEMKIN Laminar Flame Speed Simulations Results	29
4.3	Counterflow Flames	32
4.3.1	Counterflow Configuration	33
4.3.2	CHEMKIN Opposed Flow Flame Calculations	34
4.3.2.1	Opposed Flow Model	35
4.3.2.2	Finite-Difference Approximations	38

TABLE OF CONTENTS (Continued)

CHAPTER **PAGE**

	4.3.2.3	Regrid Operation	39
	4.3.3	CHEMKIN Opposed Flow Flame Simulations Results	42
	4.3.4	UNICORN Counterflow Flame Calculations - Computational Domain	46
	4.3.5	UNICORN Counterflow Flame Simulations Results	47
	4.3.6	Counterflow Flame Results Validation - Comparison CHEMKIN-UNICORN	51
	4.3.7	Effects of Equivalence Ratio	53
5	**EFFECTS OF MIXTURE LEWIS NUMBER**		60
	5.1	Definition of Lewis Number	60
	5.2	Calculation of the Lewis Number	62
	5.2.1	Thermal Diffusivity Calculation	62
	5.2.2	Mass Diffusivity Calculation	63
	5.2.3	Lewis Number Calculation	64
	5.3	Collection of Results	65
	5.4	Concluding Remarks	72
6	**STRETCH EFFECT**		74
	6.1	Flame Stretch	74
	6.2	Strain Rate	75
	6.3	The Effect of Strain Rate on Temperature	77
	6.4	The Effect of Strain Rate on Heat Release Rate	82
	6.5	Computation of Unstretched Flame Speed	85
	6.5.1	Unstretched Flame Speed Results	86
	6.5.2	Unstretched Flame Speed with Heat Radiation	89
	6.6	Flame Stretch with Non-Equidiffusion	91
	6.7	Flame Stability	96
7	**EXTINCTION OF LEAN SYNGAS FLAMES**		100
	7.1	Stretch Effect: Extinction at High Strain Rate	101
	7.2	Stretch Effect: Extinction at Low Strain Rate - Effect of Radiative Heat Loss	103
	7.2.1	CHEMKIN-PRO	104
	7.2.2	Radiation Model in CHEMKIN-PRO	104
	7.2.3	Counterflow Setup Specifications	106
	7.3	Extinction at Low Strain Rate - Simulations Results	107
	7.3.1	Effect of Heat Radiation on Burning Velocity	111
	7.4	Summary of Extinction by Stretch	112
	7.5	Nitrogen Dilution Effects	114
	7.5.1	74% Nitrogen Dilution	114
	7.5.2	80% Nitrogen Dilution	115

TABLE OF CONTENTS (Continued)

CHAPTER **PAGE**

7.5.3 84% Nitrogen Dilution 115
7.5.4 85% Nitrogen Dilution 116

8 CONCLUSIONS 127

APPENDICES 132
Appendix A 133
Appendix B 140

CITED LITERATURE 142

VITA 146

LIST OF TABLES

TABLE		PAGE
I	EQUILIBRIUM CALCULATION FOR 50% H_2 - 50% CO SYNGAS, $\Phi = 0.75$.	10
II	EQUILIBRIUM CALCULATION FOR 50% H_2 - 50% CO SYNGAS, $\Phi = 1.25$.	11
III	EQUILIBRIUM CALCULATION FOR 50% H_2 - 50% CO SYNGAS, WITH 50% N_2 DILUTION, $\Phi = 1.00$.	11
IV	EQUILIBRIUM CALCULATION FOR 20% H_2 - 80% CO SYNGAS, WITH 50% N_2 DILUTION, $\Phi = 1.00$.	12
V	PARAMETERS FOR REGRID OPERATION.	42
VI	THERMAL CONDUCTIVITY, SPECIFIC HEAT, AND MASS DIFFUSION OF THE SPECIES AT 1 ATM AND 300 K.	65
VII	MOLE FRACTION AND MASS DENSITY OF THE SPECIES AT 1 ATM AND 300 K AT DIFFERENT Φ.	65
VIII	MASS FRACTION OF THE SPECIES AT 1 ATM AND 300 K AT DIFFERENT Φ.	66
IX	TOTAL THERMAL CONDUCTIVITY, TOTAL SPECIFIC HEAT, AND TOTAL THERMAL DIFFUSIVITY OF THE SPECIES AT 1 ATM AND 300 K AT DIFFERENT Φ.	66
X	LEWIS NUMBER OF 50% H_2 - 50% CO SYNGAS (WITH 68% N_2 DILUTION) AT DIFFERENT Φ, OBTAINED WITH THE DIFFUSION- AND THE VOLUME-BASED APPROACHES.	67
XI	LEWIS NUMBER OF DIFFERENT SYNGAS COMPOSITIONS (WITHOUT DILUTION) AT DIFFERENT Φ. THE REMAINING PART OF FUEL VOLUME FRACTION IS OCCUPIED BY CO.	68
XII	LEWIS NUMBER OF DIFFERENT SYNGAS COMPOSITIONS (WITH 68% N_2 DILUTION) AT DIFFERENT Φ. THE REMAINING PART OF FUEL VOLUME FRACTION IS OCCUPIED BY CO.	69
XIII	LEWIS NUMBER OF THE INDIVIDUAL SPECIES OF A MIXTURE OF METHANE+HYDROGEN (71% CH_4 + 29% H_2) FUEL AND AIR (Φ=0.52), AS CALCULATED IN THIS WORK AND BY HAWKES ET AL.	72
XIV	MAXIMUM TEMPERATURE AND BURNING VELOCITY OF THREE FLAMES WITH THE SAME k.	76

LIST OF TABLES (Continued)

TABLE		PAGE
XV	STRETCHED FLAME SPEED OF A SYNGAS (50% H_2 - 50% CO) MIXTURE WITH 68% N_2 DILUTION AND Φ=0.8, AT DIFFERENT k.	86
XVI	STRETCHED FLAME SPEED OF A SYNGAS (50% H_2 - 50% CO) MIXTURE WITH 68% N_2 DILUTION, AT DIFFERENT Φ AND k, EVALUATED AT THE REACTION ZONE BARYCENTER.	89
XVII	COMPARISON OF THE UNSTRETCHED FLAME SPEED OF A SYNGAS (50% H_2 - 50% CO) MIXTURE WITH 68% N_2 DILUTION, AT DIFFERENT Φ, COMPUTED BY NEGLECTING AND CONSIDERING RADIATION.	91
XVIII	LOW AND HIGH EXTINCTION STRAIN RATES OF A MIXTURE OF 50% H_2 - 50% CO SYNGAS (WITH 80% N_2 DILUTION) AND AIR, AT DIFFERENT Φ.	112

LIST OF FIGURES

FIGURE		PAGE
1	Laminar premixed flame speed of syngas with 68% nitrogen dilution by volume as a function of equivalence ratio.	30
2	Counterflow configuration schematic for premixed syngas-air twin flames.	34
3	Temperature and axial velocity profiles for syngas (50% H_2 and 50% CO) flame with Φ=0.8 and 68% N_2 dilution, obtained with CHEMKIN	44
4	Species mole fraction profiles for syngas (50% H_2 and 50% CO) flame with Φ=0.8 and 68% N_2 dilution.	45
5	Temperature and axial velocity profiles for syngas (50% H_2 and 50% CO) flame with Φ=0.8 and 68% N_2 dilution, obtained with UNICORN.	47
6	Species concentration profile as a function of axial coordinate (50% H_2 and 50% CO syngas, 68% N_2 dilution, Φ=0.8), obtained with UNICORN.	48
7	OH mole fraction and temperature iso-contours in two-dimensional coordinates (in mm) (50% H_2 and 50% CO syngas, 68% N_2 dilution, Φ=0.8) obtained with UNICORN.	49
8	Temperature and axial velocity profiles as functions of axial coordinate (50% H_2 and 50% CO syngas, 68% N_2 dilution, Φ=0.8). CHEMKIN vs UNICORN comparison.	51
9	Reactant species concentration profile as a function of axial coordinate (50% H_2 and 50% CO syngas, 68% N_2 dilution, Φ=0.8). CHEMKIN (solid line) vs UNICORN (dashed line) comparison. . .	52
10	Product species concentration profile as a function of axial coordinate (50% H_2 and 50% CO syngas, 68% N_2 dilution, Φ=0.8). CHEMKIN (solid line) vs UNICORN (dashed line) comparison.	53
11	Temperature (a) and axial velocity (b) profiles for different Φ values (50% H_2 and 50% CO syngas, 68% N_2 dilution), obtained with CHEMKIN (solid lines) and UNICORN (dashed lines).	55
12	H_2 and O_2 mole fraction profiles along the axial coordinate (50% H_2 and 50% CO syngas, 68% N_2 dilution) for different Φ values, obtained with CHEMKIN (solid line) and UNICORN (dashed line).	56
13	CO_2 mole fraction profiles along the axial coordinate (50% H_2 and 50% CO syngas, 68% N_2 dilution) for different Φ values, obtained with CHEMKIN (solid line) and UNICORN (dashed line).	57

LIST OF FIGURES (Continued)

FIGURE		PAGE
14	OH mole fraction profiles along the axial coordinate (50% H_2 and 50% CO syngas, 68% N_2 dilution) for different Φ values, obtained with CHEMKIN (solid line) and UNICORN (dashed line).	58
15	OH mole fraction and temperature iso-contours in two-dimensional coordinates (in mm) (50% H_2 and 50% CO syngas, 68% N_2 dilution) for (a) Φ=0.8, (b) Φ=0.7, and (c) Φ=0.6, obtained with UNICORN.	59
16	Lewis number as a function of equivalence ratio for H_2, CO, and different syngas compositions (without dilution).	70
17	Lewis number as a function of equivalence ratio for H_2, CO, and different syngas compositions (diluted with N_2 by 68% in volume).	71
18	Temperature profiles in the axial direction for premixed flames (50% H_2 and 50% CO syngas, 68% N_2 dilution) computed at different strain rates and (a) Φ=0.8, (b) Φ=0.6.	78
19	Flame temperature as a function of strain rate (50% H_2 and 50% CO syngas, 68% N_2 dilution) indicating high strain rate extinction for different Φ, obtained with CHEMKIN.	79
20	Axial temperature profiles in the flame region near the stagnation plane (50% H_2 and 50% CO syngas, 68% N_2 dilution, Φ=0.8) for different strain rates.	80
21	HRR profiles at different strain rates for (a) Φ=0.8 and (b) Φ=0.6. (50% H_2 and 50% CO syngas, 68% N_2 dilution).	83
22	HRR profiles along the axial direction at different strain rates (50% H_2 and 50% CO syngas, 68% N_2 dilution, Φ=1.6).	84
23	Unburned flame speed as a function of the strain rate for different equivalence ratios (50% H_2 and 50% CO syngas with 68% N_2 dilution). The circles represent the results of the single simulations.	87
24	Unburned flame speed as a function of the strain rate (obtained with OPPDIFF) and unstretched laminar flame speed values (obtained with PREMIX) for Φ=0.8 and Φ=0.6 (50% H_2 and 50% CO syngas with 68% N_2 dilution).	88
25	Unburned flame speed as a function of the strain rate for different equivalence ratios (50% H_2 and 50% CO syngas with 68% N_2 dilution), considering *heat radiation*. The circles represent the results of the single simulations.	90
26	Axial velocity profile for syngas (50% H_2 and 50% CO) flame with Φ=0.8 and 68% N_2 dilution. Identification of the burned and unburned flame speed.	92
27	*Downstream* (burned) flame speed of 50% H_2 and 50% CO syngas (with 68% N_2 dilution) as a function of the strain rate for different equivalence ratios. The circles represent the results of the single simulations.	93

LIST OF FIGURES (Continued)

FIGURE		PAGE
28	*Downstream* (burned) flame speed as a function of strain rate for rich (Φ=1.6, *solid lines*) and lean (Φ=0.6, *dashed lines*) mixtures with different syngas compositions (with 68% N_2 dilution).	94
29	OH mole fraction as a function of strain rate for rich (Φ=1.6, *solid lines*) and lean (Φ=0.6, *dashed lines*) mixtures with different syngas compositions (with 68% N_2 dilution).	96
30	Normalized burned laminar flame speed as a function of the Karlovitz number at Φ=1.6 (solid lines) and Φ=0.6 (dashed lines) for different syngas composition (H_2 content is indicated in the legend, while the remaining part is CO), at ambient temperature and pressure. Circles indicate single numerical simulations results at varying k.	97
31	Temperature profiles along flow semi-axis of a (a) Φ=0.5 and a (b) Φ=0.6 syngas/air mixtures (with 80% N_2 dilution), obtained with CHEMKIN-PRO (non-radiating and radiating models).	117
32	Temperature profiles along flow axis of a (a) Φ=0.5 and a (b) Φ=0.6 syngas/air mixtures (with 80% N_2 dilution) at different k, obtained with CHEMKIN-PRO.	118
33	Flame temperature as a function of a small range of low strain rate (50% H_2 and 50% CO syngas, 80% N_2 dilution) for Φ=0.5 and Φ=0.6, obtained with CHEMKIN-PRO. Non-radiating (solid lines) and radiating (dashed lines) models.	119
34	Difference of the maximum temperatures of *radiating* and *non-radiating* models as a function of strain rate (50% H_2 and 50% CO syngas, 80% N_2 dilution) for Φ=0.5 and Φ=0.6.	120
35	Burning velocity as a function of a small range of low strain rate (50% H_2 and 50% CO syngas, 80% N_2 dilution) for Φ=0.5 and Φ=0.6, obtained with CHEMKIN-PRO. Non-radiating (solid lines) and radiating (dashed lines) models.	121
36	Extinction strain rate (logarithmic scale) as a function of equivalence ratio (50% H_2 and 50% CO syngas, 80% N_2 dilution). Results obtained with CHEMKIN-PRO.	122
37	OH mole fraction and temperature iso-contours in two-dimensional coordinates (in mm) (50% H_2 and 50% CO syngas, 74% N_2 dilution) for (a) Φ=0.8, (b) Φ=0.7, and (c) Φ=0.6, obtained with UNICORN.	123
38	OH mole fraction and temperature iso-contours in two-dimensional coordinates (in mm) (50% H_2 and 50% CO syngas, 80% N_2 dilution) for (a) Φ=0.8, (b) Φ=0.7, and (c) Φ=0.6, obtained with UNICORN.	124
39	Temperature profiles for different Φ values (50% H_2 and 50% CO syngas, 84% N_2 dilution), obtained with CHEMKIN.	125

LIST OF FIGURES (Continued)

FIGURE		PAGE
40	OH mole fraction and temperature iso-contours in two-dimensional coordinates (in mm) (50% H_2 and 50% CO syngas, 84% N_2 dilution, Φ=0.8), obtained with UNICORN. Flame extinction shown by evolution in time.	126
41	Axial velocity profile as a function of axial coordinate (50%H_2 and 50%CO syngas, 68% N_2 dilution), obtained with CHEMKIN, for (a) Φ=0.7 and (b) Φ=0.6.	133
42	Temperature profile as a function of axial coordinate (50%H_2 and 50%CO syngas, 68% N_2 dilution), obtained with CHEMKIN, for (a) Φ=0.7 and (b) Φ=0.6.	134
43	Species concentration profile profile as a function of axial coordinate (50%H_2 and 50%CO syngas, 68% N_2 dilution), obtained with CHEMKIN, for (a) Φ=0.7 and (b) Φ=0.6.	134
44	Axial velocity profile as a function of axial coordinate (50%H_2 and 50%CO syngas, 68% N_2 dilution), obtained with UNICORN, for (a) Φ=0.7 and (b) Φ=0.6.	135
45	Temperature profile as a function of axial coordinate (50%H_2 and 50%CO syngas, 68% N_2 dilution), obtained with UNICORN, for (a) Φ=0.7 and (b) Φ=0.6.	136
46	Species concentration profile profile as a function of axial coordinate (50%H_2 and 50%CO syngas, 68% N_2 dilution), obtained with UNICORN, for (a) Φ=0.7 and (b) Φ=0.6.	137
47	Axial velocity profile as a function of axial coordinate (50%H_2 and 50%CO syngas, 68% N_2 dilution). CHEMKIN vs UNICORN comparison, for (a) Φ=0.7 and (b) Φ=0.6.	137
48	Temperature profile as a function of axial coordinate (50%H_2 and 50%CO syngas, 68% N_2 dilution). CHEMKIN vs UNICORN comparison, for (a) Φ=0.7 and (b) Φ=0.6.	138
49	Reactant species concentration profile profile as a function of axial coordinate (50%H_2 and 50%CO syngas, 68% N_2 dilution). CHEMKIN vs UNICORN comparison, for (a) Φ=0.7 and (b) Φ=0.6.	138
50	Product species concentration profile profile as a function of axial coordinate (50%H_2 and 50%CO syngas, 68% N_2 dilution). CHEMKIN vs UNICORN comparison, for (a) Φ=0.7 and (b) Φ=0.6.	139
51	Modified lines of the thermodynamic data file for the San Diego chemical-kinetic mechanism	140

LIST OF ABBREVIATIONS

CFD	Computational Fluid Dynamics
HRR	Heat Release Rate

SUMMARY

In the current power generation scenario, two countervailing necessities are faced daily by designers and manufacturers of combustion systems: on the one side, the increasing energy demand and the need to respond adequately and efficiently; and on the other side, the commitment to cleaner combustion and the fulfillment of environmental measures. Among the variety of alternative fuels under development, syngas is particularly interesting, as it can be produced locally through a gasification process from biomass (as well as fossil fuels and coal). It also offers the advantages of hydrogen combustion, and it is widely available.

The purpose of the present work is to assess some syngas combustion characteristics for which literature is still fragmentary. The underlying aim is to provide combustion systems manufacturers with some useful results about characteristics and ranges of application, thus incentivizing the employment of this clean fuel. A computational study is carried out, by means of one- and two-dimensional CFD simulations. The physical model considers the classical counterflow configuration, consisting of the impingement of two opposing jets. In particular, laminar premixed syngas flames under lean conditions are considered. The effects of syngas composition, stretch, and preferential diffusion on flame speed, structure, and extinction behavior are examined. Although such issues have been broadly addressed in combustion literature for traditional fuels, flame studies of syngas are still in progress.

The Lewis numbers (Le) of several syngas/air mixtures (different in H_2/CO ratio, equivalence ratio, and N_2 dilution) are computed. Results indicate that while Le is less than or

greater than unity for lean and rich mixtures, respectively, the mixture transport properties are predominantly characterized by H_2 rather than by CO.

The combined effects of non-equidiffusion and flame stretch lead to a modification in the flame speed and structure. Since the premixed flames in a counterflow configuration are positively stretched, the effect of stretch leads to higher burning rate for mixtures with $Le < 1$, i.e., lean syngas flames, and lower burning rate for mixtures with $Le > 1$, i.e., rich syngas flames. In this sense, syngas flames exhibit an analogous behavior to hydrogen flames.

Flame stability is assessed, finding that rich syngas flames are cellularly stable, while lean syngas flames are unstable, as a consequence of the Lewis number effect.

Flame extinction limits of lean syngas flames are calculated. Extinction occurs at either too high or too low global strain rate. In the first case, it is purely induced by stretch; in the second case, gas radiation plays a crucial role. Lowly stretched (lean) flames with lower Φ are more affected by strain rate variations. Moreover, the mixture extinction limits can be extended by an increase in equivalence ratio.

Finally, the effect of N_2 dilution on syngas flames extinction is also assessed.

CHAPTER 1

INTRODUCTION

1.1 Motivations of Combustion Study

The study of combustion phenomena has accompanied the progress in science and technology of mankind for ages; predictably, research and development in this field will not stop even in the future centuries.

It is meaningful to point out that, as of 2014, more than 79 percent of the yearly primary energy production in the US was represented by combustion sources [1]. Despite of the growing popularity and employment of renewable energy sources, combustion will not be replaced by them any time soon.

Even in the propulsion sector, internal combustion engines still represent today an essential power source, since purely electric motors are not to be considered a replacement. Specifically for the improvement of engines performances, substantial development in the architecture of powertrain units has undergone a slowdown, in the last years; conversely, combustion study always plays a crucial role, not only because engine efficiency greatly relies on combustion efficiency, but also because it is a field denoted by continuous improvement. The need to more proficiently exploit the power of the fuel and achieve cleaner and lesser exhausts is surely one of the main reasons.

Combustion is in electric power generation, heating appliances, transportation systems, industrial processes, etc... Hence, it is clear how this phenomenon constitutes a big part of each individual's everyday life.

1.2 Syngas

Nowadays, energy demand is dramatically increasing day by day. Meanwhile, because of the climate change and pollution, everyday more stringent norms are enacted for emissions control; this represents a big challenge for the manufacturers of those systems that exhaust noxious gases. Therefore, it is imperative to extend the employment of alternative fuels characterized by high efficiency and clean combustion. A certainly interesting source of diversification for power generation systems is synthesis gas, or *syngas*, which finds its application in electricity production, as an additive to hydrocarbon fuels in internal combustion engines, and as a proper fuel itself in gas turbine combustors and industrial burners [2].

Synthesis gas is usually obtained through a process called *gasification*, which provides hydrogen, carbon monoxide, and carbon dioxide from fossil fuels, coal, or biomasses. One of the main advantages of syngas is that it can be produced locally anywhere, with no need to import sources.

Syngas fuel is mainly composed of H_2 and CO, with some variable content of CO_2, H_2O, N_2, CH_4, and possibly other hydrocarbons. However, in the present study, the most common case of H_2 and CO syngas composition will be considered, for the sake of simplicity.

Syngas is a low-energy density fuel; on the other hand, the employment of hydrogen as a fuel offers several advantages, e.g., high combustion performances, low noxious emissions, and a broad flammability range.

In this thesis study, the combustion characteristics of syngas will be addressed, along with the effects of flame stretch, preferential diffusion, Lewis number, and gas radiation heat loss.

1.3 Numerical Methods for Flame Calculations

Key parameters in the study of combustion, which characterize the overall reaction profitability and effects, are the following: burning temperature, flame speed, and rate of depletion/-formation of chemical species. These flame features can be evaluated by means of numerical simulations.

Throughout this work, flame studies will be approached by involving one and two-dimensional CFD simulations. Numerical methods and algorithms are employed to solve chemically reacting fluid flow problems, which are modeled by involving fluid mechanics, thermochemistry, molecular transport, and chemical kinetics principles and equations. By specifying proper convergence criteria for the employed numerical method, accurate and reliable predictions of flame structure and behavior can be obtained.

The numerical procedures adopted in the CFD codes of reference will be presented in detail in the following chapters.

CHAPTER 2

1D CFD CODE - CHEMKIN

2.1 General introduction

One of the employed tools for the numerical study of flames is CHEMKIN® software, released by Reaction Design®. It is basically a one-dimensional CFD code that allows the simulations of complex chemical reactions.

By means of CHEMKIN code, the structure, behavior, and extinction characteristics of syngas/air premixed flames will be assessed.

2.2 CHEMKIN Overview

"At its most fundamental level, CHEMKIN piece of software enables the simulation of complex chemical reactions. With the advanced capabilities now available, sophisticated Design-of-Experiments (DoE) can be created to parametrically explore potential design solutions well before costly hardware is built. CHEMKIN evolved from its origin as a Sandia National Laboratory combustion kinetics code (Chemkin II) into today's commercial-quality software suite with a user-friendly interface, industry-leading Time-to-Solution performance, and unparalleled accuracy. CHEMKIN models have been extensively validated over several decades and frequently cited in technical peer-reviewed journals" [3].

The piece of software is coded in Fortran language and presents various programs and subroutine libraries, in order to perform different reaction analyses for different physical problem types.

2.3 Employed CHEMKIN Library Codes

In the development of this work, the following codes of the CHEMKIN [4] package have been used in performing the simulations: EQUIL [5], PREMIX [6], and OPPDIFF [7] codes.

2.4 Chemical Reaction Mechanism

The study of hydrocarbon combustion is performed by employing a chemical kinetics model, entailing the definition of many chemical species and elementary processes.

Chemical reactions paths are analyzed by means of *reaction mechanisms*. They are stepwise descriptions of overall balanced chemical reactions, which are composed of *elementary processes* entailing molecular events, such as collisions and vibrations, that lead to the formation of products from reactants. In each elementary process, one or some molecules are interacting with the surrounding chemical environment, by their geometrical structure or composition modification.

Nowadays, the progress in the research and employment of alternative fuels has led to the formulation of very accurate and broad reaction mechanisms.

2.4.1 San Diego Mechanism

In the present study, the adopted chemical-kinetics mechanism is the San Diego Mechanism.

"The detailed chemistry is designed to focus on conditions relevant to flames, high temperature ignition and detonations. It was derived by beginning with simple chemical systems then

proceeding gradually to more complex systems. In this approach, the numbers of species and reactions are kept to the minimum needed to describe the systems and phenomena addressed, thereby minimizing as much as possible the uncertainties in the rate parameters employed" [8].

Three different data sets are provided altogether, which compose the complete reaction mechanism: gas-phase kinetics data file, thermodynamics data file, and gas transport data file.

2.5 CHEMKIN Equilibrium Calculations

It follows an extraction from CHEMKIN Theory Manual [9].

> In addition to chemically reacting flow applications, CHEMKIN includes an Equilibrium Reactor model. This model allows users to determine the chemical state of a mixture under equilibrium conditions. Any number of gas-phase or condensed (bulk) species can be included in an equilibrium calculation, while surface site species are ignored. In this way, the Equilibrium Reactor model can be used to determine phase equilibrium, between gas and condensed phases, as well as chemical equilibrium. All that is required is thermodynamic data for all species in each phase.
>
> An established method for evaluating chemical equilibrium is the element-potential method embodied in the Stanford software STANJAN [10]. The CHEMKIN Equilibrium Reactor employs the STANJAN library of routines in its solution method. The equilibrium determines composition equilibrium and/or phase equilibrium. The results depend only on the thermodynamic properties of the species in the user's chemistry set, as well as the starting composition and conditions specified. The starting composition determines the relative amount of chemical elements in the system. An initial estimate of the equilibrium

temperature can sometimes be used to select a *burned* equilibrium state from an *unburned* equilibrium state in the case where two equilibrium states are possible.

Currently, the equilibrium program assumes that the gas-phase is a mixture of ideal gases and that condensed phases are ideal solutions. The user selects atomic populations through identity of initial species and their fraction in each phase, as well as the state parameters.

The user may specify the state parameters in a number of different ways, including

- temperature and pressure;
- pressure and entropy;
- enthalpy and pressure;
- volume and entropy.

Species composition can be *frozen* in a given calculation, or the equilibrium composition can be determined. Calculations may be linked through continuations, such that the conditions calculated from a previous equilibrium case can be used as the starting point for a subsequent case with different constraints. In this way, the user can employ the Equilibrium Reactor Model to analyze stages in a thermodynamic cycle.

The Equilibrium Reactor Model is also commonly used to determine adiabatic flame temperatures for combustible gas mixtures. Such a simulation is performed by specifying an initial (reagent) gas mixture and constraining equilibrium for constant enthalpy (adiabatic) and constant pressure. The calculation can also be performed using constant

internal energy and constant volume. An initial guess for the equilibrium temperature of 1000 K or above is usually needed to cause the equilibrium solver to find the burned-gas solution. For accurate adiabatic-flame temperature calculations, it is important to include all radical species that might occur in the flame, as well as stable reactants and products.

In the following subsection, the equations solved and the methodology used for determining chemical and phase equilibria of arbitrary systems are discussed.

2.5.1 Minimization of Gibb's Free Energy

It follows an extraction from CHEMKIN Theory Manual [9].

The basic theory for the element-potential method of determining equilibrium is based on the minimization of Gibb's free energy. The Gibb's function of a system is:

$$G = \sum_{k=1}^{K} \overline{g}_k N_k \tag{2.1}$$

where $\overline{g}_k$ is the partial molal Gibb's function and N_k is the number of moles of each k species in the system. K is the total number of species.

For ideal-gas mixtures or ideal solutions, the partial molal Gibb's functions are given by:

$$\overline{g}_k = g_k(T, P) + RT \ln X_k \tag{2.2}$$

where $\overline{g}_k(T, P)$ is the Gibbs function for the pure species k, evaluated at the system temperature and pressure; R is the universal gas constant; X_k and is the mole fraction

of the kth species. The equilibrium solution at a given temperature and pressure is the distribution of N_k that minimizes the system Gibbs function, G, subject to atomic population constraints (and non-negative N_k). The atomic population constraints are:

$$\sum_{k=1}^{K} n_{jk} N_k = p_j \qquad j = 1, ..., M \tag{2.3}$$

where n_{jk} is the number of the jth atoms that appear in the kth molecule, is the total population in moles of the jth atom in the system, and M is the total number of different elements that are present in the system. Details regarding the relationship between the partial molar Gibbs functions and the elemental potentials for the atoms, as well as the explicit form of the equations solved in the STANJAN library, are described in the STANJAN report.

2.5.2 CHEMKIN Equilibrium Simulations Results

As far as premixed flames are concerned, it is useful to evaluate the fuel/air mixture inlet composition in terms of mole fractions. Since, in the proceeding of this work, syngas/air premixed flames will be addressed, this step is preparatory for specifying the input conditions for the diverse analyses. The procedure is to be repeated every time the specified mixture composition is changed (by varying equivalence ratio, fuel dilution percentage, H_2 to CO volume ratio in syngas, etc...).

Such calculations can be performed by means of the EQUIL [5] code on CHEMKIN. In this paragraph, the initial (as well as the equilibrium) mole fractions of the chemical species of a

limited number of syngas/air mixtures are collected in Table I,Table II,Table III, and Table IV. From now on, air composition is always assumed to be: 79% N_2 and 21% O_2.

Here, only few cases are reported, for brevity.

TABLE I: EQUILIBRIUM CALCULATION FOR 50% H_2 - 50% CO SYNGAS, $\Phi = 0.75$.

Species	**Initial State Mole Fraction**	**Equilibrium State Mole Fraction**
N_2	6.01E-01	6.81E-01
H	0	1.00E-04
O_2	1.60E-01	4.58E-02
OH	0	3.61E-03
O	0	4.32E-04
H_2	1.20E-01	5.34E-04
H_2O	0	1.33E-01
HO_2	0	1.87E-06
H_2O_2	0	8.59E-08
CO	1.20E-01	2.73E-03
CO_2	0	1.33E-01
HCO	0	7.11E-11

TABLE II: EQUILIBRIUM CALCULATION FOR 50% H_2 - 50% CO SYNGAS, $\Phi = 1.25$.

Species	**Initial State Mole Fraction**	**Equilibrium State Mole Fraction**
N_2	5.18E-01	5.98E-01
H	0	1.85E-03
O_2	1.38E-01	1.37E-03
OH	0	4.10E-03
O	0	2.92E-04
H_2	1.72E-01	1.59E-02
H_2O	0	1.80E-01
HO_2	0	3.20E-07
H_2O_2	0	3.62E-08
CO	1.72E-01	6.77E-02
CO_2	0	1.31E-01
HCO	0	2.16E-08
CH_2O	0	4.37E-10

TABLE III: EQUILIBRIUM CALCULATION FOR 50% H_2 - 50% CO SYNGAS, WITH 50% N_2 DILUTION, $\Phi = 1.00$.

Species	**Initial State Mole Fraction**	**Equilibrium State Mole Fraction**
N_2	6.58E-01	7.40E-01
H	0	8.56E-05
O_2	1.14E-01	2.88E-03
OH	0	1.21E-03
O	0	5.97E-05
H_2	1.14E-01	1.12E-03
H_2O	0	1.27E-01
HO_2	0	1.67E-07
H_2O_2	0	1.58E-08
CO	1.14E-01	5.26E-03
CO_2	0	1.23E-01
HCO	0	1.40E-10
CH_2O	0	2.42E-12

TABLE IV: EQUILIBRIUM CALCULATION FOR 20% H_2 - 80% CO SYNGAS, WITH 50% N_2 DILUTION, $\Phi = 1.00$.

Species	**Initial State Mole Fraction**	**Equilibrium State Mole Fraction**
N_2	6.58E-01	7.39E-01
H	0	6.27E-05
O_2	1.14E-01	4.18E-03
OH	0	9.35E-04
O	0	8.57E-05
H_2	4.57E-02	4.40E-04
H_2O	0	5.03E-02
HO_2	0	1.53E-07
H_2O_2	0	8.18E-09
CO	1.83E-01	8.45E-03
$CO2$	0	1.97E-01
HCO	0	1.56E-10
CH_2O	0	1.52E-12

CHAPTER 3

2D CFD CODE - UNICORN

3.1 General Introduction

As an addition to CHEMKIN one-dimensional simulations, the study of premixed flames is conducted also by means of two-dimensional numerical simulations, performed with the UNICORN code. Not only they represent an accurate prediction of flame structure and characteristics (including laminar premixed flames extinction) in two directions of the flow, but also they are useful to provide a verification of the 1D simulations output. This *double check* is done by analyzing the numerical results in the axial direction of the flow and, subsequently, comparing them to the ones previously obtained with CHEMKIN.

3.2 UNICORN Overview

The following passage is taken from the work of Katta, Aggarwal, and Roquemore [11]:

> Three chemical-kinetics models developed for heptane combustion are incorporated into a two-dimensional CFD code, UNICORN (UNsteady Ignition and COmbustion using ReactioNs). First one is San Diego (SD) mechanism. It consists of 52 species and 544 elementary reactions. The second one is Lawrence Livermore National Laboratory (LLNL) mechanism. It consists of 160 species and 1540 reactions. And the third one is National Institute of Standards and Technology (NIST) mechanism. It consists of 197 species and

2926 reactions. These three mechanisms were chosen as they represent state-of-the-art semi-detailed and detailed chemistries for n-heptane combustion.

UNICORN code [12] [13] [14] is a time-dependent, axisymmetric mathematical model, which is used for the simulation of unsteady reacting flows. It is capable of performing direct numerical simulations (DNSs) and has been developed/improved over several years. Its evolution has been in conjunction with experiments conducted to test its ability to predict ignition, extinction, stability limits, and the dynamic characteristics of nonpremixed and premixed flames of various fuels. It solves for u- and v-momentum equations, continuity, and enthalpy- and species-conservation equations on a staggered-grid system. The body-force term due to the gravitational field is included in the axial-momentum equation for simulating vertically mounted flames. A clustered mesh system is employed to trace the large gradients in flow variables near the flame surface. Details of the finite-differencing schemes and the methodologies used for handling stiff species-conservation equations are given in Refs. [12], [14].

3.3 UNICORN Computational Model

UNICORN gives the results of the physical problem by solving the enthalpy, mass flow rate, species, and momenta conservation equations in the two directions. The code also includes detailed chemistry, thermodynamic, transport, and heat radiation models.

Furthermore, the algorithm offers the possibility to employ a uniform or non-uniform computational grid for the solution of the numerical problem.

Deeper understanding of the code may be acquired by referring to literature: [12], [13], [14], [15],and [16].

3.4 Setting up a Numerical Simulation with UNICORN

Two Fortran codes are employed for running flame simulations with UNICORN: unicorng2.f and unicornd-hept-sd.f. The former is a basic single-reaction mechanism that only accounts for the formation of combustion products (H2O, CO2, and N2) from reactants (hydrocarbons/fuels, O2, and N2); the latter is a state-of-the-art detailed chemistry mechanism.

An input file is needed for the problem definition; it should specify the configuration geometry, inlet conditions (inlet velocities, temperatures, and fluid compositions), boundary conditions, environment thermodynamic conditions of reference, thermo-fluid dynamics of the physical problem, mesh definition, convergence criteria.

The simulation starts when the executable file that reads the input file is run on the terminal.

The basic simulation is launched first; the so-obtained output file (FLAMEA.DATA) provides the temperature, velocity, and species profiles in the flow field. These profiles provide the detailed chemistry simulation with a suitable initial guess for the numerical method.

Once that also the complete simulation has been run, a final output file, FLAMEA.DATA, is obtained. It has to be post-processed by another Fortran-based code, unicornxyplots.f; by this post-process phase, the 2D results are further analyzed and plotted. It is of interest to analyze the results in the axial direction of the flow, thereby using a one-dimensional approach, to investigate, for instance, the temperature, fluid velocity, and species concentration distributions

along the domain axis. Conversely, a two-dimensional approach is expedient for studying the flow properties in both directions, axially and radially, and the iso-contours are plotted by using a graphics piece of software, namely, Tecplot [17].

CHAPTER 4

SYNGAS LAMINAR PREMIXED FLAMES

Main framework of this thesis is the analysis of laminar premixed flames of lean syngas / air mixtures. This goal is accomplished by employing a counterflow configuration (described in detail in Section 4.3.1) for numerical simulations.

4.1 Laminar Premixed Flames Fundamentals

This section is devoted to some introductory definitions and remarks.

It is useful to report some classical definitions of the key words [18].

> "[...] A *flame* is a self-sustaining propagation of a localized combustion zone. The flame should be localized; that is, the flame occupies only a small portion of the combustible mixture at any one time [...]"
>
> A flame is said to be laminar if it propagates at subsonic velocities.
>
> "[...] In a premixed flame, the fuel and the oxidizer are mixed at the molecular level prior the occurence of any significant chemical reaction [...]"

Here follows the definition of a very important flame property, namely, *flame speed*, because of its critical effect on the flame shape and stability.

> "[...] A reference frame for the coordinate system must be established. A flame may be freely propagating, as occurs when a flame is initiated in a tube containing a combustible

> gas mixture. The appropriate coordinate system would be fixed to the propagating combustion wave. An observer riding with the flame would experience the unburned mixture approaching at the flame speed, S_L. [...] The reactants enter the flame with a velocity equal to the flame propagation velocity, S_L" [18]

A steady flame is said to be stationary if its flame speed matches the normal component of the unburned gas velocity at every point.

4.2 Laminar Flame Speed

Having asserted its significance over the general flame behavior, it is clear that flame speed must always be assessed, in the proceeding of this study.

Flame speed is affected by three properties of the burning mixture, namely, the reaction rate, the thermal diffusivity, and the flame temperature. Therefore, flame speed is a characteristic value for a given mixture (at fixed inlet temperature and pressure, and stoichiometry) and it changes when its composition is varied.

In all practical applications, it is important to assure that the *flashback* phenomenon is avoided. It is a hazardous condition strictly related to the flame speed, which consists on the propagation of the flame upstream through the burner port, up to its tube, and, eventually, to the gas mixer or fuel storage unit (with obvious catastrophic consequences). It is originated whenever the local fluid flow velocity is smaller than the flame speed. This condition is expressed by:

$$S_u > S_L \tag{4.1}$$

where S_u is the velocity of the *unburned* mixture and S_L is the *flame* speed.

For this and other reasons, evaluating the flame speed of each mixture under analysis is always a preliminary step, in this work. Such study is carried out by employing PREMIX [6] code on CHEMKIN.

4.2.1 CHEMKIN Laminar Flame Speed Calculation

In this chapter, the equations governing steady, isobaric, quasi-one-dimensional flame propagation will be presented.

It follows an extraction from CHEMKIN Theory Manual [9].

> The Premixed Flame Models solve the set of governing differential equations that describe the flame dynamics using implicit finite difference methods, as well as, a combination of time-dependent and steady-state methods. The solver algorithm employed automates coarse-to-fine grid refinement as a means to enhance the convergence properties of the steady-state approach and as a means to provide optimal mesh placement.
>
> The Flame-speed Calculation Model involves a freely propagating flame. This configuration is used to determine the characteristic flame speed of the gas mixture at specified pressure and inlet temperature. In this case there are no heat losses (by definition) and thus the temperatures should be computed from the energy equation. Flame speed depends, in part, on the transport of heat, and predicting the temperature distribution is an integral part of the flame speed calculation.

4.2.1.1 1D Flame Equations

It follows an extraction from CHEMKIN Theory Manual [9].

For these equations, the 1-dimensional flow assumption is made with uniform inlet conditions. The governing conservation equations reduce to:

Continuity

$$\dot{M} = \rho u A \tag{4.2}$$

Energy

$$\dot{M}\frac{\mathrm{d}T}{\mathrm{d}x} - \frac{1}{c_p}\frac{\mathrm{d}}{\mathrm{d}x}(\lambda A\frac{\mathrm{d}T}{\mathrm{d}x}) + \frac{A}{c_p}\sum_{k=1}^{K}\rho Y_k V_k c_{pk}\frac{\mathrm{d}T}{\mathrm{d}x} + \frac{A}{c_p}\sum_{k=1}^{K}\dot{\omega}_k h_k W_k + \frac{A}{c_p}\dot{Q}_{rad} = 0 \tag{4.3}$$

Species

$$\dot{M}\frac{\mathrm{d}Y_k}{\mathrm{d}x} + \frac{\mathrm{d}}{\mathrm{d}x}(\rho A Y_k V_k) - A\dot{\omega}_k W_k = 0 \qquad (k = 1, ..., K_g) \tag{4.4}$$

Equation of State

$$\rho = \frac{P\overline{W}}{RT} \tag{4.5}$$

In these equations x denotes the spatial coordinate; $\dot{M}$ the mass flow rate (which is independent of x); T the temperature; Y_k the mass fraction of the kth species (there are K_g species); P the pressure; u the velocity of the fluid mixture; ρ the mass densoty; W_k the molecular weight of the kth species; $\overline{W}$ the mean molecular weight of the mixture; R the universal gas constant; λ the thermal conductivity of the mixture; c_p the constant

pressure heat capacity of the mixture; c_{pk} the constant pressure heat capacity of the kth species; $\dot{\omega}_k$ the molar rate of production by chemical reaction of the kth species per unit volume; h_k the specific enthalpy of the kth species; V_k the diffusion velocity of the kth species; $\dot{Q}_{rad}$ the heat loss due to gas and particle radiation; and A the cross-sectional area of the stream tube encompassing the flame (normally increasing due to thermal expansion) normalized by the burner area. The user may provide an area profile (APRO) or alternatively a subroutine to specify the area as a function of the spatial coordinate. By default, the stream tube area is taken to be constant and equal to unity.

The net chemical production rate $\dot{\omega}_k$ of each species results from a competition between all the chemical reactions involving that species. It is presumed that each reaction proceeds according to the law of mass action and the forward rate coefficients are in the modified Arrhenius form,

$$k_f = AT^{\beta}\exp(\frac{-E_A}{RT}) \tag{4.6}$$

4.2.1.2 Mixture-Averaged Transport Properties

It follows an extraction from CHEMKIN Theory Manual [9].

For the mixture-averaged formula, it is assumed that the diffusion velocity is composed of three parts:

$$V_k = v_k + w_k + V_c \tag{4.7}$$

v_k is the ordinary diffusion velocity and is given in the Curtiss-Hirschfelder approximation by

$$v_k = D_{km} \frac{1}{X_k} \frac{\mathrm{d}X_k}{\mathrm{d}x} \tag{4.8}$$

where X_k is the mole fraction, and where the mixture-averaged diffusion coefficient D_km is given explicitly in terms of the binary diffusion coefficients D_kj

$$D_{km} = \frac{1 - Y_k}{\sum_{j \neq k}^{K} \frac{X_j}{D_{kj}}} \tag{4.9}$$

A non-zero thermal diffusion velocity is included only for the low molecular weight species H,H_2, and He. The trace, light-component limit is employed in determining w_k, i.e.,

$$w_k = \frac{D_{km} \Theta_k}{X_k} \frac{1}{T} \frac{\mathrm{d}T}{\mathrm{d}x} \tag{4.10}$$

where Θ_k is the thermal diffusion ratio. The sign of Θ_k makes the lower molecular weight species diffuse from low to high temperature regions.

The correction velocity V_c (independent of species but a function of the distance x) is included to insure that the mass fractions sum to unity or equivalently

$$\sum_{k=1}^{K} Y_k V_k = 0 \tag{4.11}$$

4.2.1.3 Multicomponent Transport Properties

It follows an extraction from CHEMKIN Theory Manual [9].

For the multicomponent option, the transport property evaluation follows the method described by Dixon-Lewis multicomponent diffusion coefficients, thermal conductivities and thermal diffusion coefficients are computed through the solution of a system of equations involving the binary diffusion coefficients, the species mole fractions, and the thermodynamic and molecular properties of the species. These equations result in the determination of ordinary multicomponent diffusion coefficients, D_{kj}, for species k diffusing in species j, as well as species thermal diffusion coefficients and thermal conductivities.

For the multicomponent formulation, the correction velocity, V_c, is not required and the diffusion velocity is defined as:

$$V_k = v_k + w_k \tag{4.12}$$

Now, the ordinary diffusion velocity term is given by:

$$v_k = \frac{1}{X_k \overline{W}} \sum_{j \neq k}^{K} W_j D_{kj} d_j \tag{4.13}$$

Here $\overline{W}$ is the mean molar mass, W_j is the molar mass of species j, and d_j is defined as:

$$d_j = \nabla X_k + (X_k - Y_k) \frac{1}{P} \nabla P \tag{4.14}$$

The thermal diffusion velocity is given as:

$$w_k = \frac{D_k^T}{\rho Y_k} \frac{1}{T} \nabla T \tag{4.15}$$

where D_k^T is the thermal diffusion coefficient for species k. The multicomponent option is considerably more accurate than the mixture-averaged approach when thermal diffusion effects are important.

4.2.1.4 Boundary Conditions

It follows an extraction from CHEMKIN Theory Manual [9].

The boundary conditions may be deduced from the early work of Curtiss and Hirschfelder. The temperature and mass flux fractions ($\varepsilon_k = Y_k + \rho Y_k V_k A/\dot{M}$)) are specified at the cold boundary, and vanishing gradients are imposed at the hot boundary.

For freely propagating flames, $\dot{M}$ is an eigenvalue and must be determined as part of the solution. Therefore, an additional constraint is required, or alternatively one degree of freedom must be removed from the problem. It is chosen to fix the location of the flame by specifying and fixing the temperature at one point. This is sufficient to allow for the solution of the flame speed eigenvalue $\dot{M}$. This point must be selected in such a way as to insure that the temperature and species gradients "nearly" vanish at the cold boundary. If this condition is not met then the resultant $\dot{M}$ will be too low because some heat will be lost through the cold boundary. More details on boundary conditions are described in the following.

The boundary conditions are relatively easily implemented. At the cold boundary the mass flux fractions and the temperature are specified, i.e.

$$\varepsilon_{k,1} - Y_{k,1} - (\frac{\rho A Y_k V_k}{\dot{M}})_{j=1\frac{1}{2}} = 0 \tag{4.16}$$

and

$$T_1 - T_b = 0 \tag{4.17}$$

where $\varepsilon_{k,1}$ is the inlet reactant fraction of the kth species and T_b is the specified burner temperature. At the hot boundary the vanishing of all gradients is specified, i.e.,

$$\frac{Y_{k,J} - Y_{k,J-1}}{x_J - x_{J-1}} = 0 \tag{4.18}$$

and

$$\frac{T_J - T_{J-1}}{x_J - x_{J-1}} = 0 \tag{4.19}$$

The boundary conditions for $\dot{M}$ depend on whether the given problem is a burner-stabilized or a freely propagating flame.

4.2.1.5 Finite-Difference Approximations

It follows an extraction from CHEMKIN Theory Manual [9].

The first task in solving the flame problem is to discretize the governing conservation equations. Finite difference approximations are used on a non-uniform grid with points

numbered from 1 at the cold boundary to J at the hot boundary. On the convective terms the user has the choice of using either first order windward differences or central differences. Both cases are illustrated using the convective term in the energy equation. The windward difference is given as

$$(\dot{M}\frac{\mathrm{d}T}{\mathrm{d}x})_j \approx \dot{M}_j(\frac{T_j - T_{j-1}}{x_j - x_{j-1}}) \tag{4.20}$$

where the index j refers to the mesh point. The central difference formula is

$$(\dot{M}\frac{\mathrm{d}T}{\mathrm{d}x})_j \approx \dot{M}_j(\frac{h_{j-1}}{h_j(h_j + h_{j-1})}T_{j+1} + \frac{h_j - h_{j-1}}{h_j h_{j-1}}T_j - \frac{h_j}{h_{j-1}(h_j + h_{j-1})}T_{j-1}) \tag{4.21}$$

where $h_j = x_{j+1} - x_j$. The windward difference formula introduces artificial diffusion on a coarse mesh; this has the effect of spreading out the solution and making the convergence of Newtons method less sensitive to the starting estimate. However, because the mesh is refined in regions of high gradient, the artificial diffusion becomes relatively unimportant after the solution has progressed to the fine meshes. Nevertheless, for a given mesh, the windward difference approximation is less accurate than the central difference formula. Therefore, the central difference formula may be preferred on finer meshes or in cases where the solution is converging without difficulty.

The first derivative in the summation term in the energy Equation 4.3 is always approximated by a central difference formula,

$$(\frac{\mathrm{d}T}{\mathrm{d}x})_j \approx (\frac{h_{j-1}}{h_j(h_j+h_{j-1})}T_{j+1} + \frac{h_j - h_{j-1}}{h_j h_{j-1}}T_j - \frac{h_j}{h_{j-1}(h_j+h_{j-1})}T_{j-1}) \tag{4.22}$$

and the coefficients in the summation are evaluated at j.

The second derivative term in the energy equation is approximated by the following second order central difference:

$$\frac{\mathrm{d}}{\mathrm{d}x}((\lambda A)\frac{\mathrm{d}T}{\mathrm{d}x})_j \approx (\frac{2}{x_{j+1}-x_{j-1}})[(\lambda A)_{j+\frac{1}{2}}(\frac{T_{j+1}-T_j}{x_{j+1}-x_j}) + (-(\lambda A)_{j+\frac{1}{2}})(\frac{T_j - T_{j-1}}{x_j - x_{j-1}})] \tag{4.23}$$

The coefficients in this formula (at $j \pm 1/2$) are evaluated using the averages of the dependent variables between mesh points.

The diffusive term in the species conservation equation is approximated in a similar way, but it appears to be different because it has been written using diffusion velocities. The ordinary Equation 4.8 and thermal Equation 4.10 diffusion velocities are approximated at the $j \pm 1/2$ positions as illustrated by the following mixture-averaged evaluation:

$$(Y_k v_k)_{j+1/2} \approx -(\frac{W_k D_{km}}{\overline{W}})_{j+1/2}(\frac{X_{k,j+1} - X_{k,j}}{x_{j+1} - x_j}) \tag{4.24}$$

and

$$(Y_k w_k)_{j+1/2} \approx -(\frac{W_k D_{km} \Theta_k}{\overline{W} T})_{j+1/2} (\frac{T_{j+1} - T_j}{x_{j+1} - x_j}) \tag{4.25}$$

Since the mole fraction of a species can be zero, difficulties are avoided by forming $Y_k V_k$, which is the expression needed in Equation 4.15, rather than V_k itself ($Y_k = X_k W_k / \overline{W}$). After the diffusion velocities are computed at all the mesh midpoints, the correction velocity V_c is computed at the midpoints from

$$V_c = \sum_{k=1}^{K} (v_k + w_k) \tag{4.26}$$

Upon forming the full diffusion velocities $V_k = v_k + w_k + V_c$ the diffusion term is evaluated with the following difference approximation.

$$\frac{\mathrm{d}}{\mathrm{d}x}(\rho A Y_k V_k)_j \approx \frac{(\rho A Y_k V_k)_{j+1/2} - (\rho A Y_k V_k)_{j-1/2}}{x_{j+1/2} - x_{j-1/2}} \tag{4.27}$$

All the non-differentiated terms, such as the chemical production rate terms, are evaluated at the mesh points j. Coefficients not appearing within derivatives are also evaluated at the mesh points.

4.2.2 Effects of Nitrogen Dilution

The dilution of the fuel by means of an inert gas, e.g., molecular nitrogen, N_2, has the effect of reducing the explosion likelihood and is a largely employed safety measure when flammable gas is used. This effect results from the drop in laminar burning velocity due to the decreased

thermal diffusivity of the diluted fuel / air mixture (with a corresponding reduced flame temperature).

Syngas is a blend of H_2 and CO and, thus, it exhibits a relatively high burning velocity; this is because of the very high flame speed of hydrogen with respect to hydrocarbons. For instance, reference flame speed values [18] for stoichiometric mixtures at 1 atm and room temperature are S_L=210 cm/s and S_L=40 cm/s for hydrogen and methane, respectively.

Hence, in the simulations of the study, a certain amount of fuel dilution must be included, for the aim of reducing the mixture flame speed; this is a commonly adopted procedure to contain the velocity at which the flammable mixture should be injected, still in the fulfillment of Equation 4.1.

4.2.3 CHEMKIN Laminar Flame Speed Simulations Results

Numerical simulations were carried out with CHEMKIN *Laminar Premixed Flame Calculation* subroutine to evaluate the laminar flame speed of premixed syngas/air flames.

"The Flame-speed Calculator simulates a freely propagating flame, in which the point of reference is a fixed position on the flame. In this coordinate system, the flame speed is defined as the inlet velocity (velocity of unburned gas moving towards the flame) that allows the flame to stay in a fixed location" [19].

A syngas composition of 50%H_2 and 50%CO has been chosen. The fuel is also diluted with nitrogen by 68% of its volume, with the following resulting composition: X_{H2}=0.16, X_{O2}=0.16, and X_{N2}=0.68. The air composition specified in the model will be hereafter the *standard air* one: X_{N2}=0.79 and X_{O2}=0.21.

The following problem input data are also specified: mixture inlet temperature T_{in}=300 K, mixture pressure p_{in}=1 atm.

In figure 1, the laminar flame speed of lean syngas mixture is plotted as a function of the equivalence ratio. The resulting curve shows that, in the lean mixture domain, the laminar flame speed increases almost linearly with equivalence ratio.

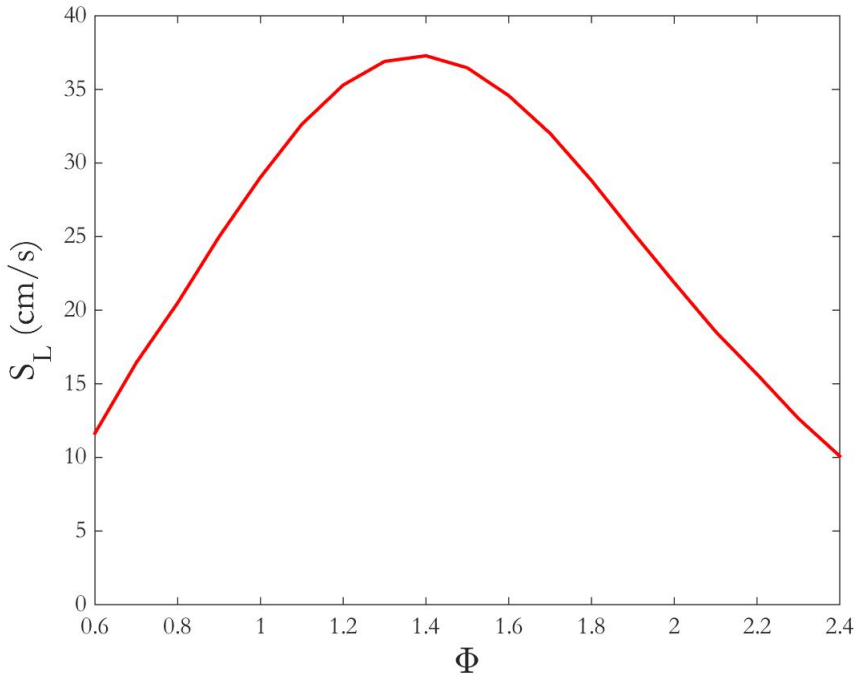

Figure 1: Laminar premixed flame speed of syngas with 68% nitrogen dilution by volume as a function of equivalence ratio.

Precisely, the flame speed reads the following values corresponding to values of equivalence ratio Φ=0.8, Φ=0.7, and Φ=0.6:

at Φ=0.6: S_L = 11.6 cm/s

at Φ=0.7: S_L = 16.4 cm/s

at Φ=0.8: S_L = 20.8 cm/s

These results represent important reference values, for the development of computational studies discussed in the continuation of this work; the axial flow velocity before the flame should never go below the corresponding flame speed value, at a given equivalence ratio.

A validation of the San Diego mechanism with PREMIX code for syngas flames has already been provided in literature [20].

4.3 Counterflow Flames

In the present thesis, premixed syngas/air flames are examined by means of one (CHEMKIN code) and two (UNICORN code) -dimensional computational studies of counterflow configuration.

Counterflow flames have been extensively used for fundamental experimental and numerical investigation of a variety of combustion phenomena, because this configuration reduces the two or three-dimensionality of the fluid flow to a one-dimensional problem; thus, the obtained flame is nearly one-dimensional and the fluid properties are considered to vary only along the axial direction of the flow. Consequently, the flame chemistry, structure, and extinction characteristics can be easily analyzed in the so-produced flat flames.

Another advantage of employing this geometry is the possibility to modify the residence time, which is an important parameter affecting the flame, e.g., its burning velocity, flame stability, diffusion and heat loss phenomena, chemical reactions, and, ultimately, extinction.

Lastly, in stagnation flames, e.g., counterflow flames, the stretch rate (see Section 6.1) and strain rate (see Section 6.2) coincide; since the flame is nearly flat and stationary, flame stretch only accounts for the aerodynamic strain. It has been shown [21] that "the concept of flame stretch is applied to interpret such practical flame phenomena as flame stabilization and flame-front instability, determination of laminar flame speeds and flammability limits, concentration and temperature modifications in flame chemistry". This seems to be an interesting feature in the control of the flame, because the global strain rate can be imposed by changing the inlet conditions of the mixture (as discussed in Section 6.2).

4.3.1 Counterflow Configuration

A counterflow configuration is depicted in figure 2. The axisymmetric geometry is composed of two concentric, circular nozzles located on the same axis and whose gas mixture streams are flowing towards each other; an axisymmetric flow field is thus obtained. The momentum flux balance of the opposed flows provides the existence of a stagnation plane between the two nozzles. This practically constitutes a physical limit for the flow, as if a wall were present.

In the present study, the nozzles are issuing premixed fuel/oxidizer streams. Consequently, two (premixed) *twin flames* are established, one on either side of the stagnation plane. Flame fronts are marked in red.

Here, the inlet flow velocities and the mixture compositions are the same at the nozzles exits; hence, the stagnation plane is expected to be at the axial coordinate midpoint.

It follows the definition of geometry parameters referred to the system under study:

Total length: $L = 1.5$ cm (in the axial direction, x)

Mixture nozzle radius: $r = 1.4$ cm (in the radial direction, y)

Nitrogen nozzle radius: $r_{N2} = 3.0$ cm (in the radial direction, y)

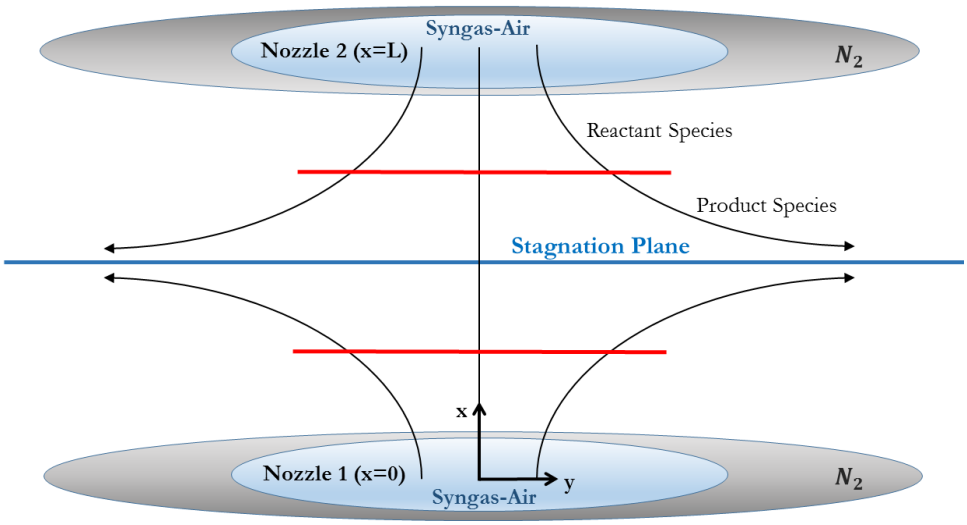

Figure 2: Counterflow configuration schematic for premixed syngas-air twin flames.

4.3.2 CHEMKIN Opposed Flow Flame Calculations

In order to compute a steady-state solution for axisymmetric flames in a counterflow geometry, CHEMKIN OPPDIFF [7] code is employed. The opposed-flow flame configuration, which presents a 2 or 3-D flow model, has a simplification by the hypothesis that fluid properties vary as a function of the axial coordinate only. Therefore, a one-dimensional model is obtained, with obvious analysis advantages.

Neglecting the so-called edge effects, the temperature, velocity, and species profiles of the gas phase in the core flow can be predicted.

4.3.2.1 Opposed Flow Model

The present section is devoted to the description of the conservation equations and assumptions governing counterflow flames. Regardless of the nature of the flame, i.e., diffusion or premixed, the following equations hold for such a geometry.

The above-mentioned equations are obtained by means of a similarity transformation, which renders the two-dimensionality of the flow approximated by a single coordinate, namely, the axial direction. The conservation equations of the system will depend on the latter.

It follows an extraction from CHEMKIN Theory Manual [9].

In the following equations, ξ represents either the radial direction r for the axisymmetric case, or the perpendicular direction y for the planar case. The coordinate parameter n allows to present one set of equations for both cases, with $n = 3$ for the 3-D axisymmetric flow and $n = 2$ for the 2D planar case.

At steady-state, conservation of mass in cylindrical or planar coordinates is

$$\frac{\partial(\rho u)}{\partial x} + \frac{1}{\xi^{n-2}} \frac{\partial(\rho v_\xi \xi^{n-2})}{\partial \xi} = 0 \tag{4.28}$$

where u and v_ξ are the axial and radial (or cross-flow) velocity components, and ρ is the mass density.

Following von Karman, who recognized that v_ξ/ξ and other variables should be functions of x only, the following definitions are given:

$$G(x) = \frac{-(\rho v_\xi)}{\xi} \qquad F(x) = \frac{\rho u}{(n-1)}$$

for which the continuity Equation 4.28 reduces to

$$G(x) = \frac{\mathrm{d}F(x)}{\mathrm{d}x} \tag{4.29}$$

for the axial velocity u. Since F and G are functions of x only, so are ρ, u, T and Y_k.

The perpendicular momentum equation is satisfied by the eigenvalue

$$H = \frac{1}{\xi^{n-2}}\frac{\partial p}{\partial \xi} = 0 \tag{4.30}$$

The perpendicular momentum equation is

$$H - (n-1)\frac{\mathrm{d}}{\mathrm{d}x}(\frac{FG}{\rho}) + \frac{nG^2}{\rho} + \frac{\mathrm{d}}{\mathrm{d}x}[\mu\frac{\mathrm{d}}{\mathrm{d}x}(\frac{G}{\rho})] = 0 \tag{4.31}$$

Energy and species conservation are

$$\rho u\frac{\mathrm{d}T}{\mathrm{d}x} - \frac{1}{c_p}\frac{\mathrm{d}}{\mathrm{d}x}(\lambda\frac{\mathrm{d}T}{\mathrm{d}x}) + \frac{\rho}{c_p}\sum_k c_{pk}Y_kV_k\frac{\mathrm{d}T}{\mathrm{d}x} + \frac{1}{c_p}\sum_k h_k\dot{\omega}_k + \frac{1}{c_p}\dot{Q}_{rad} = 0 \tag{4.32}$$

where $\dot{Q}_{rad}$ is the optically-thin radiation heat loss from the gas and particle.

$$\rho u \frac{\mathrm{d}Y_k}{\mathrm{d}x} + \frac{\mathrm{d}}{\mathrm{d}x}(\rho Y_k V_k) - \dot{\omega}_k W_k = 0 \qquad k = 1, ..., K \tag{4.33}$$

where the diffusion velocities are given by either the multicomponent formulation

$$V_k = \frac{1}{X_k \overline{W}} \sum_{j \neq k}^{K} W_j D_{k,j} \frac{\mathrm{d}X_j}{\mathrm{d}x} - \frac{D_k^T}{\rho Y_k} \frac{1}{T} \frac{\mathrm{d}T}{\mathrm{d}x} \tag{4.34}$$

or the mixture-averaged formulation

$$V_k = -\frac{1}{X_k} D_{km} \frac{\mathrm{d}X_k}{\mathrm{d}x} - \frac{D_k^T}{\rho Y_k} \frac{1}{T} \frac{\mathrm{d}T}{\mathrm{d}x} \qquad where \qquad D_{km} = \frac{1 - Y_k}{\sum_{j \neq k}^{K} \frac{X_j}{D_{jk}}} \tag{4.35}$$

and $D_{k,j}$, D_{km}, $D_j k$ and D_k^T are the multicomponent, mixture-averaged, binary, and thermal diffusion coefficients, respectively.

The boundary conditions for the lower (1) and upper (2) streams at the nozzles are

$$x = 0: \qquad F = \frac{\rho_1 u_1}{(n-1)}; \qquad G = 0; \qquad T = T_1; \qquad \rho u Y_k + \rho Y_k V_k = (\rho u Y_k)_1 \tag{4.36}$$

$$x = L: \qquad F = \frac{\rho_2 u_2}{(n-1)}; \qquad G = 0; \qquad T = T_2; \qquad \rho u Y_k + \rho Y_k V_k = (\rho u Y_k)_2 \tag{4.37}$$

In the present study, the problem is two-dimensional, therefore $n = 2$ in the previous equations.

Again from CHEMKIN Theory Manual [9]:

> The inflow boundary conditions (Equation 4.36 and Equation 4.37) specify the total mass flux, including diffusion and convection, rather than the fixing species mass fraction $Y_k = Y_k, F$. If gradients exist at the boundary, these conditions allow diffusion into the nozzle.
>
> The differential Equation 4.29 through Equation 4.33 and boundary conditions Equation 4.36 and Equation 4.37 form a boundary value problem for the dependent variables (F, G, H, T, Y_k). The GAS-PHASE KINETICS Subroutine Library provides the reaction rates and thermodynamic properties, while the TRANSPORT package evaluates the transport properties for these equations.

4.3.2.2 Finite-Difference Approximations

It follows an extraction from CHEMKIN Theory Manual [9].

> Discretization of the differential equations uses conventional finite differencing techniques for non-uniform mesh spacing. Diffusive terms use central differences, with truncation error that is second-order in the mesh spacing. For better convergence, convective terms use upwind differencing, which uses the sign of the velocity to choose which direction the

spatial difference will go. If $u_j = 0$, for example, then the convective term in the energy equation is differenced as:

$$\rho u \frac{\mathrm{d}T}{\mathrm{d}x} \approx \rho_i u_j (\frac{T_j - T_{j-1}}{x_j - x_{j-1}}) \tag{4.38}$$

The truncation error of this approximation is first-order in the mesh spacing, leading to what is often called "artificial diffusion", but this form avoids unwanted oscillations during the solution on a coarse mesh. Alternatively, the convective terms can be centrally differenced, but the default windward differencing is recommended.

4.3.2.3 Regrid Operation

It follows an extraction from CHEMKIN Theory Manual [9].

A Regrid operation is specified by supplying a new number of grid points during a restart or continuation, which allow a new flame solution to begin from an initial guess based on the solution of a previous flame.

The steady-state solver, TWOPNT, automatically refines the grid by adding points in regions where they are needed to resolve the first and second derivatives of the solution, using criteria controlled by the Gradient and Curvature grid parameters.

The adaptive grid control based on solution *gradient* and *curvature* is set to 0.1 and 0.5, respectively.

Again from CHEMKIN Theory Manual [9]

However, TWOPNT does not move or remove points. If it reaches a maximum number of points (internally defined by the dimensions), a warning message is printed and the adaptation is terminated. In some cases, then, it may be necessary to reduce the number of points when starting a new solution from a previous result. The Regrid operation redefines the solution guess on the user-specified number of mesh points.

The Regrid operation is different from the grid-point insertion operation performed by TWOPNT. Both operations attempt to resolve the gradient and curvature in the solution, except that TWOPNT considers all solution components, whereas Regrid only considers the temperature profile. TWOPNT only adds points, leaving the old points as they were, but Regrid alters the location and solution of all the points interior to the boundaries. Regrid computes new locations for exactly the given number of points, and then interpolates the solution from the previous grid to obtain a new approximation of the solution. Regrid does not conserve any properties of the solution; in fact, it tends to smooth the solution by the error inherent in the interpolation.

Regrid redistributes a weighting function of the first and second derivatives of the temperature. The profiles of the other dependent variables are ignored on the assumption that the temperature profile defines the flame location well enough for the purposes of realigning the mesh for an initial condition. The redistribution uses a transformation from the physical coordinate x to a new coordinate η

$$\frac{\mathrm{d}x}{\mathrm{d}\eta} W(x,T) = C \tag{4.39}$$

with the weighing function,

$$W(x,T) = 1 + b_1\left|\frac{\mathrm{d}T}{\mathrm{d}x}\right| + b_2\left|\frac{\mathrm{d}^2T}{\mathrm{d}x^2}\right| \tag{4.40}$$

Integration over the entire domain defines the constant

$$C = \frac{1}{N-1}\int_0^L W(x,T)\mathrm{d}x \tag{4.41}$$

Integrating over a portion of the domain gives an expression for the point locations in η-space

$$\eta = 1 + \frac{1}{C}\int_0^x W(x,T)\mathrm{d}x \tag{4.42}$$

The new grid locations x come by interpolation between the computed values of η defined using the old mesh, onto a uniform mesh in η-space. Since $d\eta$ is constant on this uniform mesh, the solution to Equation 4.39 states that is $W(x,T)dx$ constant, so the new values of will be concentrated where the weighting function is large.

A set of parameters for the Regrid operation, which is performed at each restart or continuation, is presented in Table V.

Thereby, a new solution guess on 20 points will be created, devoting 60 percent of the points to resolving gradients, with equal weighting of gradient and curvature in the temperature profile.

TABLE V: PARAMETERS FOR REGRID OPERATION.

Parameter	Value
Number of Grid Points for Regrid	20
Percent of Grids for Regrid	60%
Ratio of Gradient to Curvature Adaptation	1.0

4.3.3 CHEMKIN Opposed Flow Flame Simulations Results

Simulations results obtained with CHEMKIN are presented in this section.

The distance between the two nozzles is L=1.5 cm and the global strain rate (defined in Section 6.2) is k= 175 s^{-1}, with the corresponding inlet velocity of v_{in}=65.6 cm/s at the two nozzles exits.

The thermodynamic conditions at the inlet are: T_{in}=300 K, p_{in}=1 atm.

The simulations entail a parametric study with three fuel-lean mixture cases with Φ=0.8, Φ=0.7, and Φ=0.6. However, for the sake of brevity, only the results with Φ=0.8 are reported here. Those for Φ=0.7 and Φ=0.6 can be found in Appendix (see Section A.1).

In figure 3, the temperature and axial velocity profiles along the flow axis, x, are depicted. Axial velocity is zero at the stagnation plane, i.e., exactly at the midpoint of the geometry (x=0.75 cm). Moving from one side of the stagnation plane to the other, axial velocity switches sign, but its magnitude is the same.

Moreover, it can be observed that the flow is decelerating down from its inlet velocity value, because of the presence of the stagnation plane. The rapid increase in axial velocity indicates the location of the flame. This behavior can be explained by recalling the conservation of mass:

$$\rho_u A S_u = \rho_b A S_b \tag{4.43}$$

Here subscripts u and b indicate the *unburned* and *burned* states of the mixture. Since the cross sectional flow area is conserved, and the burned gas has a lower density than the unburned gas ($\rho_b < \rho_u$), it follows that: $S_b > S_u$.

The temperature profile in figure 3 exhibits a steep increase occurring in correspondence of the two flames. The maximum temperature is then achieved in the central region of the domain.

The chemical species profiles are plotted as a function of the axial coordinate in figure 4. The blue, orange, and yellow curves are those of the reactants, and indicate the H_2, CO, and O_2 molar concentrations, respectively. Since a lean mixture is considered, the fuel species are completely consumed, while O_2 is partially consumed. It is interesting to note that H_2 (blue) starts getting consumed earlier compared to CO (orange), since it is a more reactive species. The initial decrease of H_2, before its reaction with O2, is due to its high diffusivity.

The purple and green curves are those of the products species, i.e., H_2O and CO_2, respectively. Here again, it is worth pointing out that H_2O starts forming slightly before CO_2 does.

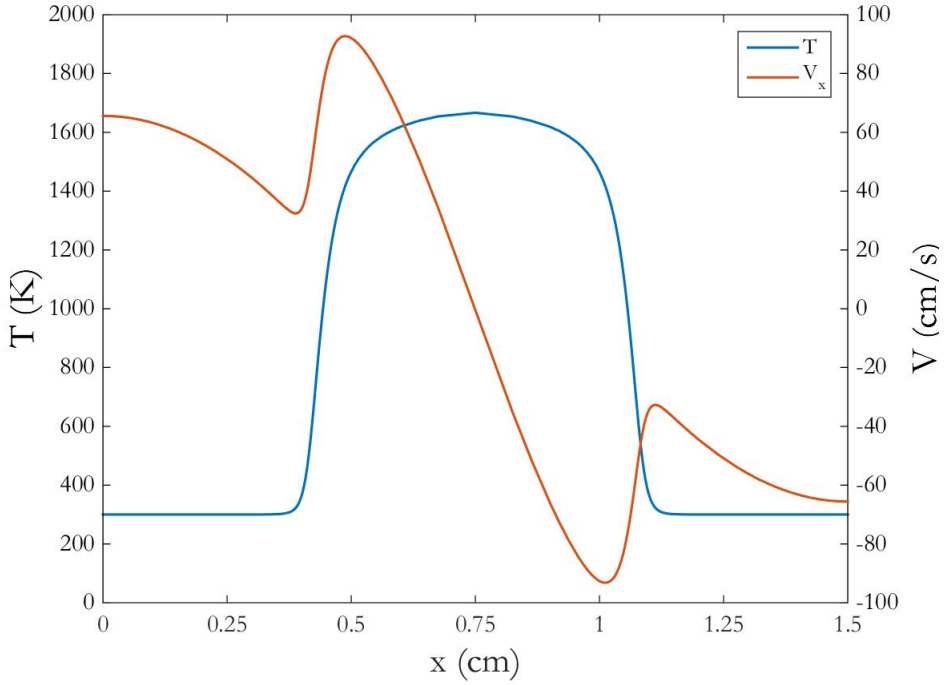

Figure 3: Temperature and axial velocity profiles for syngas (50% H_2 and 50% CO) flame with Φ=0.8 and 68% N_2 dilution, obtained with CHEMKIN

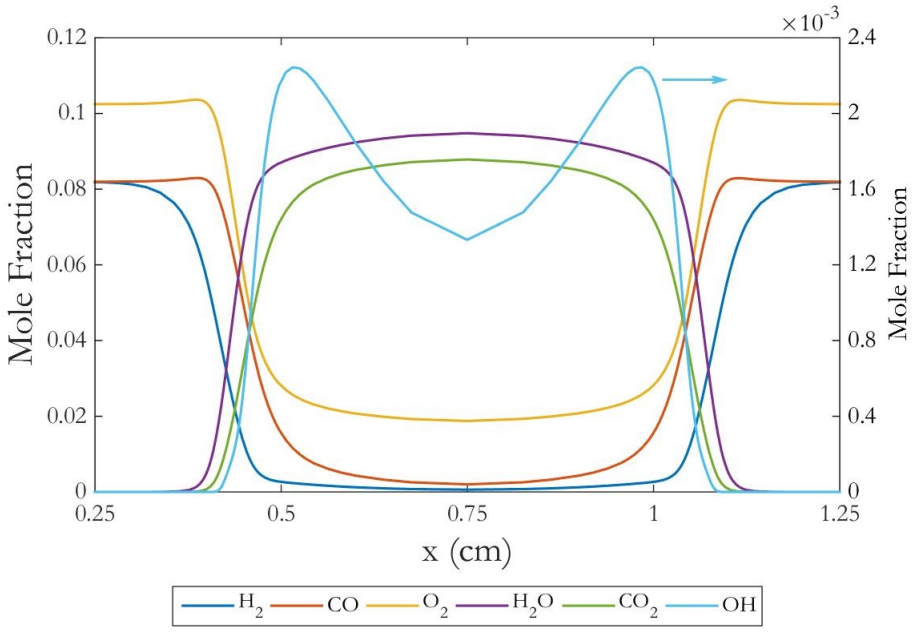

30

Figure 4: Species mole fraction profiles for syngas (50% H_2 and 50% CO) flame with Φ=0.8 and 68% N_2 dilution.

The light blue curve refers to OH mole fraction and is plotted on the secondary axis; it is an intermediate product of combustion and its concentration is lower than those of reactants and final products by approximately two orders of magnitude. Its production occurs in the flame zone and its final burnout is not completed, since, in the central region, OH concentration decreases but does not reach zero.

4.3.4 UNICORN Counterflow Flame Calculations - Computational Domain

The same problem of the previous section is solved numerically by employing the UNICORN code.

In this section, the computational domain for 2D UNICORN simulations is defined so as to reproduce the physical counterflow configuration.

Firstly, it must be noted that the configuration is axisymmetric; therefore, half of the domain is sufficient to consistently describe the phenomenon. The axial distance between nozzles is then set to L=1.5 cm, while their radii are the same and equal to 1.4 cm. The syngas mixture streams are enclosed by simultaneous nitrogen streams on both sides, extending from 1.4 to 3 cm radial distance from the flow axis.

The computational grid is composed of 301 uniformly placed nodes along the axial direction and 31 nodes along radial direction that thicken in the fuel flow zone (at small distance from the domain centerline).

There are six boundary conditions referring to the geometry: one lateral side of the domain (for instance, the left hand-side) is characterized by a symmetry condition; the other lateral side (the right hand-side) has a free surface boundary condition; the top and bottom represent

the two inflow boundaries, one for the fuel mixture and the other for the nitrogen jet. The inflow boundary conditions require the specification of the velocity, temperature, and fluid composition (expressed in species mass fractions) at each boundary.

4.3.5 UNICORN Counterflow Flame Simulations Results

The same simulations of Section 4.3.3 are run with the UNICORN piece of software. Results are presented in figure 5 and figure 6.

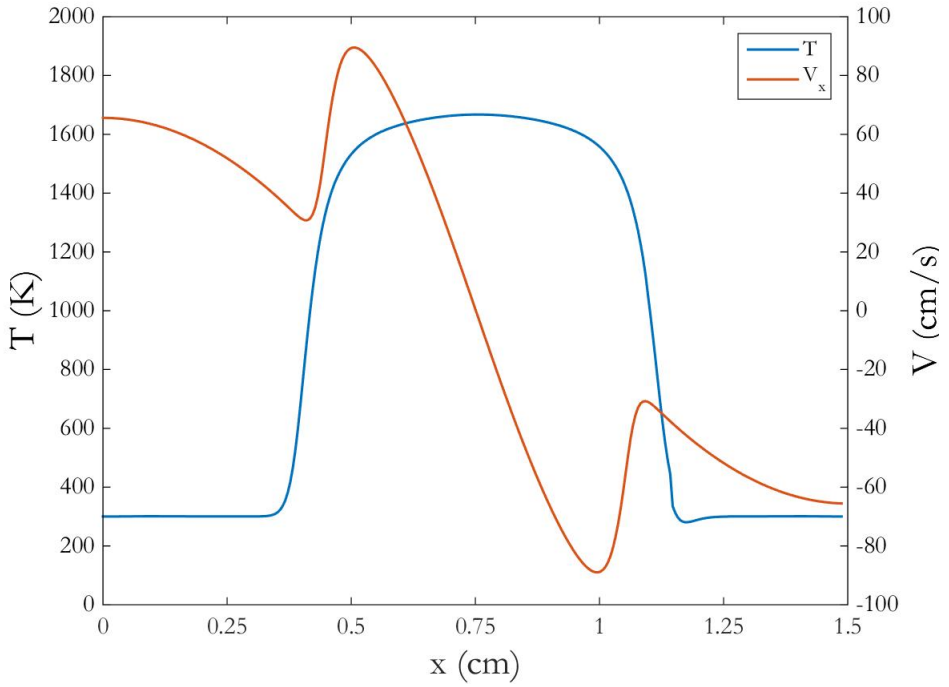

Figure 5: Temperature and axial velocity profiles for syngas (50% H_2 and 50% CO) flame with Φ=0.8 and 68% N_2 dilution, obtained with UNICORN.

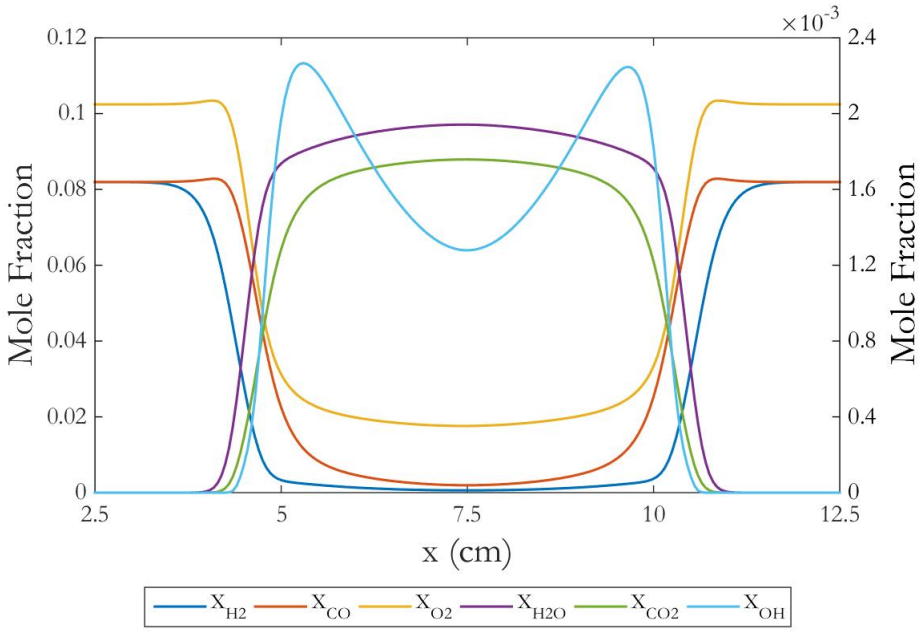

Figure 6: Species concentration profile as a function of axial coordinate (50% H_2 and 50% CO syngas, 68% N_2 dilution, Φ=0.8), obtained with UNICORN.

Analogous considerations as those in Section 4.3.3 can be drawn.

The charts for the cases Φ=0.7 and Φ=0.6 can be found in Appendix (see Section A.2).

By post-processing the solution of UNICORN two-dimensional code and plotting it with Tecplot, the iso-contours of OH mole fraction and temperature are obtained and shown in figure 15.

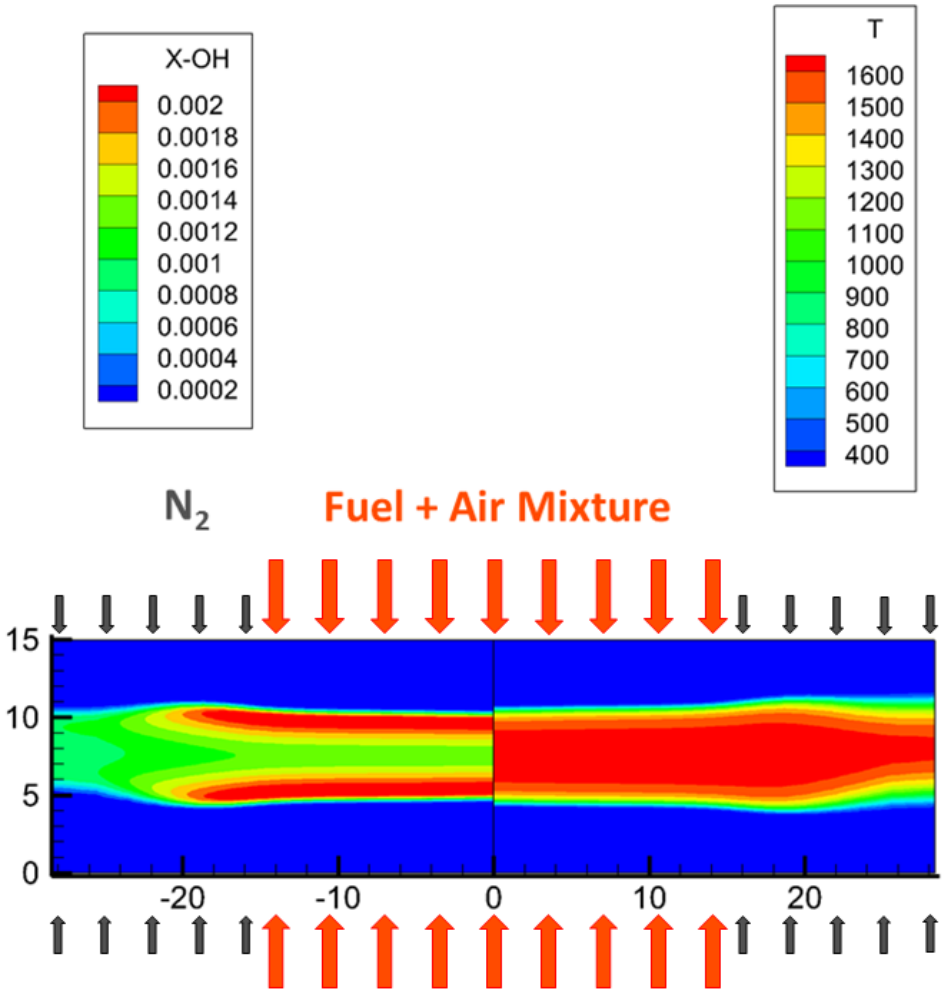

Figure 7: OH mole fraction and temperature iso-contours in two-dimensional coordinates (in mm) (50% H_2 and 50% CO syngas, 68% N_2 dilution, Φ=0.8) obtained with UNICORN.

The OH mole fraction contours are particularly useful to identify the location where flames establish. The temperature iso-contours plot depicts how the peak temperature is reached in the region between the flames.

4.3.6 Counterflow Flame Results Validation - Comparison CHEMKIN-UNICORN

A validation of the results can be achieved by comparing the outputs of CHEMKIN and UNICORN codes. The profiles of temperature, axial velocity, and species molar concentration are plotted, in figure 8, figure 9, and figure 10. The same charts for Φ=0.7 and Φ=0.6 are reported in Appendix (see Section A.3).

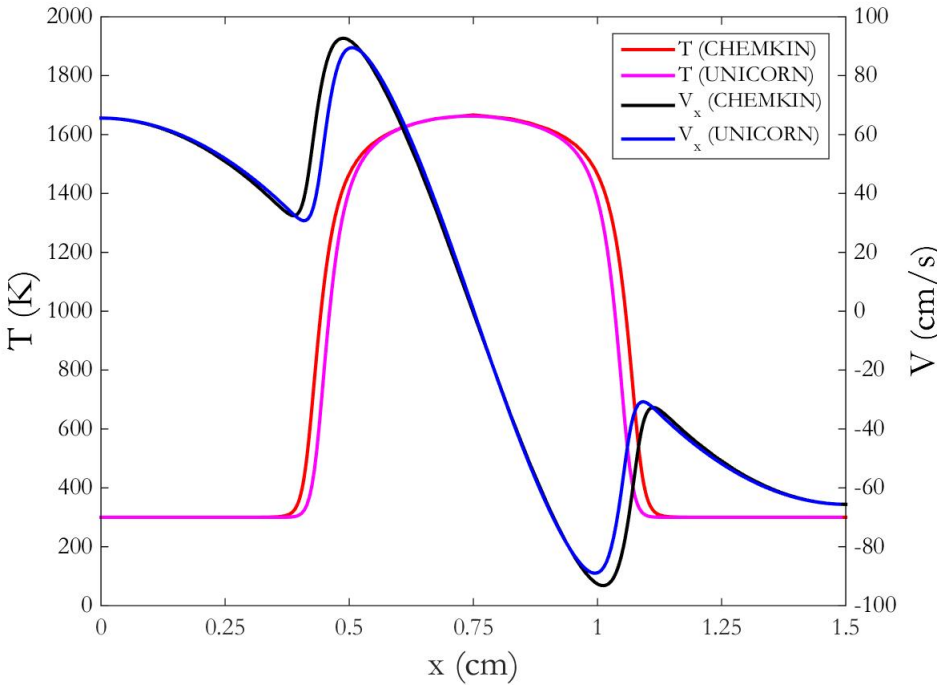

Figure 8: Temperature and axial velocity profiles as functions of axial coordinate (50% H_2 and 50% CO syngas, 68% N_2 dilution, Φ=0.8). CHEMKIN vs UNICORN comparison.

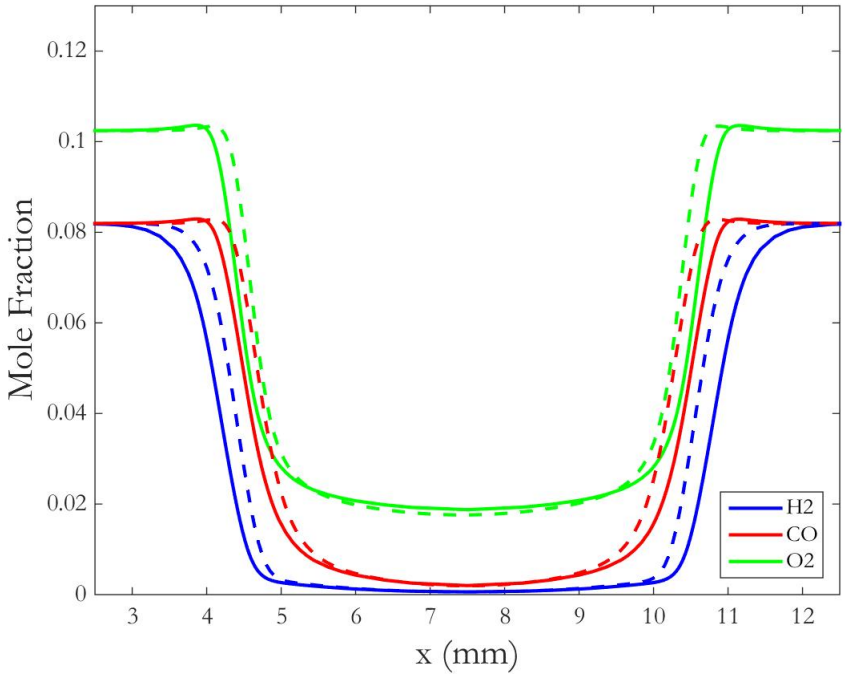

Figure 9: Reactant species concentration profile as a function of axial coordinate (50% H_2 and 50% CO syngas, 68% N_2 dilution, Φ=0.8). CHEMKIN (solid line) vs UNICORN (dashed line) comparison.

Looking at the charts, it is worth noticing that both the temperature and species concentration profiles match very well for CHEMKIN and UNICORN simulations.

However, a small difference exists: CHEMKIN predicts combustion to occur slightly earlier than UNICORN. This is probably due to the fact that the latter includes a radiative heat loss model, while the former does not.

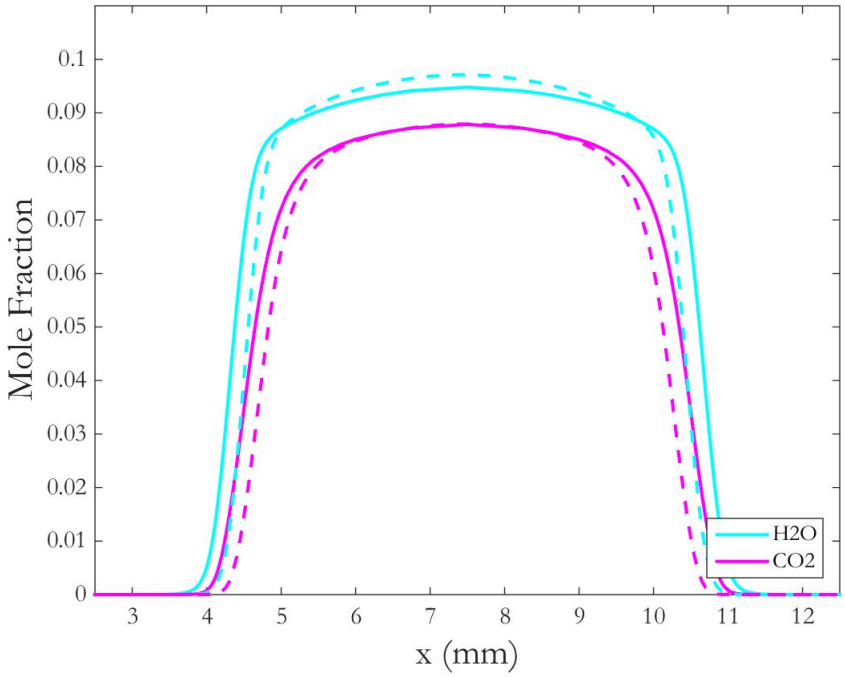

Figure 10: Product species concentration profile as a function of axial coordinate (50% H_2 and 50% CO syngas, 68% N_2 dilution, Φ=0.8). CHEMKIN (solid line) vs UNICORN (dashed line) comparison.

4.3.7 Effects of Equivalence Ratio

The effects of equivalence ratio on the flame parameters are here examined. Three equivalence ratio values are employed for the parameter study: Φ=0.6, Φ=0.7, and Φ=0.8.

A comparison of the temperature and axial velocity profiles for different equivalence ratios of a lean mixture of syngas and air is shown in figure 11, displaying the results obtained with CHEMKIN and UNICORN.

As it is possible to observe, the highest temperature and axial velocity peaks are achieved for burning the Φ=0.8 mixture; conversely, the lowest temperature and axial velocity (in absolute value) peaks are for Φ=0.6. Furthermore, the curves get broader for values of Φ closer to stoichiometry; this means that combustion occurs earlier for more stoichiometric mixtures.

An analogous observation derives from the analysis of figure 12, figure 13, and figure 14, showing the species molar concentration profiles for varying equivalence ratio.

In figure 12 the reactant species profiles are presented, namely, H_2 and O_2, while figure 13 and figure 14 present the product species profiles, namely, CO_2 and OH (intermediate product), respectively. With leaner mixtures, the amount of molecular oxygen not consumed at the end of the reaction is increasing as equivalence ratio decreases.

The iso-contours of OH mole fraction and temperature for the three different values of equivalence ratio are shown in figure 15.

The OH mole fraction contours show that flames establish closer to the stagnation plane for leaner mixtures, and they present a thinner reaction zone. This is reflected by the flame temperature contours, showing that less stoichiometric mixtures have lower flame temperatures. For both contours, the higher burning rate of richer mixtures is evidenced by the intensity of the colors of the shade of red.

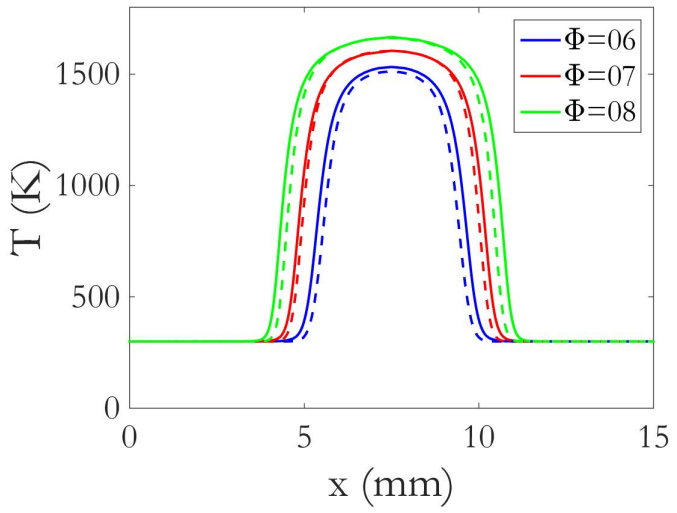

(a)

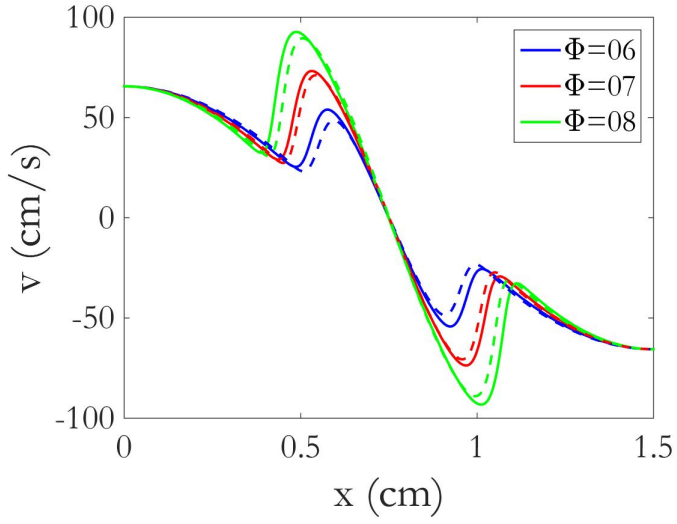

(b)

Figure 11: Temperature (a) and axial velocity (b) profiles for different Φ values (50% H_2 and 50% CO syngas, 68% N_2 dilution), obtained with CHEMKIN (solid lines) and UNICORN (dashed lines).

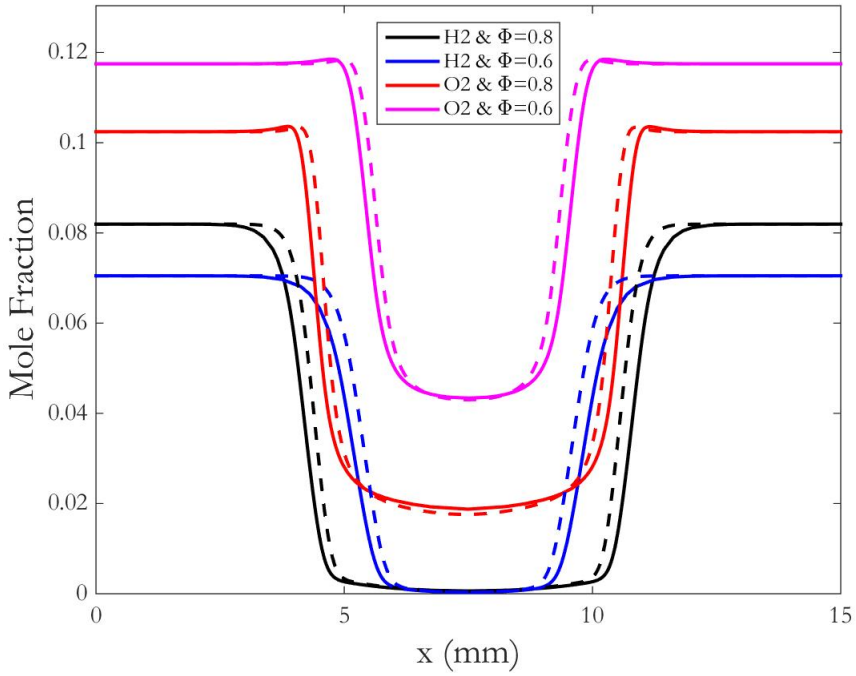

Figure 12: H_2 and O_2 mole fraction profiles along the axial coordinate (50% H_2 and 50% CO syngas, 68% N_2 dilution) for different Φ values, obtained with CHEMKIN (solid line) and UNICORN (dashed line).

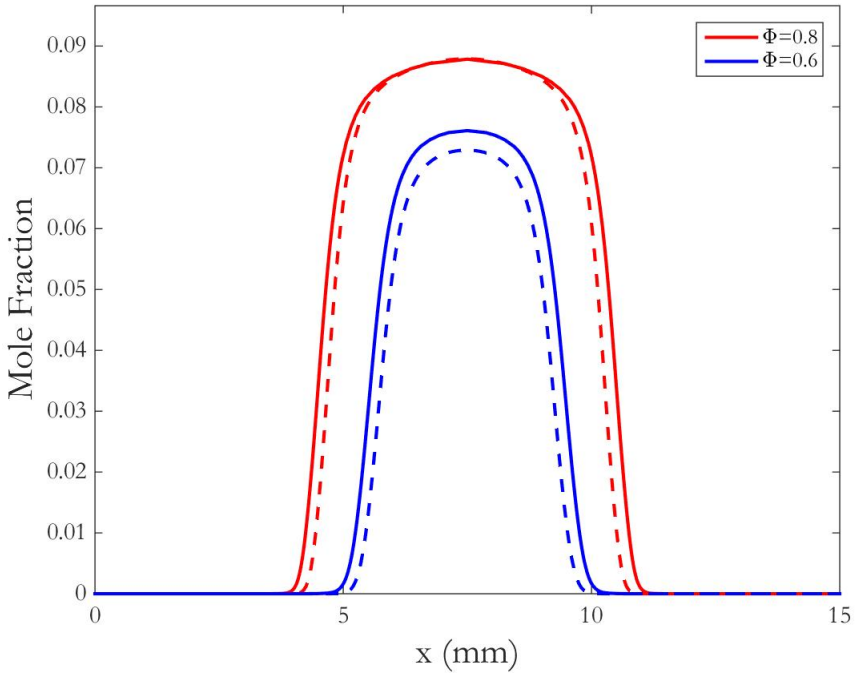

Figure 13: CO_2 mole fraction profiles along the axial coordinate (50% H_2 and 50% CO syngas, 68% N_2 dilution) for different Φ values, obtained with CHEMKIN (solid line) and UNICORN (dashed line).

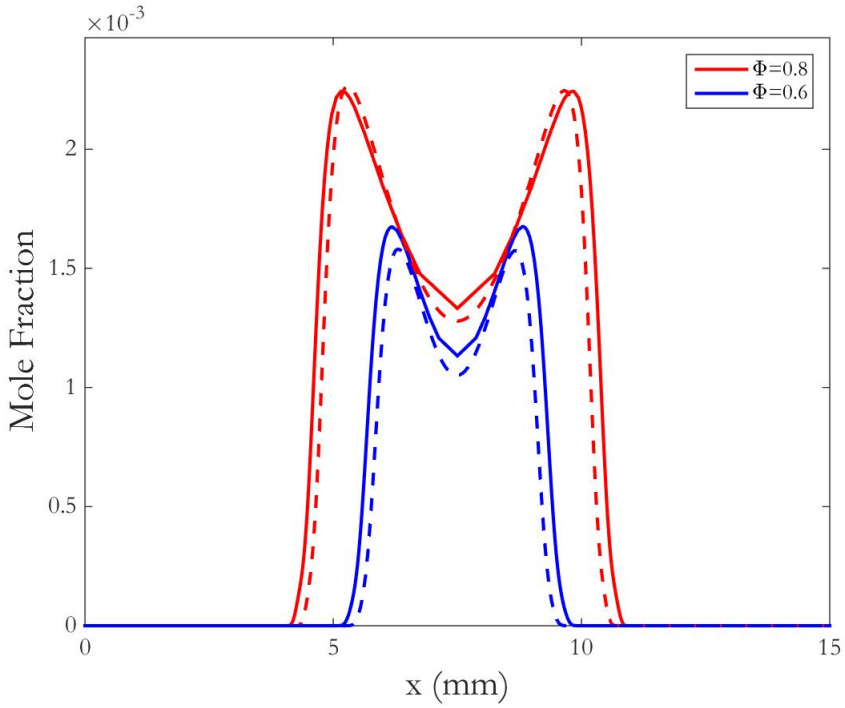

Figure 14: OH mole fraction profiles along the axial coordinate (50% H_2 and 50% CO syngas, 68% N_2 dilution) for different Φ values, obtained with CHEMKIN (solid line) and UNICORN (dashed line).

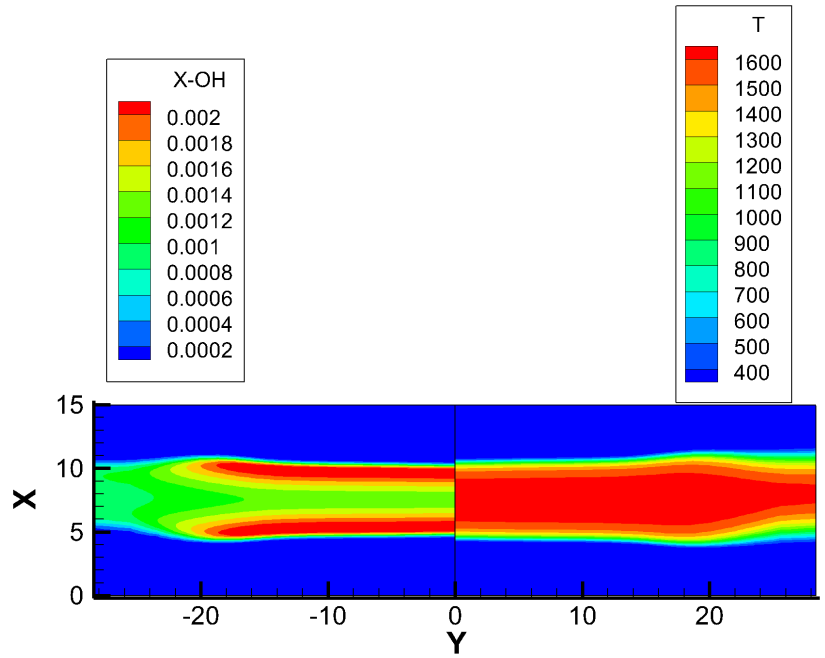

(a) Φ=0.8

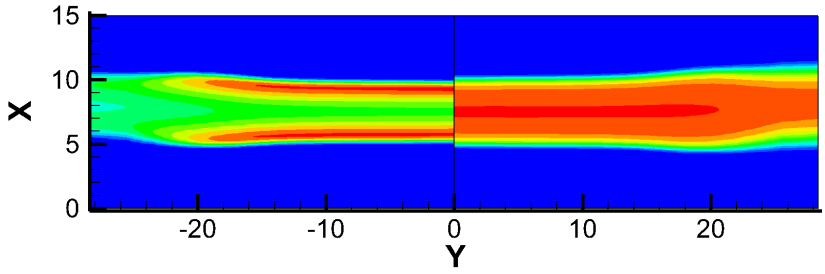

(b) Φ=0.7

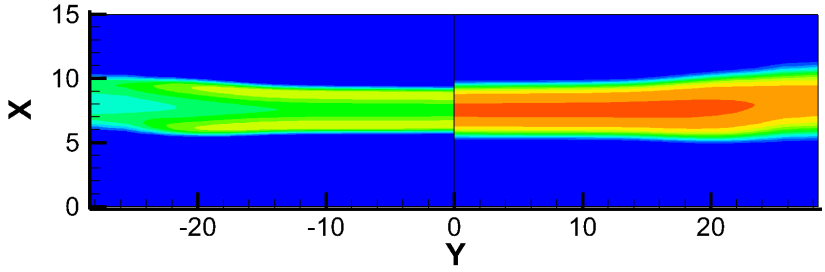

(c) Φ=0.6

Figure 15: *OH* mole fraction and temperature iso-contours in two-dimensional coordinates (in *mm*) (50% H_2 and 50% *CO* syngas, 68% N_2 dilution) for (*a*) Φ=0.8, (*b*) Φ=0.7, and (*c*) Φ=0.6, obtained with UNICORN.

CHAPTER 5

EFFECTS OF MIXTURE LEWIS NUMBER

A description of the flame energy is provided by preferential diffusion. A source of heat loss from the flame is represented by thermal diffusion; on the other hand, chemical energy of controlling species is provided to the flame by mass diffusion. *Lewis number* is a measure of the balance of these two diffusive phenomena, whose assessment leads to the identification of the prevailing one.

In simple combustion problems, the assumption that Lewis number is unity is frequently made, in order to simplify the energy conservation equation; this is a key assumption for the formulation of the so-called *Shvab-Zeldovich energy equation*. However, in the present thesis, it is of interest to study more realistic cases, for which Lewis number differs from one, and to evaluate how this physical quantity affects the flame parameters.

Specifically, a predictive evaluation of the stretch effect on flames (see chapter 6) starts from the analysis of preferential diffusion, i.e., the mixture Lewis number.

5.1 Definition of Lewis Number

Lewis number is defined as the ratio between thermal diffusivity and mass diffusivity and is useful to determine the energy balance/unbalance of the flame. If one of the two phenomena is dominant with respect to the other, flame temperature differs from the adiabatic one, T_{ad}, thus effecting the flame behavior.

The definition of Lewis number for a single fuel mixture is straightforward:

$$Le_i = \frac{\alpha}{D_i} \tag{5.1}$$

where α is the mixture thermal diffusivity and D_i is the mass diffusivity of the deficient reactant, i.e., fuel for lean and oxidizer for rich mixtures.

Nevertheless, being syngas composed of two different fuels, namely, H_2 and CO, its Lewis number estimation is not trivial. For a mixture with two fuel components, literature offers several *effective* Lewis number formulations. There are basically three different formulations:

Heat release - based (H):

$$Le_H = 1 + \frac{Q_1(Le_1 - 1) + Q_2(Le_2 - 1)}{Q_1 + Q_2} \tag{5.2}$$

Volume - based (V):

$$Le_V = X_1 Le_1 + X_2 Le_2 \tag{5.3}$$

Diffusion - based (D):

$$Le_D = \frac{\alpha}{X_1 D_{1/N2} + X_2 D_{2/N2}} \tag{5.4}$$

where subscripts 1 and 2 indicate the first or second component of the fuel, Q is the amount of released heat, X is the molar fraction, and $D_{i/N2}$ is the mass (or molecular) diffusivity with respect to nitrogen.

Bouvet et al. [22] showed that the volumetric weighted approach is the most consistent for some of the most important alkanes, e.g., methane, propane, and octane; on the other hand, for syngas mixtures (especially for lean mixtures), the most suitable approach has been found to be the diffusion-based one, since H_2 has an overwhelming effect on CO regarding the stability of the flame. Therefore, Equation 5.4 is used for the calculation of syngas Lewis number. The obtained results will be compared to those obtained by employing the volume-based formulation.

5.2 Calculation of the Lewis Number

This section is devoted to the evaluation of the mixture Lewis number through a series of sequential steps, elucidated in the following subsections.

5.2.1 Thermal Diffusivity Calculation

The mixture *thermal diffusivity*, α, is expressed as:

$$\alpha = \frac{\lambda}{\rho_u c_p} \tag{5.5}$$

The thermodynamic properties in Equation 5.5 must be evaluated for a mixture of syngas (composed of 16% CO, 16% H2, and 68% N2, in moles) and standard air.

Thermal conductivity, λ_{mix}, for gas mixtures is obtained by:

$$\lambda_{mix} = \frac{1}{2}\left(\sum_{k=1}^{N} X_k \lambda_k + \frac{1}{\sum_{k=1}^{N} \frac{X_k}{\lambda_k}}\right) \tag{5.6}$$

Where X_k are the mole fractions, λ_k are the thermal conductivities (at T=300K, p=1atm), and N is the total number of species in the mixture.

The *unburned mixture density*, ρ_u, is the density value at axial distance x=0 cm, i.e., at the inlet, of 1D CHEMKIN opposed flow simulations.

The mixture *heat capacity*, $c_{p,mix}$, is computed by employing an average heat capacity of the mixture by weighing the mass fractions of the components with their heat capacity:

$$c_{p,mix} = \sum_{k=1}^{N} Y_k c_{p,k} \tag{5.7}$$

5.2.2 Mass Diffusivity Calculation

The empirical formula for *mass diffusivity* is:

$$D_{AB} = 0.0018583\sqrt{T^3(\frac{1}{M_A} + \frac{1}{M_B})}\frac{1}{p\sigma_{AB}^2\Omega_{D,AB}} \tag{5.8}$$

where T is the temperature (K), M is the molecular weight of the component, p is the pressure (atm), σ_{AB} is the characteristic diameter of the molecules called the *collision diameter* (Angstrom), and $\Omega_{D,AB}$ is a dimensionless quantity called the *collision integral* and is a function of dimensionless temperature. Species B is $N2$.

The collision diameter, σ_{AB}, of Equation 5.8 is calculated as:

$$\sigma_{AB} = \frac{1}{2}(\sigma_A + \sigma_B) \tag{5.9}$$

where σ_A and σ_B are the Lennard-Jones parameters, whose values are given in literature [23].

The collision integral, $\Omega_{D,H2-CO}$, is evaluated starting from the dimensionless temperature (function of Lennard-Jones parameters given in literature) $\frac{kT}{\varepsilon_{AB}}$:

$$\frac{\varepsilon_{AB}}{k} = \sqrt{\frac{\varepsilon_A}{k}\frac{\varepsilon_B}{k}} \tag{5.10}$$

A different value of the Lennard-Jones collision integral, $\Omega_{D,AB}$, corresponds to a specified dimensionless temperature. A linear interpolation of the data given in [23] may be necessary.

5.2.3 Lewis Number Calculation

Employing the values of thermal and mass diffusivities previously calculated, the Lewis number is found as follows.

- *For lean mixtures*, *fuel Lewis number* must be evaluated. Its expression is the following:

$$Le = \frac{\alpha}{X_{H2}D_{H2/N2} + X_{CO}D_{CO/N2}} \tag{5.11}$$

  It is important to point out that the thermal diffusivity, α, is an overall property referring to the final air/fuel mixture; on the contrary, the molar fractions X_{H2} and X_{CO} refer to the fuel composition only (for instance, for syngas composed of 50% H_2 and 50% CO, it follows: $X_{H2} = X_{CO} = 0.5$).

- *For rich mixtures*, *oxidizer Lewis number* must be evaluated. Its expression is the following:

$$Le = \frac{\alpha}{D_{O2/N2}} \tag{5.12}$$

5.3 Collection of Results

The present section collects the initial thermodynamic data and summarizes the numerical results for each parameter involved in the Lewis number calculation, in the case considered above, i.e., 50% H_2 - 50% CO syngas with 68% N_2 dilution.

TABLE VI: THERMAL CONDUCTIVITY, SPECIFIC HEAT, AND MASS DIFFUSION OF THE SPECIES AT 1 ATM AND 300 K.

Species	λ (W/mK)	c_p (J/kgK)	$D_{x/N2}$ (m^2/s)
H_2	0.1869	14307	7.67E-05
CO	0.0250	1040	2.04E-05
N_2	0.0260	1039	2.02E-05
O_2	0.0263	918	2.05E-05

TABLE VII: MOLE FRACTION AND MASS DENSITY OF THE SPECIES AT 1 ATM AND 300 K AT DIFFERENT Φ.

Φ	X_{N2}	X_{CO}	X_{H2}	X_{O2}	$\rho(kg/m^3)$
0.6	0.74154	0.07049	0.07049	0.11748	1.08253
0.8	0.73366	0.08195	0.08195	0.10244	1.06799
1.0	0.72757	0.09081	0.09081	0.09081	1.05675
1.3	0.72065	0.10088	0.10088	0.07760	1.04397
1.6	0.71548	0.10839	0.10839	0.06774	1.03445

TABLE VIII: MASS FRACTION OF THE SPECIES AT 1 ATM AND 300 K AT DIFFERENT Φ.

Φ	Y_{N2}	Y_{CO}	Y_{H2}	Y_{O2}
0.6	0.77951	0.07091	0.00533	0.14107
0.8	0.78173	0.08731	0.00628	0.12468
1.0	0.78348	0.09778	0.00704	0.11170
1.3	0.78552	0.10995	0.00791	0.09662
1.6	0.78707	0.11922	0.00858	0.08512

TABLE IX: TOTAL THERMAL CONDUCTIVITY, TOTAL SPECIFIC HEAT, AND TOTAL THERMAL DIFFUSIVITY OF THE SPECIES AT 1 ATM AND 300 K AT DIFFERENT Φ.

Φ	λ_{mix} (W/mK)	$c_{p,mix}$ (J/kgK)	α (m^2/s)
0.6	0.0325	1089.45	2.75E-05
0.8	0.0335	1107.38	2.83E-05
1.0	0.0343	1118.95	2.9E-05
1.3	0.0353	1132.41	2.98E-05
1.6	0.0360	1142.67	3.04E-05

TABLE X: LEWIS NUMBER OF 50% H_2 - 50% CO SYNGAS (WITH 68% N_2 DILUTION) AT DIFFERENT Φ, OBTAINED WITH THE DIFFUSION- AND THE VOLUME-BASED APPROACHES.

Φ	Le_D	Le_V
0.6	0.57	0.75
0.8	0.58	0.76
1.0	1.41	1.42
1.3	1.45	1.47
1.6	1.48	1.49

As indicated in Table X, if the volume-based approach of Equation 5.3 is employed, the obtained Le values of lean mixtures are very different from those obtained by the diffusion-based approach of Equation 5.4. As mentioned, when syngas mixtures are considered, the former method yields less accurate results than the latter one, especially for lean mixtures, which appear to be overestimated by the diffusion-based formula.

An analogous procedure has been adopted to estimate the Lewis number of various fuel compositions. In the following, the obtained values of Lewis number for:

- 100% H_2 fuel
- 80% H_2 20% CO syngas
- 50% H_2 50% CO syngas
- 20% H_2 80% CO syngas
- 100% CO fuel

are listed, in both no-dilution (Table XI) and 68% N_2 dilution (Table XII) cases.

TABLE XI: LEWIS NUMBER OF DIFFERENT SYNGAS COMPOSITIONS (WITHOUT DILUTION) AT DIFFERENT Φ. THE REMAINING PART OF FUEL VOLUME FRACTION IS OCCUPIED BY CO.

Φ	$100\%H_2$	$80\%H_2$	$50\%H_2$	$20\%H_2$	$0\%H_2$
0.6	0.50	0.53	0.61	0.79	1.07
0.8	0.57	0.58	0.65	0.81	1.07
1.0	2.39	1.99	1.63	1.29	1.06
1.3	2.70	2.33	1.75	1.33	1.06
1.6	2.90	2.34	1.93	1.36	1.05

Table XI shows the Lewis number variation with fuel composition and equivalence ratio. As noted, in lean mixtures, $Le < 1$, except for pure CO. This implies that mass diffusion dominates

TABLE XII: LEWIS NUMBER OF DIFFERENT SYNGAS COMPOSITIONS (WITH 68% N_2 DILUTION) AT DIFFERENT Φ. THE REMAINING PART OF FUEL VOLUME FRACTION IS OCCUPIED BY CO.

Φ	$100\%H_2$	$80\%H_2$	$50\%H_2$	$20\%H_2$	$0\%H_2$
0.6	0.43	0.47	0.57	0.76	1.07
0.8	0.46	0.49	0.58	0.77	1.07
1.0	1.78	1.63	1.41	1.20	1.06
1.3	1.86	1.69	1.45	1.22	1.06
1.6	1.92	1.74	1.48	1.23	1.06

thermal diffusion even when H_2 is present in relatively small amounts (20% by volume). Further, as the amount of hydrogen in the fuel is increased, the mixture Lewis number decreases, because of the very high mass diffusivity of hydrogen.

Conversely, in rich mixtures, $Le > 1$, i.e., heat loss exceeds mass gain. Therefore, the flame temperature T_b is lower than the adiabatic flame temperature T_{ad}. Moreover, increased H_2 content in the fuel leads to higher values of the Le; this is due to the higher overall thermal diffusivity due to the increased H_2 mole fraction in the fuel.

For CO-air mixtures, $Le \approx 1$, as indicated in the table.

Table XII lists the values of Lewis number for syngas mixtures with 68% N_2 dilution by volume. The amount of H_2 in the fuel is reduced as a consequence of dilution, and the Lewis number is reduced, as observed by comparing the two tables.

For pure CO fuel, dilution does not yield substantial changes in the mixture Lewis number.

The data of Table XI and Table XII are plotted in figure 16 and figure 17, respectively.

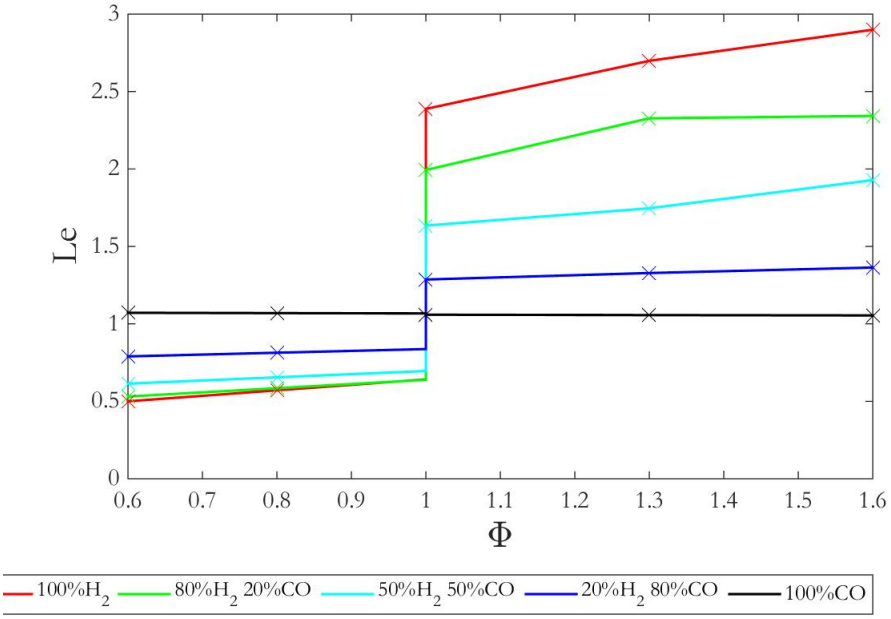

Figure 16: Lewis number as a function of equivalence ratio for H_2, CO, and different syngas compositions (without dilution).

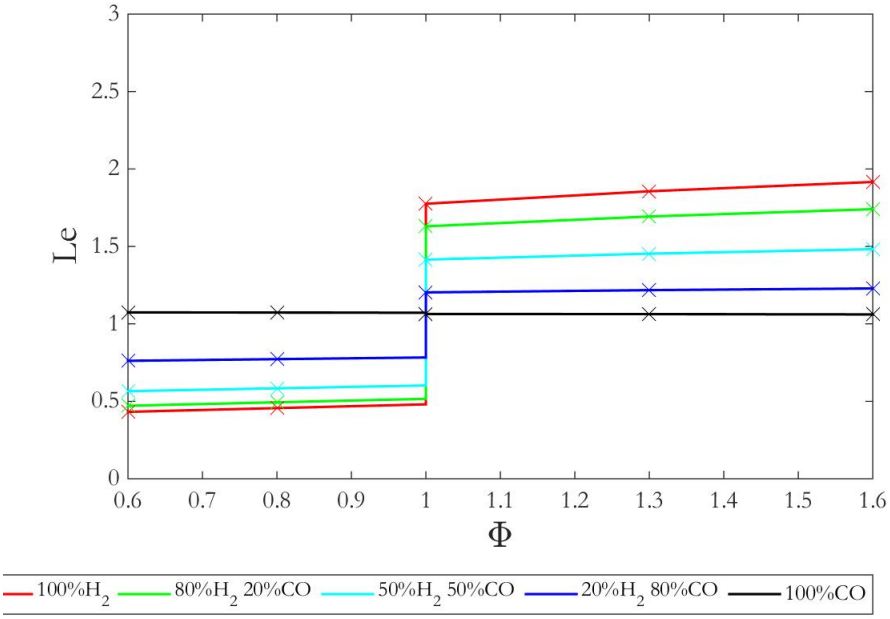

Figure 17: Lewis number as a function of equivalence ratio for H_2, CO, and different syngas compositions (diluted with N_2 by 68% in volume).

5.4 Concluding Remarks

Syngas flame behavior is essentially similar to that of hydrogen flames, since for both fuels $Le < 1$ and $Le > 1$ for lean and rich mixtures, respectively. Therefore, syngas premixed flame behavior is predominantly determined by hydrogen transport properties.

In order to validate the results, the Lewis number of individual chemical species, e.g., H_2, CH_4, N_2 and O_2, are calculated for the same mixture as that analyzed by Hawkes et al. [24] (who determined Le from "a best fit to the mixture-averaged transport coefficients of the GRI3.0 mechanism in the laminar flame"): methane/air mixture enriched with 29% H_2 by volume and with Φ=0.52 (at 300 K and 1 atm). Results are compared in Table XIII, which includes the Le values obtained by both the volume- and the diffusion-based approaches.

TABLE XIII: LEWIS NUMBER OF THE INDIVIDUAL SPECIES OF A MIXTURE OF METHANE+HYDROGEN (71% CH_4 + 29% H_2) FUEL AND AIR (Φ=0.52), AS CALCULATED IN THIS WORK AND BY HAWKES ET AL.

	H_2	CH_4	N_2	O_2
This work - Le_V	0.14	1.03	1.33	1.31
This work - Le_D	0.32	1.12	1.20	1.19
Hawkes et al.	0.29	0.98	1.04	1.10

A general agreement of the results with those provided by literature is shown, with the diffusion-based approach yielding closer Le values than the volume-based one. As mentioned,

the former is more accurate when hydrogen is present, while the latter is more suitable with alkanes.

CHAPTER 6

STRETCH EFFECT

"The concept of flame stretch was first introduced by Karlovitz [25] to describe flame extinction in the presence of velocity gradients. It was subsequently adopted by Lewis and von Elbe [26] to explain and quantify the various phenomena associated with flame stabilization. The flame curvature aspects of stretch also formed the basis for the study of flame front instability by Markstein [27]. During the past years, significant advances have been made in our understanding of flame stretch and its influence on the flame structure." [21]

Not only the study of flame stretch is very useful for the description of actual physical situations, but it has also lead to a complete re-interpretation of some flame phenomena.

6.1 Flame Stretch

Consider an arbitrary - say, isothermal - surface, A, representing the flame. Because of the underlying fluid velocity and the motion of the flame itself, A moves along the flame structure, still remaining attached to it, and undergoes a continuous deformation. The consequent flame deformation can be measured by the *stretch rate*, defined as the fractional area change of a Lagrangean surface belonging to the flame and expressed by the equation [21]:

$$K = \frac{1}{A}\frac{\mathrm{d}A}{\mathrm{d}t} \tag{6.1}$$

Basing on this formulation, a consistent general definition is provided by C.K. Law: "Stretch at any point on this surface is the time derivative of the logarithm of the area of an infinitesimal element of the surface, with the boundary of this surface element moving tangentially to the surface at the local tangential component of the fluid velocity" [21].

A kinematic formulation for the stretch rate, indicating its relation with the flame speed, is cast as [28]:

$$K = S_L\kappa + k_s \tag{6.2}$$

where κ is the local principal curvature and k_s is the strain rate.

As mentioned before, stretch is induced by the flame motion, curvature and aerodynamic strain.

6.2 Strain Rate

Based on Equation 6.2, flame stretch rate is equal to strain rate in counterflow flames. As discussed in 4.3), such flames are stationary and nearly flat, i.e., there is no curvature. Hence, the only contribution to flame stretch is due to *aerodynamic straining* caused by the axial velocity gradient because of the presence of a stagnation plane.

The flame strain rate (distinguished in normal and shear strain rate) assumes different values as function of the position in the flow domain. However, it is expedient to define a *global* strain rate, which affects flame stability, structure, and other characteristics. The *global strain rate*, k, can be expressed as [29]:

$$k = \frac{2|v_2|}{L}(1 + \frac{|v_1|\sqrt{\rho_1}}{|v_2|\sqrt{\rho_2}}) \tag{6.3}$$

where the subscripts 1 and 2 denote conditions at the two nozzles and L is the axial spacing between the nozzles. In the present study, the same mixture is fed through both nozzles, i.e., ρ_1=ρ_2=ρ_{in} and v_1=v_2=v_{in}.

Therefore, Equation 6.3 reduces to:

$$k = \frac{4|v_{in}|}{L} \tag{6.4}$$

As mentioned earlier, global strain rate is an important parameter in the study of counterflow flames. Therefore, inlet velocities are prescribed using the desired strain rate for a given value of L (fixed). This also implies equal momentum fluxes at the two nozzles exits.

Flames with the same global strain rate, k, will exhibit identical burning characteristics. For example, Table XIV shows that almost the same maximum flame temperature, T_{max}, and burning velocity, S_b, are obtained by varying the nozzle distance, L, and changing the inlet velocity, v_{in}, accordingly, in such a way to impose the same global strain rate, e.g., $k = 100s^{-1}$.

TABLE XIV: MAXIMUM TEMPERATURE AND BURNING VELOCITY OF THREE FLAMES WITH THE SAME k.

L (cm)	v_{in} (cm/s)	k (s^{-1})	T_{max} (K)	S_b (cm/s)
1.5	37.5	100	1655.9	96.7
3.0	75.0	100	1663.0	99.6
4.5	112.5	100	1662.6	100.3

The global strain rate is also a measure of the residence time, a key physical parameter in characterizing the extinction behavior of a flame.

6.3 The Effect of Strain Rate on Temperature

In figure 18 temperature profiles of various lean flames are presented. They are computed at different strain rates and at two equivalence ratios (namely, Φ=0.8 and Φ=0.6). Simulations are performed using the CHEMKIN software.

As indicated, the distance between the twin flames decreases as the strain rate is increased (and as Φ is decreased, as explained in Section 4.3.7). As k increases, the flames establish at locations closer to the stagnation plane as a consequence of the reduced flow time.

The effect of stretch rate on flame temperature is analyzed in figure 19, which plots the peak flame temperature against the strain rate, for Φ=0.6, 0.7, and 0.8.

In accordance with previous studies of counterflow premixed flames [30], it is indicated that for $Le < 1$, as stretch rate increases, the flame temperature increases and reaches a maximum at certain strain rate, and subsequently the flame temperature decreases. The flame is extinguished close to the stagnation plane, for the range of strain rate values where a rapid decrease in temperature is observed. In his work, Graham Dixon-Lewis [31] has reported an analogous behavior for lean laminar premixed methane-air flames (same Lewis number effect as lean syngas-air mixtures).

As expected, the peak temperature is lower for leaner mixtures. Moreover, for leaner mixtures, the flame extinction occurs at a lower strain rate.

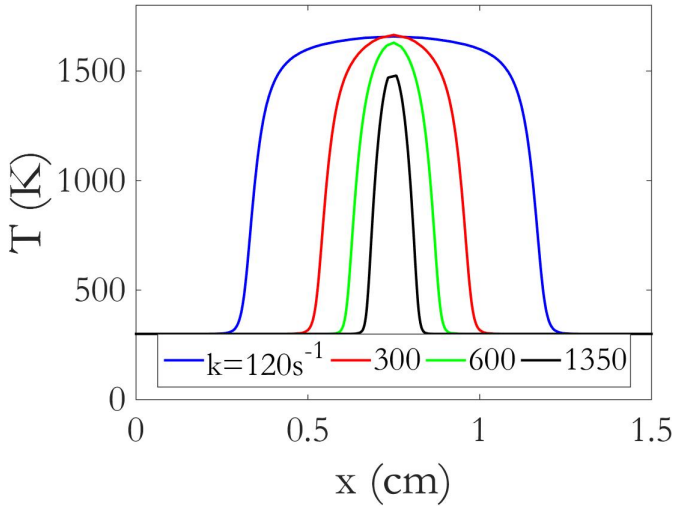

(a) Φ=0.8

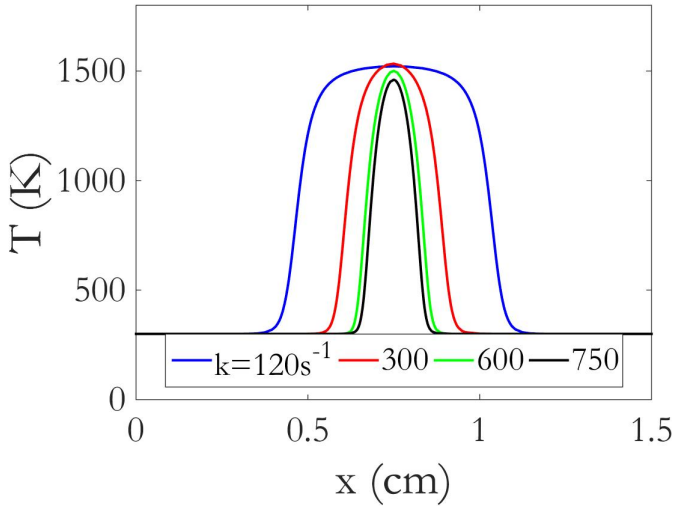

(b) Φ=0.6

Figure 18: Temperature profiles in the axial direction for premixed flames (50% H_2 and 50% CO syngas, 68% N_2 dilution) computed at different strain rates and (a) Φ=0.8, (b) Φ=0.6.

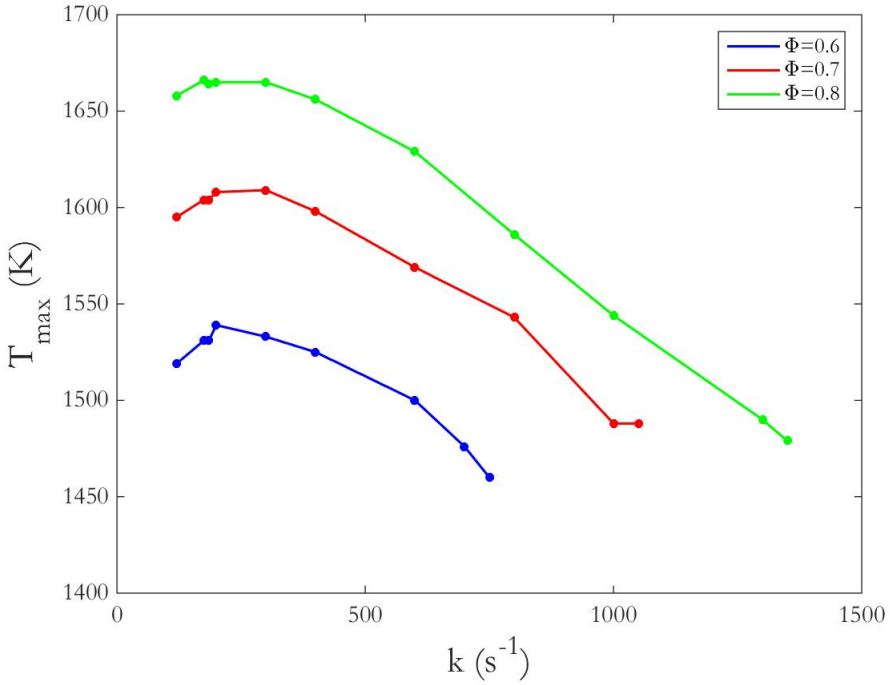

Figure 19: Flame temperature as a function of strain rate (50% H_2 and 50% CO syngas, 68% N_2 dilution) indicating high strain rate extinction for different Φ, obtained with CHEMKIN.

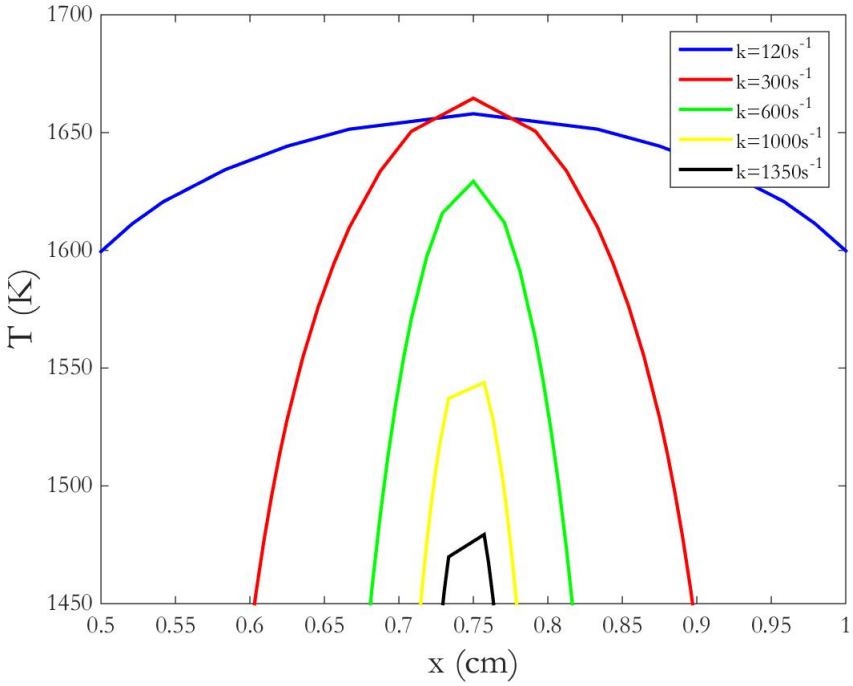

Figure 20: Axial temperature profiles in the flame region near the stagnation plane (50% H_2 and 50% CO syngas, 68% N_2 dilution, Φ=0.8) for different strain rates.

In figure 20, a zoomed view of the temperature distributions in the flame is shown near the stagnation plane, for Φ=0.8 and different strain rates.

As strain rate is increased from 120 to 300 s^{-1}, the peak temperature increases. This can be explained by the Lewis number effect for $Le < 1$, which causes the preferential diffusion of the excess reactant, i.e., the oxidizer, thus "enriching" the mixture in the proximity of the center axis of the flow. However, with further increase in strain rate, the peak temperature decreases,

because the final equilibrium temperature of the mixture is affected by diffusive and reactive aspects of the problem.

6.4 The Effect of Strain Rate on Heat Release Rate

In figure 21 the heat release rate (HRR) profiles along the axial direction are presented at different strain rates, for Φ=0.8 and Φ=0.6. For mixtures with Lewis number smaller than unity, it is observed that the maximum HRR continuously increases with global strain rate (while, as expected, it decreases as equivalence ratio is reduced).

A case of fuel rich mixture, namely, Φ=1.6, is also examined, as $Le > 1$ for this case. In figure 22 heat release rate profiles are plotted for different strain rates. Also in this case, the twin flames are established closer to the stagnation plane, as the strain rate is increased. In contrast to lean mixtures, increasing the strain rate leads to a reduction in the peak HRR for rich mixtures.

It is known that the trend of HRR as a function of the stretch rate depends on the Lewis number [21]. Precisely, it is a result of how this parameter affects the maximum flame temperature (as seen in the previous section): HRR (temperature) increases / decreases with stretch for $Le < 1$ / $Le > 1$.

These results are consistent with those reported by Choi et al. [30].

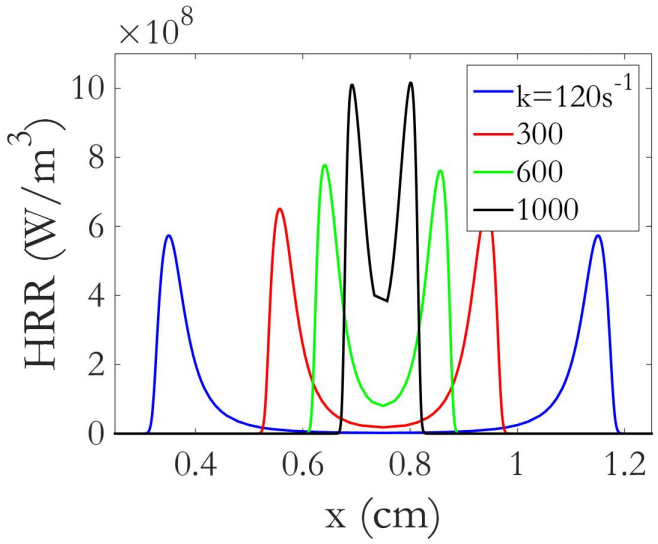

(a) Φ=0.8

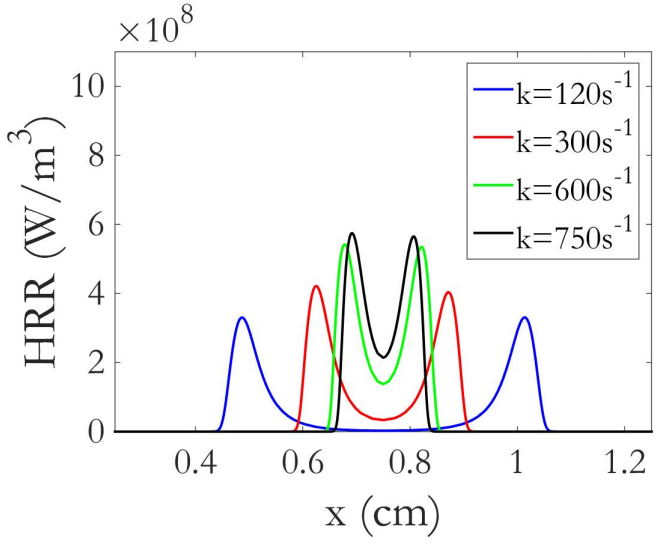

(b) Φ=0.6

Figure 21: HRR profiles at different strain rates for (a) Φ=0.8 and (b) Φ=0.6. (50% H_2 and 50% CO syngas, 68% N_2 dilution).

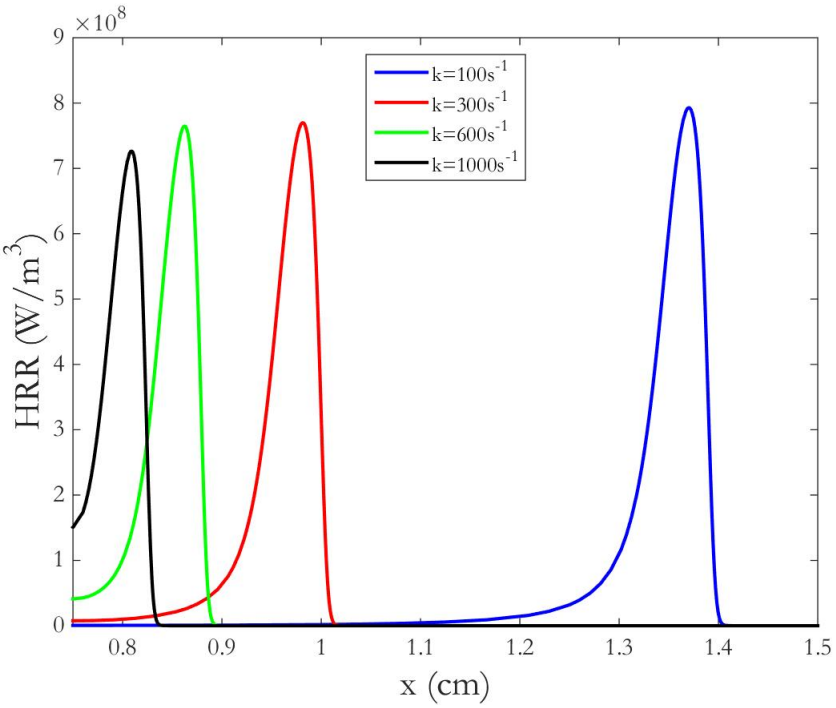

Figure 22: HRR profiles along the axial direction at different strain rates (50% H_2 and 50% CO syngas, 68% N_2 dilution, Φ=1.6).

6.5 Computation of Unstretched Flame Speed

Computation of counterflow premixed flames can be used to extract both the stretched and *unstretched flame speed*. The latter is determined by subtracting out the stretch effects from the stretched laminar flame speed, S_u.

In the symmetrical opposed flow flame configuration, the minimum point in the axial velocity profile (before the flame) is identified as the stretched *upstream (unburned) flame speed* S_u, corresponding to the imposed stretch rate (see figure 3). "Thus, by plotting S_u versus the global strain rate k, the unstretched flame speed S_u^0 can be determined through linear extrapolation to k=0" [21].

One-dimensional CHEMKIN opposed flow simulations are carried out for the analysis.

As an example, for the case of a 50% H_2 and 50% CO syngas mixture, with 68% N_2 dilution, Φ=0.8, and strain rate value of $k_1 = 175s^{-1}$, the stretched flame speed corresponding to the minimum axial velocity is $S_{u,1} = 32.4cm/s$. Then, in order to compute the unstreched flame speed, S_u^0, stretched flame speeds at different strain rates, $S_{u,i}$, must be determined; they are indicated in Table XV.

Subsequently, a numerical curve fitting method is employed to find the analytical law that expresses the linear proportionality between k and S_u.

Finally, the value of the *unstretched upstream flame speed* obtained by a linear extrapolation procedure is $S_u^0 = 24.2cm/s$.

The procedure is then repeated for the other equivalence ratios, namely, Φ=0.7 and Φ=0.6.

TABLE XV: STRETCHED FLAME SPEED OF A SYNGAS (50% H_2 - 50% CO) MIXTURE WITH 68% N_2 DILUTION AND Φ=0.8, AT DIFFERENT k.

$k_i(s^{-1})$	$S_{u,i}(cm/s)$
120	29.9
175	32.4
185	32.9
200	33.6

6.5.1 Unstretched Flame Speed Results

The results of the previous section are summarized in figure 23, which plots the unburned flame speed, S_u, against the strain rate, k. The *unstretched* unburned flame speeds are obtained from the intersection of the curves with the vertical axis: $S_u^0 = 20.8cm/s$ for Φ=0.7 and $S_u^0 = 17.4cm/s$ for Φ=0.6.

The unburned flame speed curves of figure 23 are monotonically increasing functions of the strain rate; the underlying reason is the proportionality between strain rate and mixture inlet velocity.

The three curves can be approximated by straight lines having equation: $S_u = S_u^0 - \ell_u k$. It has been proven [32] [33] [34] that the slope of the linear fit, ℓ_u, is the Markstein length of the flame (strain sensitivity of the mixture) of the unburned gas, which is negative in this case.

A validation of this procedure is provided by the comparison with the unstretched flame speed of a freely propagating flame at the same conditions, obtained using the PREMIX code. In figure 24 a quite large difference is shown in the predicted unstretched flame speed of the

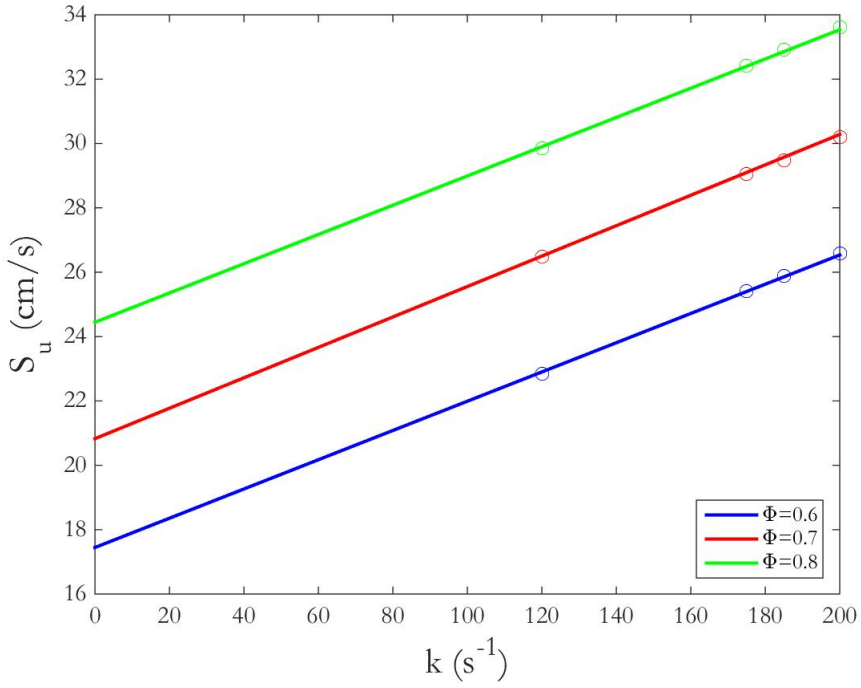

Figure 23: Unburned flame speed as a function of the strain rate for different equivalence ratios (50% H_2 and 50% CO syngas with 68% N_2 dilution). The circles represent the results of the single simulations.

Φ=0.8 mixture by the two methods; precisely, the value of S_u^0=24.2 cm/s predicted by the linear extrapolation method from counterflow simulations indicates a relative error of 15% with respect to the *exact* value of S_L=20.8 cm/s predicted by the laminar flame speed calculation simulation of a freely propagating flame.

Such a large uncertainty is mainly due to the adopted definition of unburned flame speed in the counterflow simulation. Another method proposed in literature [35] is that of determining the unburned flame speed by extrapolation of the axial velocity (before the flame) to the

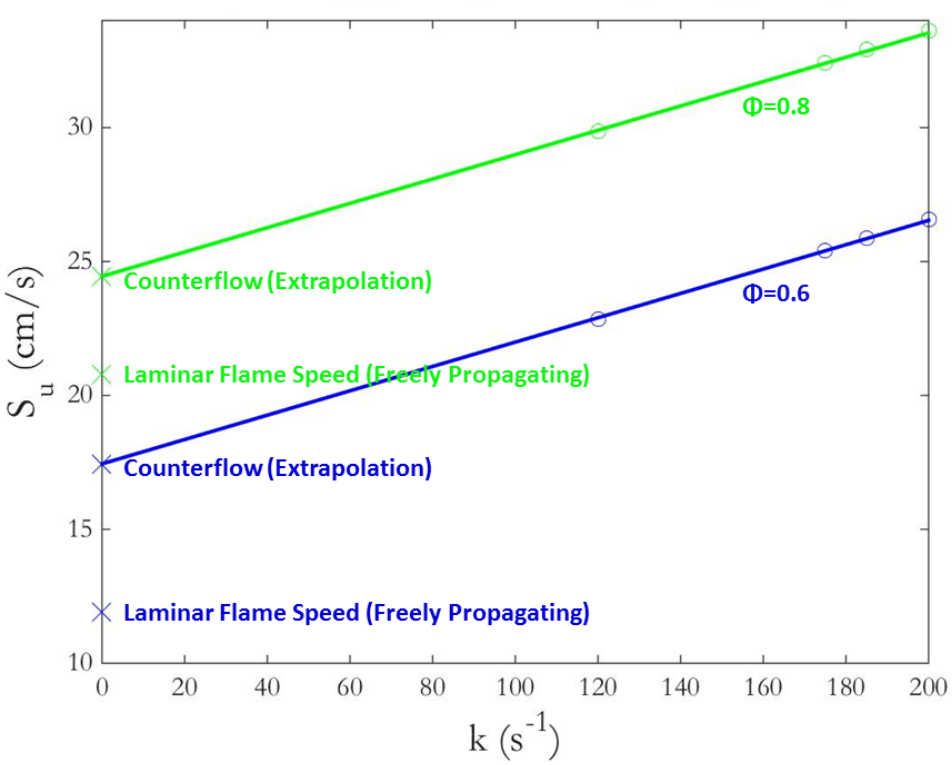

Figure 24: Unburned flame speed as a function of the strain rate (obtained with OPPDIFF) and unstretched laminar flame speed values (obtained with PREMIX) for Φ=0.8 and Φ=0.6 (50% H_2 and 50% CO syngas with 68% N_2 dilution).

barycenter of the reaction zone. This provides lower values of the unburned flame speed, i.e., a value of the unstretched flame speed closer to S_L evaluated with PREMIX. However, the assessment, either theoretical or experimental, of the reaction zone barycenter is not always easy.

Table XVI reports the values of the stretched flame speed at the reaction zone barycenter for the corresponding imposed strain rates.

TABLE XVI: STRETCHED FLAME SPEED OF A SYNGAS (50% H_2 - 50% CO) MIXTURE WITH 68% N_2 DILUTION, AT DIFFERENT Φ AND k, EVALUATED AT THE REACTION ZONE BARYCENTER.

$k_i(s^{-1})$	$S_{u,i}(cm/s)$ ($\Phi = 0.8$)	$S_{u,i}(cm/s)$ ($\Phi = 0.6$)
120	22.9	15.4
175	23.5	16.0
185	24.0	16.8
200	24.1	17.2

Through a linear extrapolation to k=0 of these sets of data, the unstretched flame speeds are calculated: S_u^0=21.0 cm/s and S_u^0=12.6 cm/s for Φ=0.8 and Φ=0.6, respectively. These results are in close agreement with those obtained with CHEMKIN laminar flame speed calculations and confirm the consistency of the calculations.

6.5.2 Unstretched Flame Speed with Heat Radiation

While the inclusion of heat radiation in the computational model will be described in Section 7.2.2, it is useful to analyze here the effect of radiative heat losses on the unburned flame speed, in order to observe the difference with the adiabatic case.

As it will be discussed in the following, radiative effects become important with high residence time, i.e., with low strain rate. Therefore, no substantial change in the unburned flame speed is registered for high values of k, while a deviation of S_u from the linear trend occurs when k is decreased. This is shown in figure 25.

The unburned flame speed is slightly lower than that in the adiabatic case; moreover, it undergoes a moderate decay at low strain values, due to the reduction in flame temperature

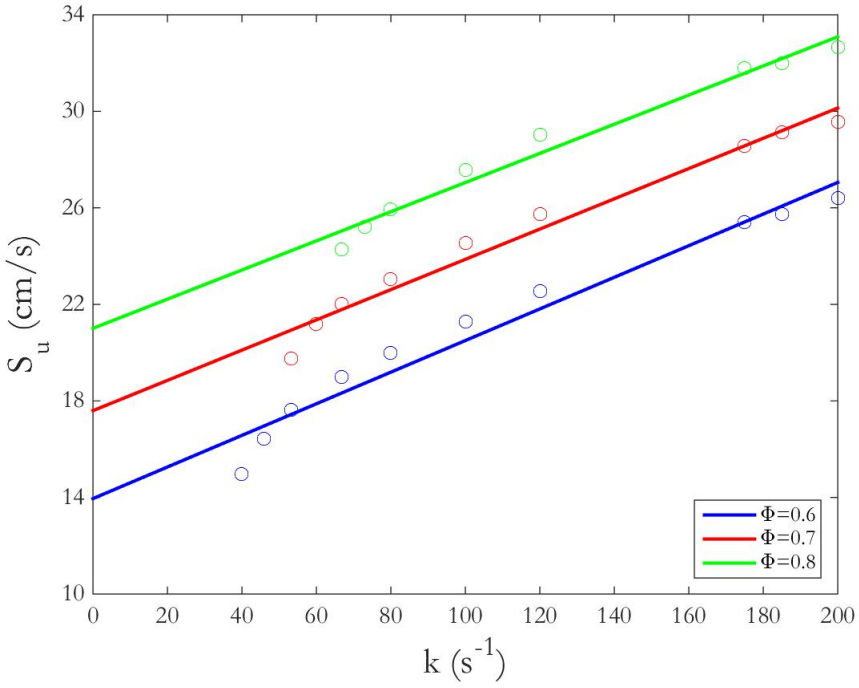

Figure 25: Unburned flame speed as a function of the strain rate for different equivalence ratios (50% H_2 and 50% CO syngas with 68% N_2 dilution), considering *heat radiation*. The circles represent the results of the single simulations.

resulting from radiation. Consequently, the extrapolated *unstretched* flame speeds are lower than those obtained in Section 6.5.1, as shown in Table XVII.

TABLE XVII: COMPARISON OF THE UNSTRETCHED FLAME SPEED OF A SYNGAS (50% H_2 - 50% CO) MIXTURE WITH 68% N_2 DILUTION, AT DIFFERENT Φ, COMPUTED BY NEGLECTING AND CONSIDERING RADIATION.

Φ	$S_u^0(cm/s)$ (no rad)	$S_u^0(cm/s)$ (rad)
0.6	17.4	14.0
0.7	20.8	17.6
0.8	24.2	21.0

6.6 Flame Stretch with Non-Equidiffusion

As discussed earlier, syngas/air flames exhibit a behavior that is similar to premixed hydrogen/air flames. Consequently,

- $Le < 1$ for lean mixtures
- $Le > 1$ for rich mixtures

The burning velocity, S_b, of the fluid mixture in a counterflow geometry is considered to be the axial flow velocity in the point of the domain where the heat release rate peaks. In figure 26 the axial velocity profile of the mixture analyzed in 4.3.3 has been reported, in order to distinguish the velocity values corresponding to S_u and S_b.

In figure 27, the burned mixture velocity, S_b, is plotted as a function of the strain rate, k. The blue curve is representative of the condition Φ=0.6 ($Le < 1$), while the red curve is representative of the condition Φ=1.6 ($Le > 1$).

As indicated in figure 27, for $Le < 1$, burning velocity increases with strain rate, since a positive stretch has the effect of increasing the fuel concentration of lean syngas/air mixtures,

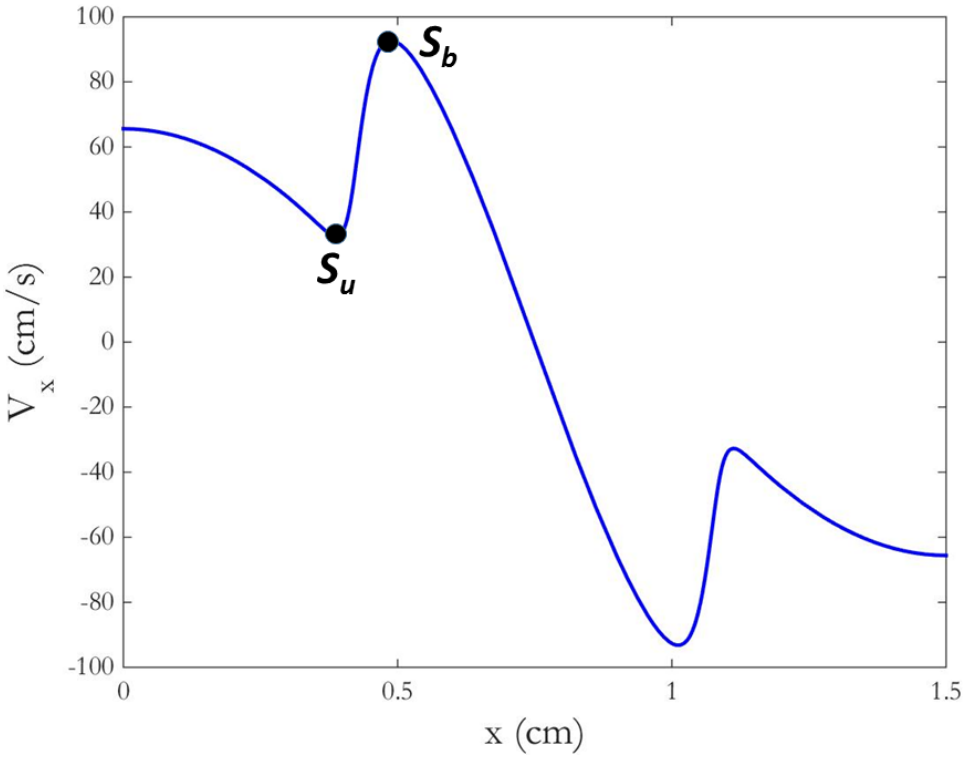

Figure 26: Axial velocity profile for syngas (50% H_2 and 50% CO) flame with Φ=0.8 and 68% N_2 dilution. Identification of the burned and unburned flame speed.

thereby enhancing burning rate. The opposite holds for $Le > 1$, i.e., lower burning velocities with increasing stretch. In this case, thermal diffusion dominates and leads to a reduction in temperature and thus lower burning rate.

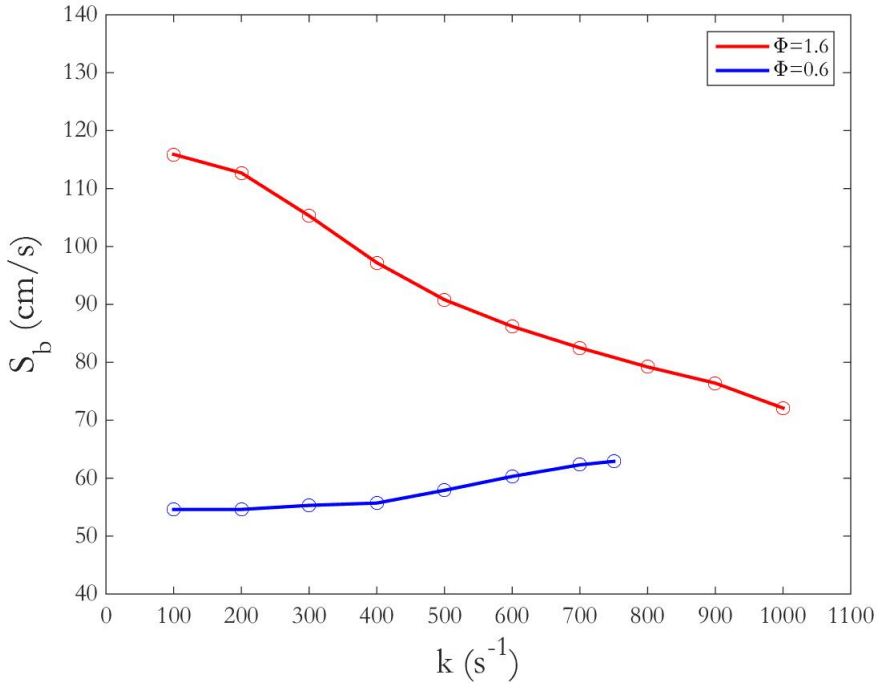

Figure 27: *Downstream* (burned) flame speed of 50% H_2 and 50% CO syngas (with 68% N_2 dilution) as a function of the strain rate for different equivalence ratios. The circles represent the results of the single simulations.

Results are now presented for different syngas fuel compositions (with 68% N_2 dilution), highlighting the effect of Lewis number.

The burning velocity is plotted in figure 28 as a function of the strain rate for the rich and lean mixture cases. The upper bounds are chosen sufficiently close to the extinction strain rate, while the lower bounds are in compliance with the flashback avoidance condition.

In figure 28 it is shown that these three different fuel compositions have the same trend for increasing strain rate, i.e., the burning velocity, S_b, is an increasing function of k for lean mix-

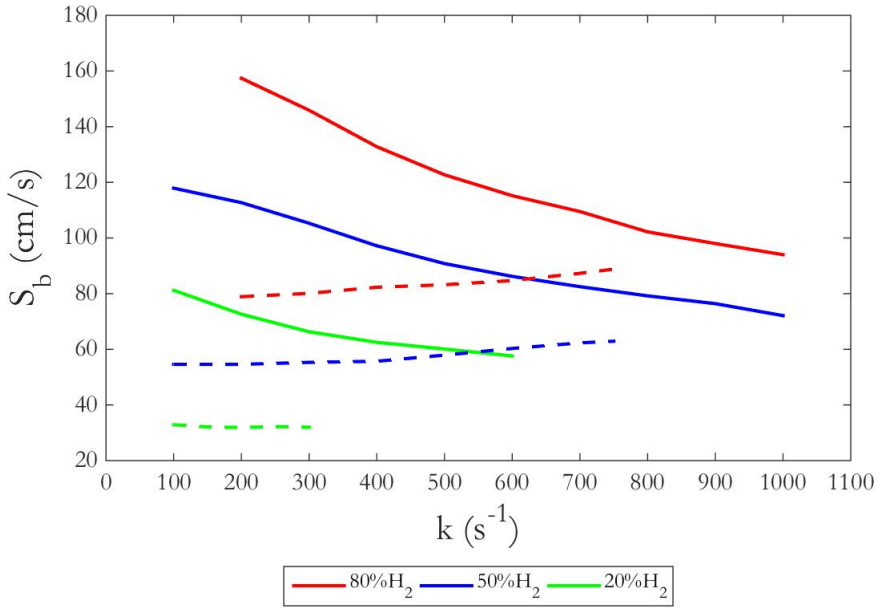

Figure 28: *Downstream* (burned) flame speed as a function of strain rate for rich (Φ=1.6, *solid lines*) and lean (Φ=0.6, *dashed lines*) mixtures with different syngas compositions (with 68% N_2 dilution).

tures (having $Le < 1$) and a decreasing function of k for rich mixtures ($Le > 1$). Furthermore, as the CO content is increased, the curves are shifted downwards, thus showing how hydrogen has the effect of enhancing the flame intensity in syngas fuel mixtures.

A first order - numerical curve fitting method is then employed to obtain an equation for each of the three curves corresponding to rich mixtures, since they exhibit the largest dependence on strain rate (an analogous procedure has been carried out in Section 6.5.1 for the unburned flame speed of lean mixtures). The so-obtained linear equations are:

- For $H_2 = 80\%$: $S_b = 166.9144 - 0.0786k$
- For $H_2 = 50\%$: $S_b = 120.2133 - 0.0512k$
- For $H_2 = 20\%$: $S_b = 82.6467 - 0.0455k$

The so-obtained equations are in the form: $S_b = S_b^0 - \ell_b k$ [35], where S_b^0 (cm/s) is the unstretched burned flame speed, and ℓ_b (cm) is the Markstein length of the burned gas. In the formulation provided by Davis et al. [35], the dependence of ℓ_b on a factor of $(1 - 1/Le)$ is indicated. This explains the different flame behavior when Le switches from $Le < 1$ to $Le > 1$.

The Lewis number effect on the burning rate is also shown in figure 29, where OH mole fraction is plotted as a function of strain rate for different combinations of syngas compositions and equivalence ratios. OH concentration is an increasing function of strain rate for lean mixtures, i.e., burning rate increases with stretch for $Le < 1$. The opposite holds for rich mixtures ($Le > 1$).

Moreover, an increase of the H_2 content in the syngas mixture leads to an increase of the burning rate when Φ=0.6 and a decrease of it when Φ=1.6. The underlying reason is that Le is lower with lower H_2 content for lean mixtures, as seen in Section 5.3; therefore, heat diffusion is reduced, thus positively affecting the burning rate. Viceversa, Le increases with H_2 content for rich mixtures, and the burning rate decreases.

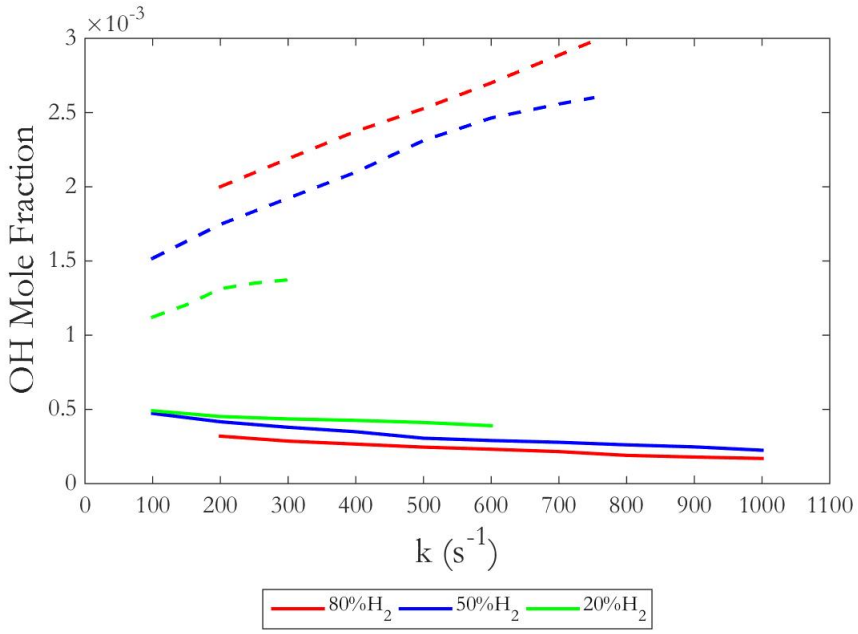

Figure 29: *OH* mole fraction as a function of strain rate for rich (Φ=1.6, *solid lines*) and lean (Φ=0.6, *dashed lines*) mixtures with different syngas compositions (with 68% N_2 dilution).

6.7 Flame Stability

The Karlovitz number, *Ka*, of the flame is defined by the following expression [36]:

$$Ka = \frac{k\delta}{S_b} \tag{6.5}$$

Here, δ is the flame thickness, obtained analytically through the following formula [18]:

$$\delta = \frac{2\alpha}{S_b} \tag{6.6}$$

and α is the thermal diffusivity of the mixture.

The curves of figure 30 are obtained by linearly fitting several 1-D counterflow simulations results on a normalized burned laminar flame speed (S_b^0/S_u) - Karlovitz number (Ka) plot, for different values of equivalence ratio ($\Phi = 0.6$ and $\Phi = 1.6$) and for different syngas composition ($80\%H_2 + 20\%CO$, $50\%H_2 + 50\%CO$, and $20\%H_2 + 80\%CO$). The unstretched burned flame speed, S_b^0, is obtained for each case analogously as in Section 6.5.

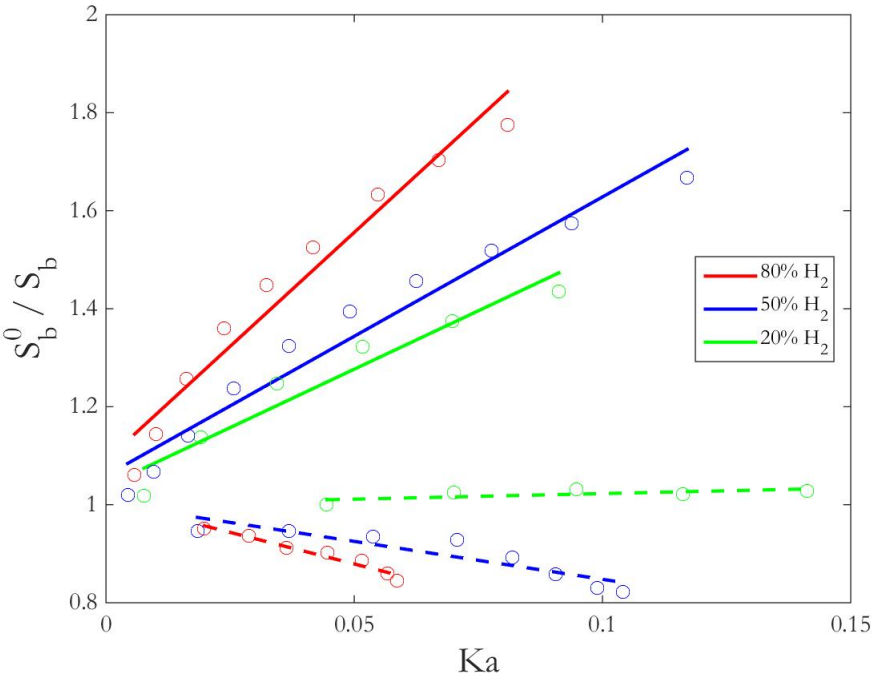

Figure 30: Normalized burned laminar flame speed as a function of the Karlovitz number at Φ=1.6 (solid lines) and Φ=0.6 (dashed lines) for different syngas composition (H_2 content is indicated in the legend, while the remaining part is CO), at ambient temperature and pressure. Circles indicate single numerical simulations results at varying k.

The slope of the curves yields the Markstein number, Ma. "$Ma > 0$ and $Ma < 0$ correspond to diffusively stable and unstable conditions, respectively" [36]. Therefore, the lean syngas flames in figure 30, represented by curves with negative slopes (except the 80% CO one, which is almost horizontal), are cellularly unstable and present wrinkles on their surface ("cellular instabilities due to stretch and thermal-diffusion effects lead to the wrinkling of the flame surface with regions of local extinction and robust burning" [37]). Conversely, rich syngas flames have positive slopes and are cellularly stable. This is explained by the Lewis number effect: "if an initially planar flame is perturbed into one containing alternating convex and concave segments towards the unburned mixture, then for $Le > 1$ the burning is intensified at the concave segment and weakened at the convex segment, leading to smoothing of the wrinkles, that is, the flame is stable. Conversely, for $Le < 1$ the flame is unstable" [36].

According to the previous considerations, the straight lines of figure 30 will be represented by equations in the following form: $S_b^0/S_b = 1 + MaKa$. Thereby, the equations obtained by linearly fitting the simulations numerical results will provide the Markstein number of each flame. The actual equations obtained in this way are presented below:

- For $H_2 = 80\%$ ($\Phi = 1.6$ and $\Phi = 0.6$):

  $S_b^0/S_b = 1.09 + 9.30Ka$ and $S_b^0/S_b = 1.01 - 2.58Ka$

- For $H_2 = 50\%$:

  $S_b^0/S_b = 1.06 + 5.69Ka$ and $S_b^0/S_b = 1.00 - 1.55Ka$

- For $H_2 = 20\%$:

$$S_b^0/S_b = 1.04 + 4.77Ka \qquad \text{and} \qquad S_b^0/S_b = 1.00 + 0.22Ka$$

Moreover, "the magnitude of Ma provides a measure of the flame speed sensitivity to stretch. Thus, for $Ma > 0$ a decrease in Ma and for $Ma < 0$ an increase in its magnitude indicate an increased propensity for diffusive instability" [36]. It follows that the more unstable flames of figure 30 are the 20% H_2 (solid green) and the 80% H_2 (dashed red) ones for rich and lean conditions, respectively. This is explained by the effect of the reduced Lewis number on the diffusive instability: indeed, as seen in Section 5.3, these mixtures are characterized by the lowest Le among the other rich/lean mixtures.

CHAPTER 7

EXTINCTION OF LEAN SYNGAS FLAMES

Flame extinction is a phenomenon of essential importance in the field of combustion. As such, it has been extensively studied for both premixed and diffusion flames.

"Flame extinction represents one of the fundamental and classical phenomena in combustion science. It is important to a variety of combustion systems in transportation and power generation applications. Flame extinguishment studies are directly relevant to the safe and reliable operation of these combustion systems" [38].

In the present work, a study of the extinction of *lean premixed syngas/air flames* is carried out by examining how some chemical-kinetic parameters affect this phenomenon. Two main factors influencing extinction are addressed: the effects of flame stretch and nitrogen dilution.

7.1 Stretch Effect: Extinction at High Strain Rate

In this section, dedicated to flame extinction by stretch, computations refer to fuel/oxidizer pre-mixtures with the following composition:

- fuel: X_{N2}=0.68, X_{H2}=0.16, and X_{CO}=0.16;
- oxidizer: air, whose composition is X_{N2}=0.79 and X_{O2}=0.21.
- equivalence ratio: Φ=0.8, 0.7, and 0.6.

The flow axial velocity increases with strain rate, up to a point where the completion of chemical reactions is not guaranteed, as a consequence of the reduced flow time. Flame extinction may occur for too high values of the strain rate. Furthermore, a tight coupling exists between flame stretch and Lewis number effect [30]: flame extinction can be originated from insufficient reaction time combined with preferential diffusion.

According to the above statements, the reached extinction limit is originated purely by strain. Were the mixture stoichiometric with no preferential diffusion phenomena, the flame would be adiabatic.

Peak temperature profiles at different Φ, obtained by 1-D counterflow simulations, have already been plotted as a function of strain rate in figure 19 of Section 6.3. This figure illustrates the effect of stoichiometry on the high-strain rate extinction limit, i.e., lower k values are sufficient to extinguish flames farther from stoichiometry. The low-strain rate domain is not investigated here (it will be addressed in the next section); simulations start from a strain rate value of $k = 100s^{-1}$.

In a counterflow configuration, the twin flames are pushed closer and closer together when strain rate is increased, and flame extinction eventually occurs at a certain threshold distance (at a *critical* strain rate value).

7.2 Stretch Effect: Extinction at Low Strain Rate - Effect of Radiative Heat Loss

In order for combustion to be sustained, a balance between radical source strength and radical removal rate must exist in the flame. When radical loss becomes larger than radical gain, the flame extinguishes.

Let us refer to the flame and the ignition temperature as T_f and T_i, respectively; the latter represents the temperature at which chemical radicals are produced in the flame. From [39]: temperature difference $(T_f - T_i)$ is a measure of the high-temperature radical source strength in the flame. It follows that, the lowest radical source strength accompanies the lowest burning temperature (for constant T_i), in the flame temperature versus strain rate profiles of figure 19. Consequently, extinction limits are approached in the left-most and right-most regions of the graph.

As mentioned, flame extinction is purely stretch-induced at high strain rates. On the contrary, in the low strain rate domain, radiative heat loss contributes significantly to the extinction mechanism.

Strictly speaking, low strain rate is equivalent to low inlet velocity, and increased residence time. At this point, it is easy to understand how radiative heat loss becomes important in the flame extinction determination. Therefore, in the low strain rate domain, extinction is caused by the combined effects of strain and radiation.

7.2.1 CHEMKIN-PRO

The analysis of non-adiabatic flames is carried out by employing CHEMKIN-PRO software.

In the following, a radiation model is included, in order to perform a detailed analysis of the combustion of lean syngas premixed flames with low stretch, comprising heat loss phenomena, by employing CHEMKIN-PRO OPPDIFF code.

7.2.2 Radiation Model in CHEMKIN-PRO

The last term of the energy conservation law (Equation 4.3) represents the amount of lost thermal power due to gas and particle radiative phenomena. The aim of the present section is to clarify how this term is obtained.

It follows an extraction from CHEMKIN Theory Manual [9].

> The radiation heat-transfer model assumes that the radiation transport is through "optically thin" media. In the optically thin limit, the local gas does not re-absorb radiation emitted from other parts of the gas, such that the radiation does not need to be considered as a separate source of energy in the energy balance. The radiation heat loss, then, is due to exchange between the gas and the surroundings and between the particles and the surroundings. The optically-thin model is computationally efficient and allows quick assessment of the effects of radiation heat loss on flame structure and emissions.
>
> The radiation model is provided as an option to calculate radiation heat loss from gas and particulate matter in unconfined, lightly sooting flames, for all CHEMKIN Flame simulators, including flat-flame burner and opposed-jet flow configurations.

The optically-thin radiation heat loss from a mixture of gas and particulates is given as

$$\dot{Q}_{rad} = 4\sigma(T^4 - T_{amb}^4) \sum_i p(X_i a_i) \tag{7.1}$$

where σ is the Stefan-Boltzmann constant, T is the gas temperature, T_{amb} is the ambient temperature, p is the gas pressure, X_i is the mole fraction of species i, and a_i is the Planck mean absorption coefficient for species i.

This last equation assumes that gas and particles locally have the same temperature, since the energy balance of the particulate phase is not solved. The mean absorption coefficients of gas species and particles are treated as thermodynamic properties and are therefore required inputs to the radiation model.

The radiating gas species in syngas combustion must be identified, in order to include them in the model.

Firstly, it must be remembered that absorption or emission of infrared energy is peculiar of molecular structures that exhibit rotational and vibrational modes and modification of dipole moment. Consequently, monoatomic and homogeneous diatomic species (for instance, H_2, N_2 and O_2) are not involved in thermal radiation phenomena. Secondly, the contribution of species existing in very small quantities and/or in colder boundaries of the flow is negligible.

According to the above statements, CO_2 and H_2O (by almost 90%) as well as CO (by approximately 10%) are responsible for almost the full thermal radiation transfer in hydrocarbon combustion.

The radiative behavior of each of the above-mentioned species is characterized by a mean thermal absorption coefficient (Planck coefficient), namely, a (which has the dimension of $m^{-1}atm^{-1}$). For more accurate computational performance, instead of using mean coefficients, the species thermal absorption coefficients are implemented in the chemistry set by using polynomial fitting to temperature [40].

The temperature polynomials for modeling radiation are reported in the following equations:

Polynomial fitting law 1

$$a_i(T) = \sum_j c_j T^j \qquad with j = 0, ..., 6 \tag{7.2}$$

Polynomial fitting law 2

$$a_i(T) = \sum_j c_j / T^j \qquad with j = 0, ..., 6 \tag{7.3}$$

To include heat radiation in the calculation, the employed chemistry set must specify the thermal absorption coefficients of the individual gas-phase species. Therefore, a *modification of the thermodynamic data file of the San Diego mechanism* (reported in Section B.1 of Appendix) has been necessary.

7.2.3 Counterflow Setup Specifications

Looking at the simplified global strain rate expression (Equation 6.4), it is clear that low strain rate values, k, are achieved by setting either a low fluid inlet velocity or a large axial distance of the nozzles. However, there is a lower bound for the imposed inlet velocity; Equa-

tion 4.1 imposes that it should never become smaller than the flame speed (otherwise the flame would blow at the nozzles).

In the syngas combustion scenario, imposing a small global strain rate is therefore challenging, considering the fuel relatively high flame speed. Consequently, in the development of this study, the system layout must be modified for allowing the analysis of low-stretched flames; precisely, the nozzles distance, L, is increased to 7.5 cm (five times larger than the $L = 1.5$ cm distance previously adopted).

Moreover, in order to further reduce the mixture flame speed, N_2 dilution is set to 80% by fuel volume and equivalence ratio is kept fixed to a low value of Φ=0.6. By simulating the flame of such mixture with CHEMKIN Laminar Flame Speed Calculation mode, the calculated flame speed at $T = 300K$ and $p = 1atm$ is: $S_L = 3.16$ cm/s.

7.3 Extinction at Low Strain Rate - Simulations Results

The first-order effects of heat loss are included in the model by considering radiation to the environment (at 300 K). Heat loss by thermal radiation emission is considered both in the flame region, and downstream from it. The radiating gas phase species are considered to be only CO, CO_2, and H_2O. Therefore, CHEMKIN Opposed Flow Flame subroutine is set up in order to encompass the optically thin model for radiation of CO, CO_2, and H_2O, as well as the Soret effect.

The mixture temperature profiles along the axial coordinate are plotted in figure 31 (only half of the geometry is shown, for symmetry reasons) for two different cases: neglecting and considering gas radiation. Results are shown for two Φ values, with strain rate slightly larger

than the respective extinction value (assessed later, in Section 7.4): Φ=0.5 with $k = 4.2s^{-1}$, and Φ=0.6 with $k = 2.8s^{-1}$.

As one can observe in figure 31, when radiative heat losses are included in the computational model, the flame front moves towards the stagnation plane. Some of this movement is associated with the change in density and strain rate structure between this and the adiabatic flame [39]. However, the major cause of this flame location change can be identified as the negative effect of temperature decrease on the flame speed.

Obviously, because of heat radiation, the maximum temperature reached by the flame is lower than that of the "adiabatic" flame. Larger temperature deviations (from adiabaticity) in equivalent points of the geometry are observed for mixture conditions that are farther from stoichiometry, as noted by comparing Φ=0.5 and Φ=0.6 plots of figure 31.

Gas temperature at the stagnation plane for Φ=0.5 is higher than that for Φ=0.6. There are two main causes for this:

- lesser heat loss due to lesser residence time associated to slightly higher strain rate;
- flame closer to the stagnation plane because of the equivalence ratio effect on the mixture ignition characteristics.

When the model accounts for radiation, a temperature well appears in the zone between the two flames. This is a consequence of the downstream heat loss induced by radiative phenomena, in a region where residence time is relatively large. In figure 32, the rapid elimination of the downstream heat loss is shown, when strain rate increases; flame fronts are pushed closer to

each other and the residence time is diminished, hence radiative heat loss becomes smaller and smaller.

In figure 33, the maximum flame temperature is plotted as a function of strain rate, for two different Φ values: Φ=0.5 (in blue) and Φ=0.6 (in red). The curves are obtained by fitting a collection of results of several 1D CHEMKIN-PRO Opposed Flow Flame simulations. Solid and dashed lines refer to simulations excluding and including gas radiation model, respectively.

As predictable, gas radiation leads to a reduction of the maximum flame temperature (with respect to the "adiabatic" case). However, this reduction is progressively attenuated with increasing strain rate. This is analyzed in figure 34, which plots the maximum-temperature difference ΔT_{max} between the cases without and with gas radiation, for the two examined Φ values.

As revealed in figure 34, the two models provide very different results at very low strain rate: temperature differences are about 75 K for Φ=0.5 and 55 K for Φ=0.6 in the points of minimum k. On the other hand, much smaller values of ΔT_{max} are registered for higher k: at a moderately low strain of 50 s^{-1}, ΔT_{max} is already diminished to around 20 K for Φ=0.6; while, for Φ=0.5, the flame temperatures of the *radiating* and *non-radiating* models almost match. Thus, the two curves exhibit a different slope, the Φ=0.5 curve being considerably steeper than the Φ=0.6 one. Radiative heat loss is larger for leaner mixtures at very low strain rates. However, the increase in strain rate compensates for this effect more rapidly than it does for more stoichiometric mixtures. Therefore, leaner flames are more susceptible to stretch changes

in the radiating behavior; indeed, the blue curve (Φ=0.5) of figure 34 displays a larger ΔT_{max} excursion than the red one (Φ=0.6), in the considered strain rate range: $4.2s^{-1} < k < 50s^{-1}$.

7.3.1 Effect of Heat Radiation on Burning Velocity

The reduction of the flame temperature at low stretch because of radiative heat loss is accompanied by a collateral reduction in the burning velocity, S_b. This is shown in figure 35, in which the curves are obtained by fitting a collection of results of several 1D CHEMKIN-PRO Opposed Flow Flame simulations. Solid and dashed lines refer to simulations excluding and including gas radiation model, respectively.

In figure 35, a more pronounced decrease is depicted at very low strain rates (near extinction), while the deviation is soon recovered at about $k = 30s^{-1}$ for both the equivalence ratios (the solid and dashed curves overlap).

7.4 Summary of Extinction by Stretch

The present section is devoted to the analysis of radiative heat loss effects on the *low strain rate - extinction* of the flame. Table XVIII collects the extinction strain rate values calculated for different mixture stoichiometries, entailing the effects of gas radiation, for L=7.5 cm. Results were obtained by means of 1D CHEMKIN-PRO Opposed Flow Flame simulations.

TABLE XVIII: LOW AND HIGH EXTINCTION STRAIN RATES OF A MIXTURE OF 50% H_2 - 50% CO SYNGAS (WITH 80% N_2 DILUTION) AND AIR, AT DIFFERENT Φ.

Φ	$k_{ext,low}(s^{-1})$	$k_{ext,high}(s^{-1})$
0.50	4.15	460
0.55	3.85	560
0.60	2.75	600
0.65	2.10	760

In figure 36 the extinction strain rate, k_ext, is plotted as a function of Φ in semi-logarithmic scale, in a narrow lean mixture domain ($0.5 < \Phi < 0.65$). Such a small range has been chosen, because flames characterized by higher equivalence ratios do not comply with the condition of Equation 4.1. The dots identify the numerical simulations results; trendlines are traced by employing a second-order polynomial fitting method.

The upper and the lower curves in figure 36 represent high- and low strain rate - extinction, respectively. Were the abscissae axis extended leftwards (to lower Φ values), the two curves

would eventually change their slope and meet in a single point (to the left of which ignition would not be possible).

The lower curve of figure 36 shows that low strain extinction limit is a decreasing function of equivalence ratio (in the lean mixtures domain). The opposite holds for extinction caused by high strain rate, i.e., the upper trendline is monotonically increasing. It follows that more stoichiometric mixtures are more prone to ignite; in the diagram, the flammable region lies between the curves, proving that the flammability range (with respect to flame stretch) can be extended by enriching the mixture.

7.5 Nitrogen Dilution Effects

Being an inert gas, nitrogen content plays a role in the flame inhibition. It is useful to clarify this concept, by invoking the definition of *physical suppressant* provided by Aggarwal: "a physical agent extinguishes the flame mainly through thermal and dilution effects" [38]. Thus, as mentioned in Section 4.2.2, the thermal diffusivity of the fuel is lowered by increasing the amount of dilution.

The studies presented here are performed by keeping fixed the strain rate ($k = 175s^{-1}$) and varying the fuel N_2 dilution percentage (in volume) case by case, until a certain *critical nitrogen dilution* value is found, for which the flame extinguishes.

Results are presented for three lean mixture cases: Φ=0.8, Φ=0.7, and Φ=0.6. Flame extinction is found to occur for different nitrogen content, when the mixture stoichiometry is varied. Precisely, smaller amounts of nitrogen dilution are sufficient for more off-stoichiometric cases.

In order to evaluate the effect of N_2 dilution on premixed flame of 50% H_2 and 50% CO syngas and air, both one and two-dimensional numerical simulations are carried out. In each of the following subsections, a different N_2 dilution percentage has been introduced in the fuel, and some meaningful simulations outputs are presented.

7.5.1 74% Nitrogen Dilution

Considering 74% N_2 fuel dilution by volume, the existence of the flame is predicted by both codes, which give very similar results.

In figure figure 37 the output of UNICORN 2D code is portrayed by employing OH mole fraction and temperature iso-contours.

A flame weakening is progressively evidenced in figure 37 by reducing the equivalence ratio from Φ=0.8 to Φ=0.7 and ultimately to Φ=0.6. However, combustion is still predicted in the three cases.

7.5.2 80% Nitrogen Dilution

Simulations with 80% N_2 dilution are now set up. The numerical results of both codes still predict mixture ignition, in this case. This is shown by figure 38, which represents the results obtained with UNICORN.

The main difference of the contours of figure 38 with respect to those of figure 37 is the fading of the colors, meaning that burning rate decreases with increasing N_2 dilution.

7.5.3 84% Nitrogen Dilution

N_2 dilution is now increased to 84%. CHEMKIN simulations identify this particular amount of N_2 dilution as the one needed to extinguish the Φ=0.6 flame, but flames still establish for Φ=0.8 and Φ=0.7. This is shown by the temperature profiles in figure 39. Conversely, no flame is predicted for any of the Φ values, with UNICORN. Extinction phenomenon is shown in figure 40: N_2 dilution is increased from 80% to 84% by volume and the evolution in time is shown.

7.5.4 85% Nitrogen Dilution

Finally, a value of N_2 dilution equal to 85% by volume is found to be the minimum one to extinguish the Φ=0.8 and Φ=0.7 flames of syngas and air mixtures, according to CHEMKIN Opposed Flow Flame simulations.

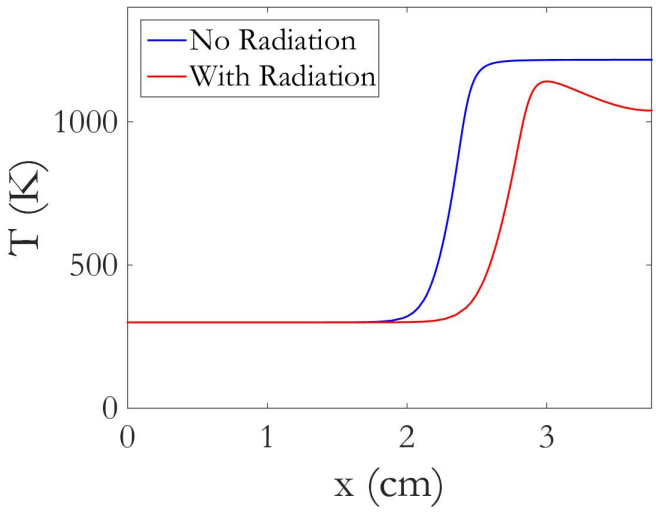

(a) Φ=0.5

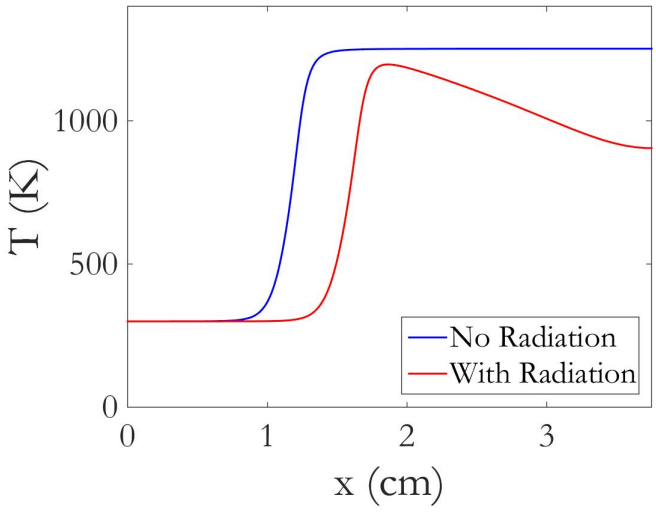

(b) Φ=0.6

Figure 31: Temperature profiles along flow semi-axis of a (*a*) Φ=0.5 and a (*b*) Φ=0.6 syngas/air mixtures (with 80% N_2 dilution), obtained with CHEMKIN-PRO (non-radiating and radiating models).

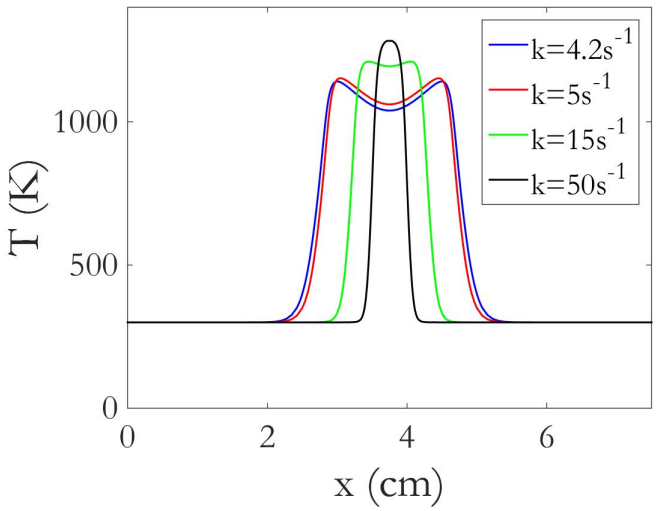

(a) Φ=0.5

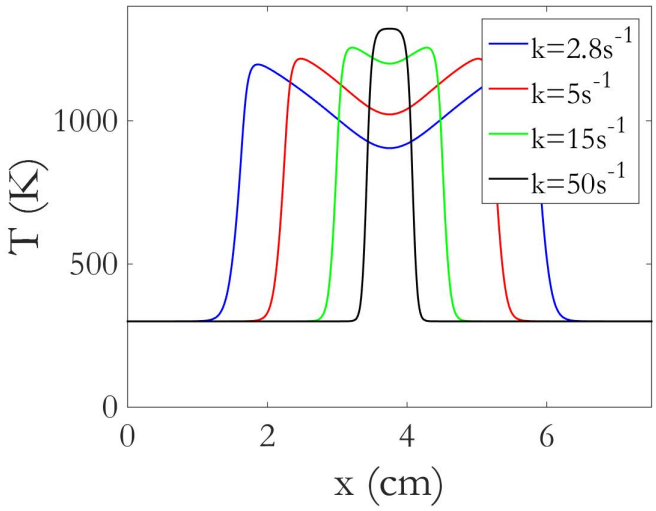

(b) Φ=0.6

Figure 32: Temperature profiles along flow axis of a (*a*) Φ=0.5 and a (*b*) Φ=0.6 syngas/air mixtures (with 80% N_2 dilution) at different k, obtained with CHEMKIN-PRO.

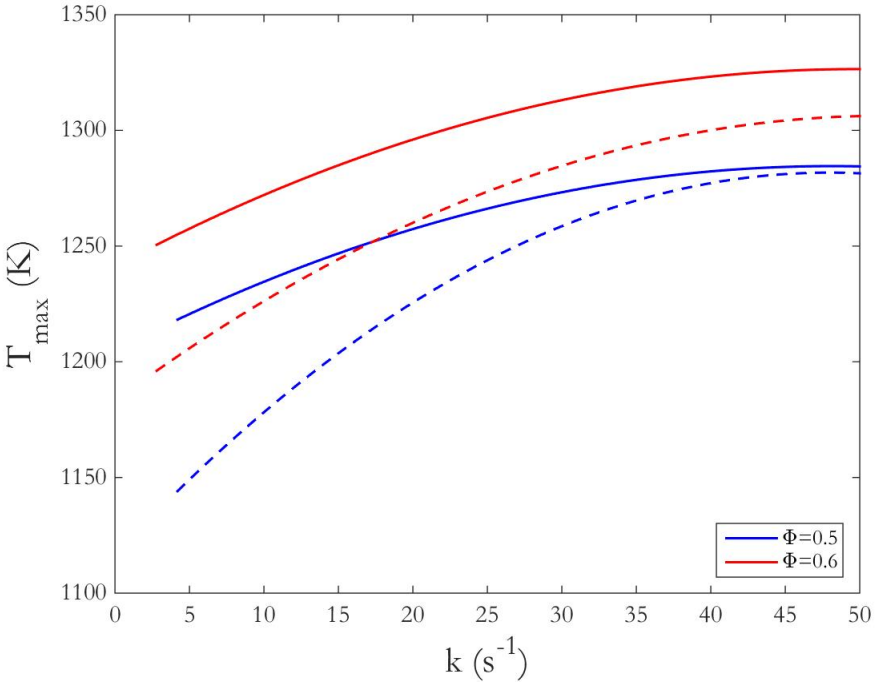

Figure 33: Flame temperature as a function of a small range of low strain rate (50% H_2 and 50% CO syngas, 80% N_2 dilution) for Φ=0.5 and Φ=0.6, obtained with CHEMKIN-PRO. Non-radiating (solid lines) and radiating (dashed lines) models.

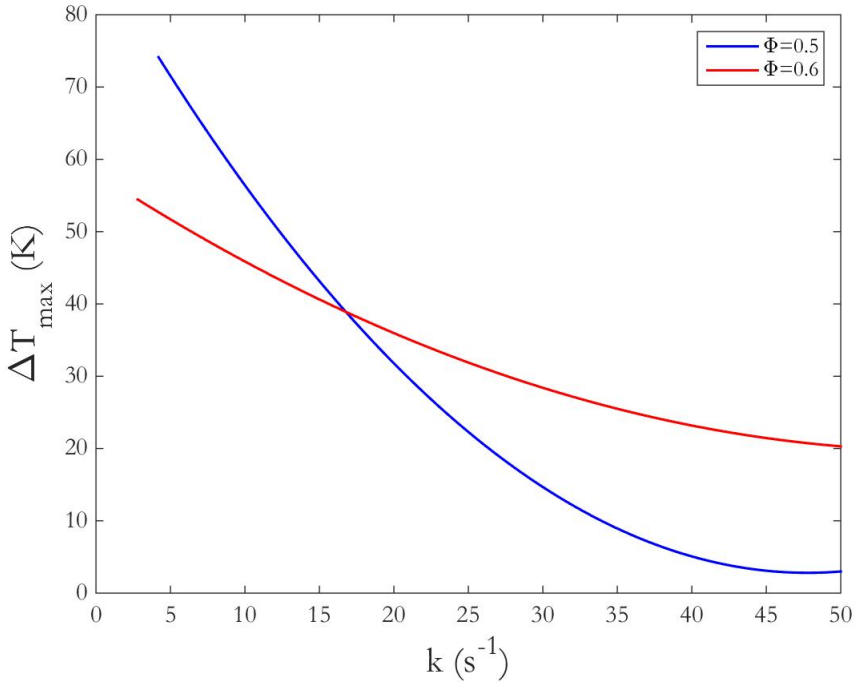

Figure 34: Difference of the maximum temperatures of *radiating* and *non-radiating* models as a function of strain rate (50% H_2 and 50% CO syngas, 80% N_2 dilution) for Φ=0.5 and Φ=0.6.

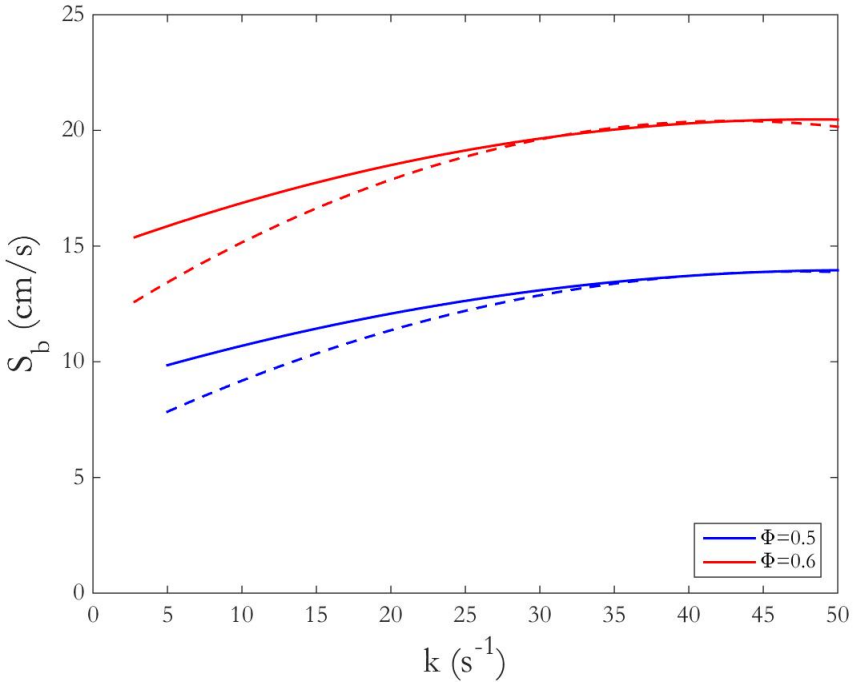

Figure 35: Burning velocity as a function of a small range of low strain rate (50% H_2 and 50% CO syngas, 80% N_2 dilution) for Φ=0.5 and Φ=0.6, obtained with CHEMKIN-PRO. Non-radiating (solid lines) and radiating (dashed lines) models.

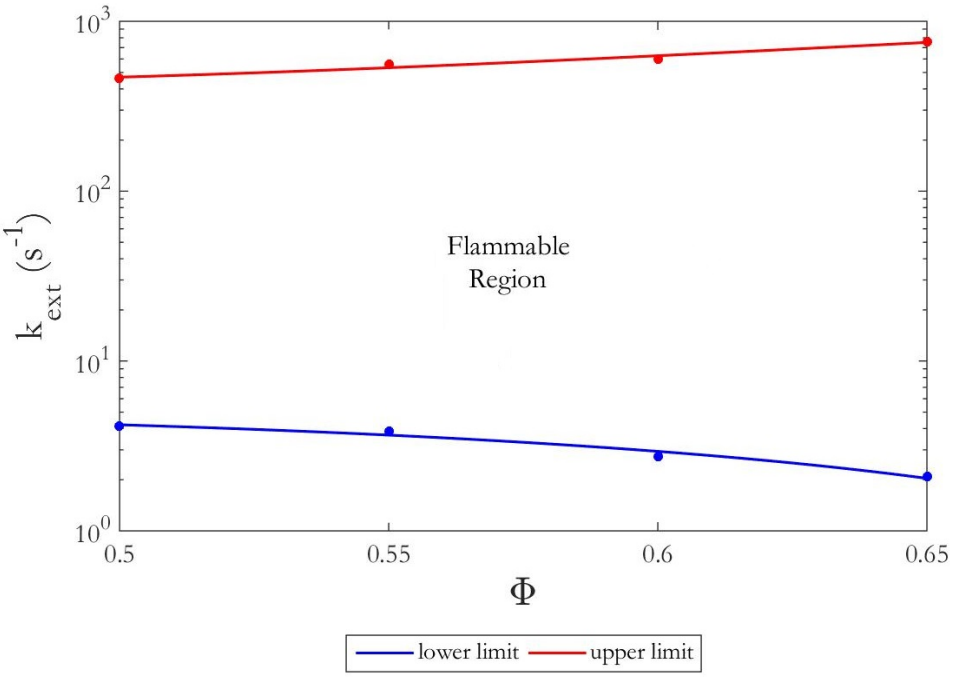

Figure 36: Extinction strain rate (logarithmic scale) as a function of equivalence ratio (50% H_2 and 50% CO syngas, 80% N_2 dilution). Results obtained with CHEMKIN-PRO.

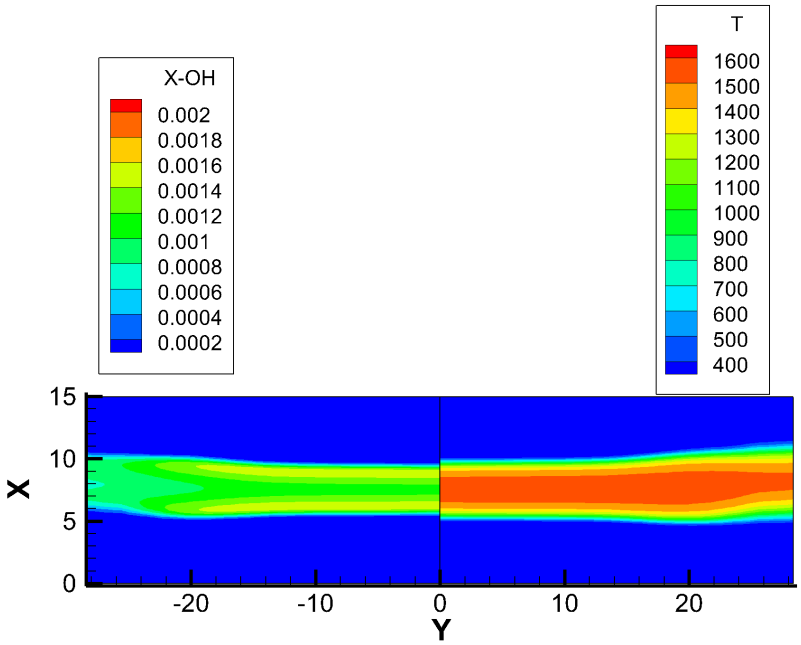

(a) Φ=0.8

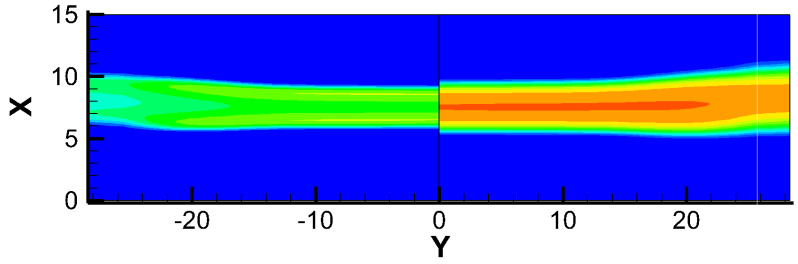

(b) Φ=0.7

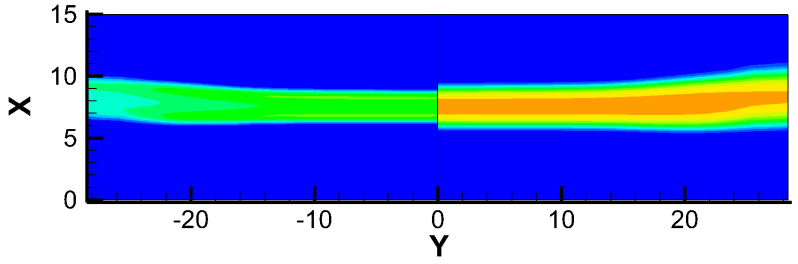

(c) Φ=0.6

Figure 37: OH mole fraction and temperature iso-contours in two-dimensional coordinates (in mm) (50% H_2 and 50% CO syngas, 74% N_2 dilution) for (a) Φ=0.8, (b) Φ=0.7, and (c) Φ=0.6, obtained with UNICORN.

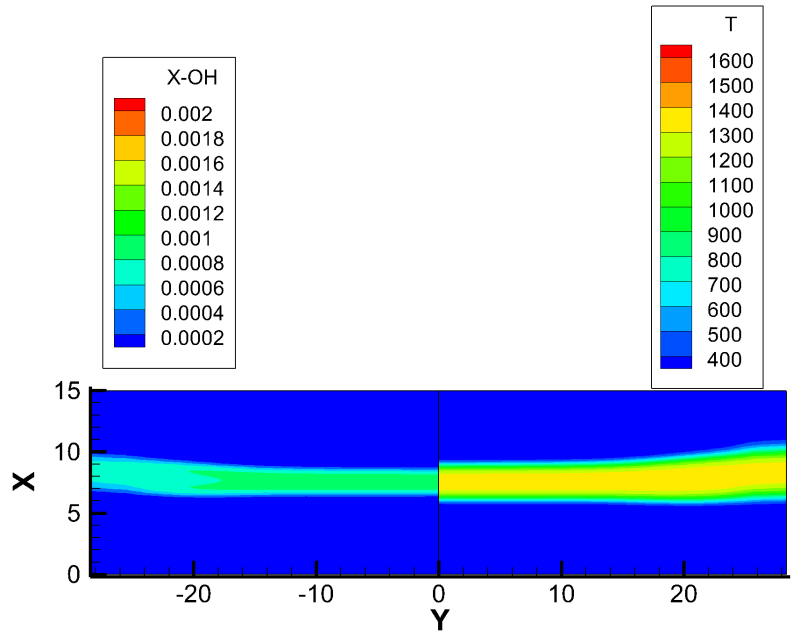

(a) Φ=0.8

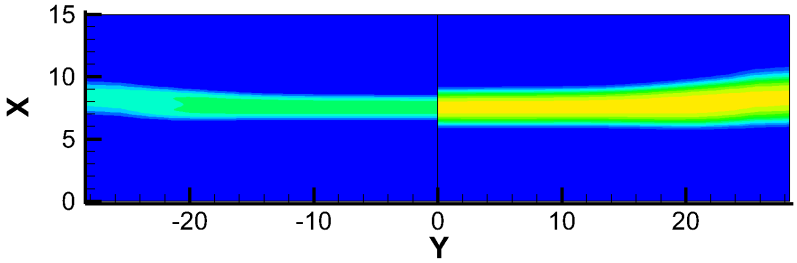

(b) Φ=0.7

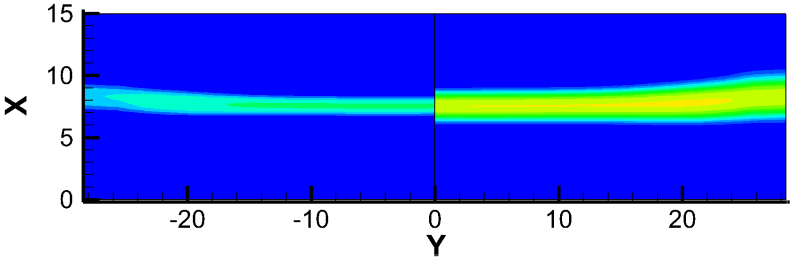

(c) Φ=0.6

Figure 38: OH mole fraction and temperature iso-contours in two-dimensional coordinates (in mm) (50% H_2 and 50% CO syngas, 80% N_2 dilution) for (a) Φ=0.8, (b) Φ=0.7, and (c) Φ=0.6, obtained with UNICORN.

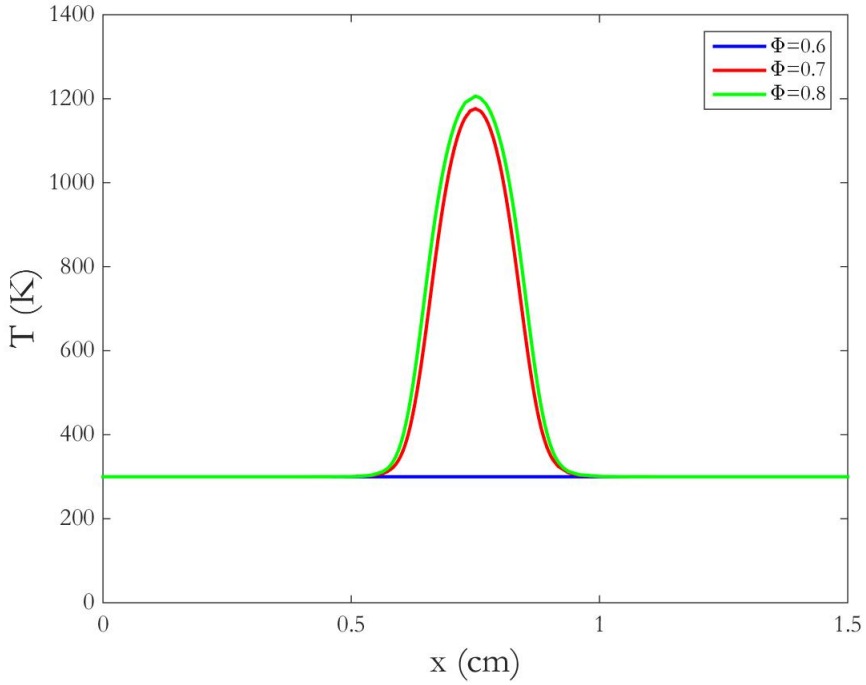

Figure 39: Temperature profiles for different Φ values (50% H_2 and 50% CO syngas, 84% N_2 dilution), obtained with CHEMKIN.

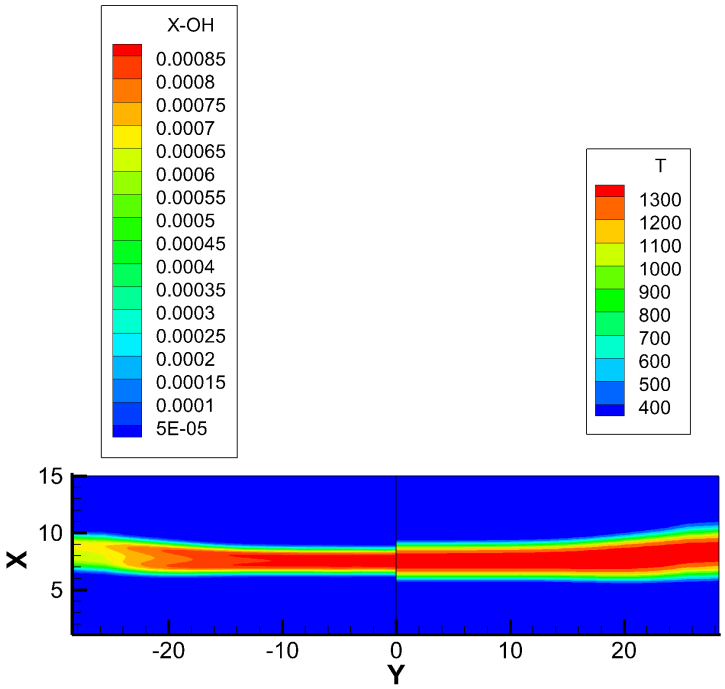

(a) Time = 2 ms

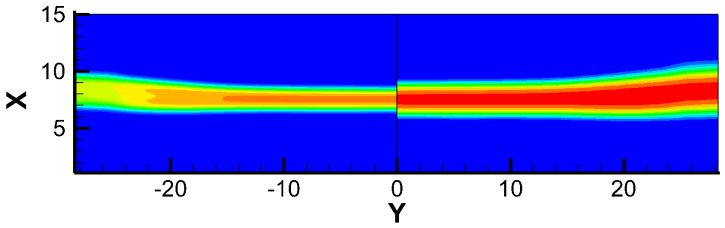

(b) Time = 15 ms

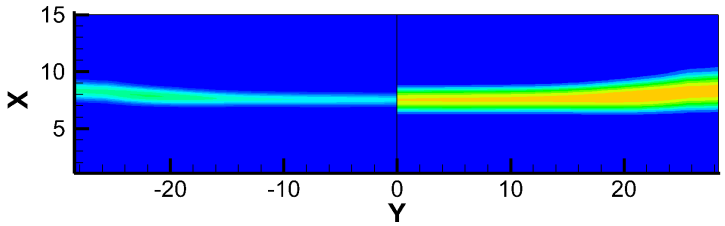

(c) Time = 37.5 ms

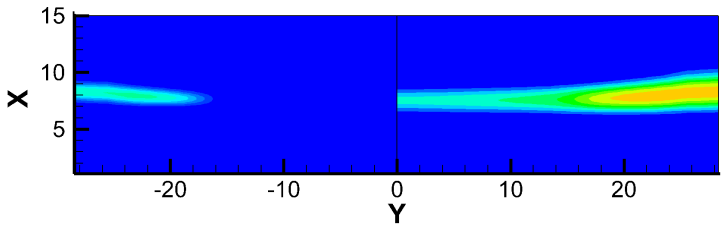

(d) Time = 45 ms

Figure 40: OH mole fraction and temperature iso-contours in two-dimensional coordinates (in mm) (50% H_2 and 50% CO syngas, 84% N_2 dilution, Φ=0.8), obtained with UNICORN. Flame extinction shown by evolution in time.

CHAPTER 8

CONCLUSIONS

In this thesis, a numerical study of laminar premixed syngas/air flames has been conducted, through one- and two-dimensional CFD simulations with CHEMKIN and UNICORN.

In the first part of the thesis a general introduction to the topic is given. The physical and mathematical models, tools, and numerical methods employed for solving the governing equations are presented.

In Chapter 4, laminar flame speed is calculated for syngas-air mixtures with varying equivalence ratio, by employing CHEMKIN PREMIX code. It has been found necessary to use N_2 dilution of 68% by volume, in order to reduce the flame speed of a mixture of 50% H_2 and 50% CO syngas and air. The reduction in flame speed was required to avoid flashback in the computatipon of counterflow moderately stretched premixed flames.

Counterflow flame simulations are performed by employing CHEMKIN OPPDIFF and UNICORN codes. In simulations, two stationary premixed twin flames on either side of the stagnation plane are obtained. The axial velocity, temperature, and species concentration profiles are obtained along the axial direction of the flow, thus leading to a one-dimensional description of the stagnation flames in a counterflow configuration. The effect of equivalence ratio on the flame structure is examined by computing flames with Φ=0.8, 0.7, and 0.6.

A comparison of numerical results obtained using 1-D and 2-D codes is presented, showing very small deviations and thus insuring accuracy and consistency.

Chapter 5 deals with preferential diffusion and includes the computation of Lewis number for a multi-component gas mixture. Lewis number is calculated for different mixture compositions, equivalence ratios, and amounts of dilution. Lewis number here is defined based on the diffusivity of the deficient reactant. This yields Le smaller than one (mass diffusion prevails) for lean mixtures, and greater than one (thermal diffusion prevails) for rich mixtures. Therefore, syngas flames are, in a sense, similar to hydrogen ones. Hydrogen content is found to be the most important parameter for the preferential diffusion, which influences the effect of stretch on flame behavior.

In Chapter 6, the effects of flame stretch are analyzed, by performing both the CHEMKIN and UNICORN simulations. It is shown that the residence time is reduced by increasing the global strain rate and flames are established at locations closer to the stagnation plane.

The flame temperature for lean syngas mixture is found to first increase with strain rate, and subsequently decrease as the strain rate is further increased. The increase in flame temperature is due to the Lewis being less than one, since the preferential diffusion of deficient reactant (mostly hydrogen), which increases the burning rate, has a more dominant effect compared to that of thermal diffusion, which decreases the burning rate. However, as the strain rate exceeds certain value, the flame temperature decreases due to the reduced residence time.

In addition, for mixture characterized by $Le < 1$, i.e., lean syngas/air flames, the maximum HRR continuously increases with global strain rate. The opposite holds for rich syngas/air mixtures ($Le > 1$).

The unstretched unburned flame speed of lean flames is then evaluated for different equivalence ratios, by post-processing the results of opposed flow numerical simulations and through a linear extrapolation method; it is also shown that unburned flame speed is a linear function of the global strain rate.

The effect of flame stretch on the burned flame speed is studied by taking into account the coupling with the Lewis number effect; two different behaviors are exhibited with increasing flame stretch, depending on Le of the mixture. Positive flame stretch has the effect of increasing the fuel concentration of lean syngas/air mixtures ($Le < 1$), thereby enhancing flame intensity, with a consequent increase in the burning velocity. The opposite holds for rich syngas/air mixtures ($Le > 1$); in this case, thermal diffusion prevails and the reduction in temperature entails a collateral reduction in the burning velocity.

Both unburned and burned velocities increase linearly with H_2 content in syngas.

A study of flame stability through the Markstein number closes the chapter, showing that rich and lean syngas flames are cellularly stable and unstable (wrinkled surface), respectively. This is explained by the Lewis number effect, which predicts a smoothing of the wrinkles for $Le > 1$. Markstein numbers are computed for different syngas H_2/CO ratio and Φ. The smaller the Markstein number, the more unstable the flame. For lean mixtures, the flame stability decreases for increasing the H_2 content; the opposite holds for rich flames. This denotes a positive effect of the Lewis number on the flame stability (one increases when the other does).

In Chapter 7, a study of flame extinction is carried out, by using both the CHEMKIN and UNICORN simulations. Two extinction mechanisms are addressed: extinction by stretch (with fixed dilution) and extinction by dilution (with fixed stretch).

Extinction by stretch occurs either for too large or too small global strain rate values. In the first case, flame extinction is exclusively induced by strain: the residence time is so small that the completion of chemical reactions is not guaranteed. In the second case, extinction occurs because the residence time is considerably large, so that radiative heat loss becomes significant and leads to flame extinction. Therefore, upper and lower bounds for k are identified, for which lean syngas/air flames can be sustained for a given equivalence ratio in a counterflow geometry. Upper bounds are calculated for equimolar-syngas and air mixtures with Φ=0.8, 0.7, and 0.6 and with 68% N_2 dilution. Upper and lower bounds are calculated for equimolar-syngas and air mixtures with Φ=0.65, 0.6, 0.55, and 0.5 and with 80% N_2 dilution.

It was necessary to modify the thermodynamic data file of the San Diego mechanism, in order to use the radiation model in CHENKIN-PRO, which is employed for the analysis of extinction at low strain rate. A comparison of the results obtained with and without radiation indicates that differences tend to reduce and eventually disappear when strain rate is increased; however, in the low strain rate domain, leaner flames show larger deviations from the quasi-adiabatic conditions.

Finally, it is demonstrated that there exists a limit amount of N_2 dilution that can be introduced in the fuel, in order to avoid the flame to extinguish. The two codes, CHEMKIN and UNICORN, present slightly different results for this. To be more specific, CHEMKIN

simulations results are reported: syngas/air mixtures (at k=175 s^{-1}) at Φ=0.6, 0.7, and 0.8 extinguish at 84%, 85%, and 85% N_2 dilution by volume of fuel, respectively.

Since it is a *new-generation* alternative fuel, syngas literature is still fragmentary. The obtained results and the predicted behavior of syngas are then intended to provide an incentive to a broader utilization of this clean fuel.

APPENDICES

Appendix A

COUNTERFLOW SIMULATIONS FOR Φ=0.7 AND Φ=0.6

A.1 CHEMKIN Opposed Flow Flame Simulations Results

Numerical simulations results obtained with CHEMKIN *Opposed Flow* subroutine are here collected, for the fuel-lean mixture cases of Φ=0.7, and Φ=0.6.

A strain rate value of k=175 $s^{-}1$ is imposed, whose corresponding inlet velocity (for L=1.5 cm), from both sides, is v_{in}=65.6 cm/s.

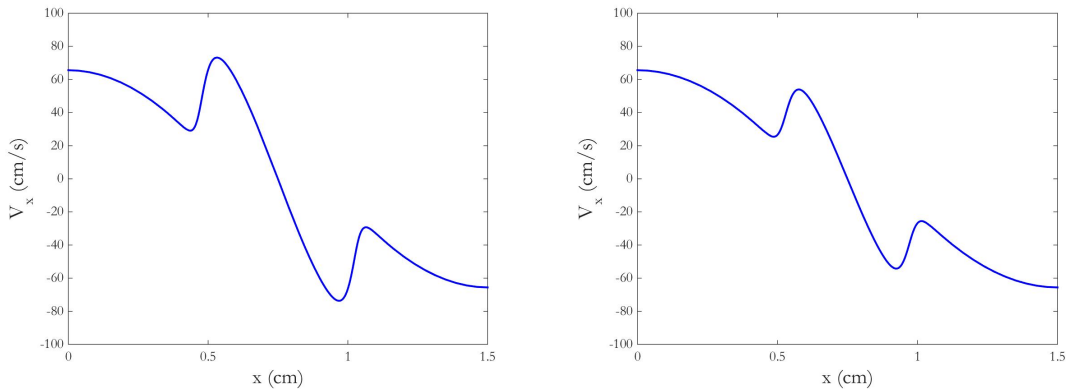

(a) Φ=0.7 (b) Φ=0.6

Figure 41: Axial velocity profile as a function of axial coordinate (50%H_2 and 50%CO syngas, 68% N_2 dilution), obtained with CHEMKIN, for (a) Φ=0.7 and (b) Φ=0.6.

APPENDIX A (Continued)

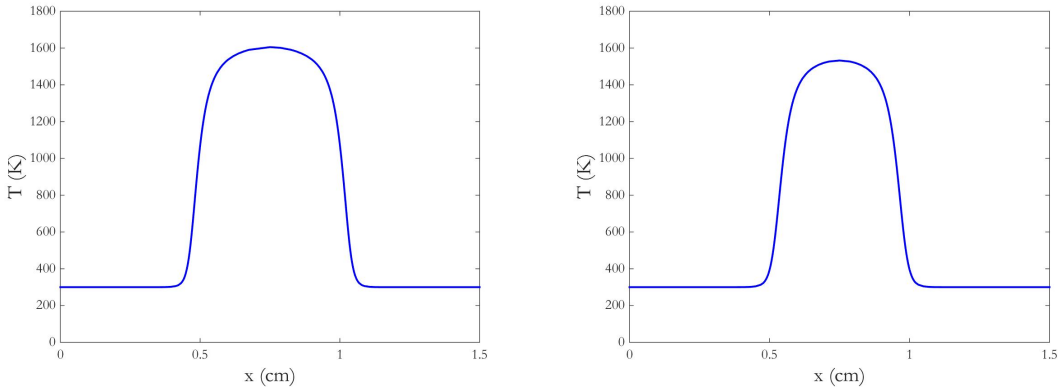

(a) Φ=0.7 (b) Φ=0.6

Figure 42: Temperature profile as a function of axial coordinate (50%H_2 and 50%CO syngas, 68% N_2 dilution), obtained with CHEMKIN, for (a) Φ=0.7 and (b) Φ=0.6.

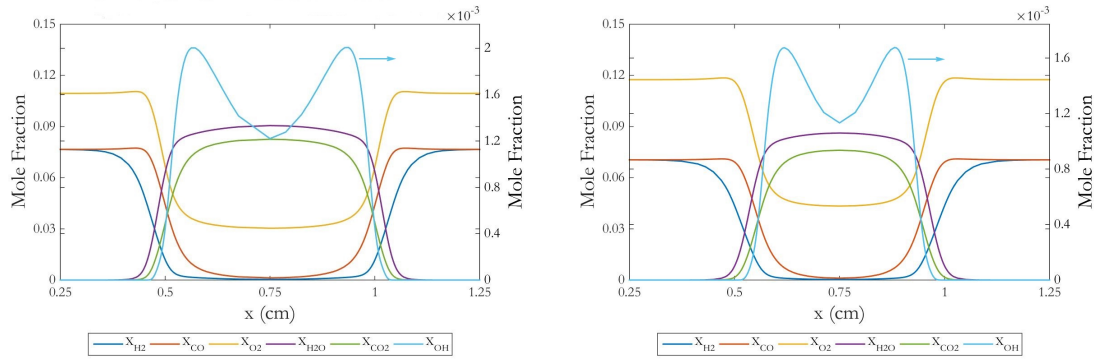

(a) Φ=0.7 (b) Φ=0.6

Figure 43: Species concentration profile profile as a function of axial coordinate (50%H_2 and 50%CO syngas, 68% N_2 dilution), obtained with CHEMKIN, for (a) Φ=0.7 and (b) Φ=0.6.

APPENDIX A (Continued)

A.2 UNICORN Counterflow Flame Simulations Results

The same simulations are run with the UNICORN code.

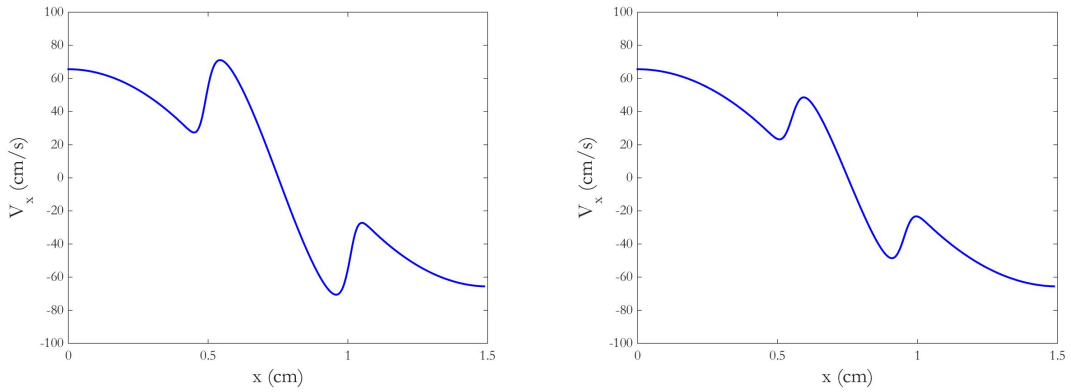

(a) Φ=0.7 (b) Φ=0.6

Figure 44: Axial velocity profile as a function of axial coordinate (50%H_2 and 50%CO syngas, 68% N_2 dilution), obtained with UNICORN, for (a) Φ=0.7 and (b) Φ=0.6.

APPENDIX A (Continued)

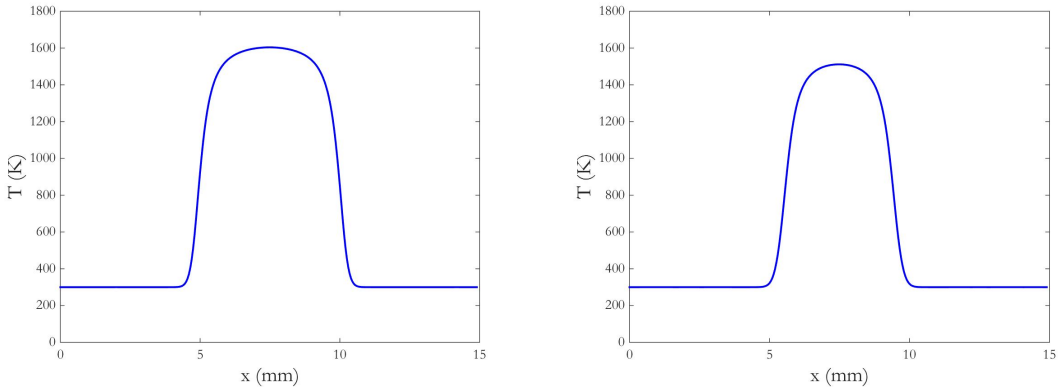

(a) Φ=0.7 (b) Φ=0.6

Figure 45: Temperature profile as a function of axial coordinate (50%H_2 and 50%CO syngas, 68% N_2 dilution), obtained with UNICORN, for (a) Φ=0.7 and (b) Φ=0.6.

A.3 Counterflow Flame Results Validation - Comparison CHEMKIN-UNICORN

APPENDIX A (Continued)

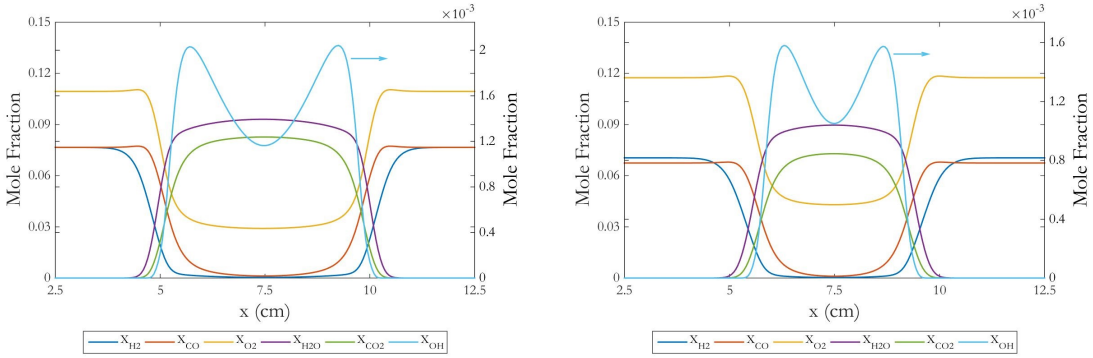

(a) Φ=0.7 (b) Φ=0.6

Figure 46: Species concentration profile profile as a function of axial coordinate (50%H_2 and 50%CO syngas, 68% N_2 dilution), obtained with UNICORN, for (a) Φ=0.7 and (b) Φ=0.6.

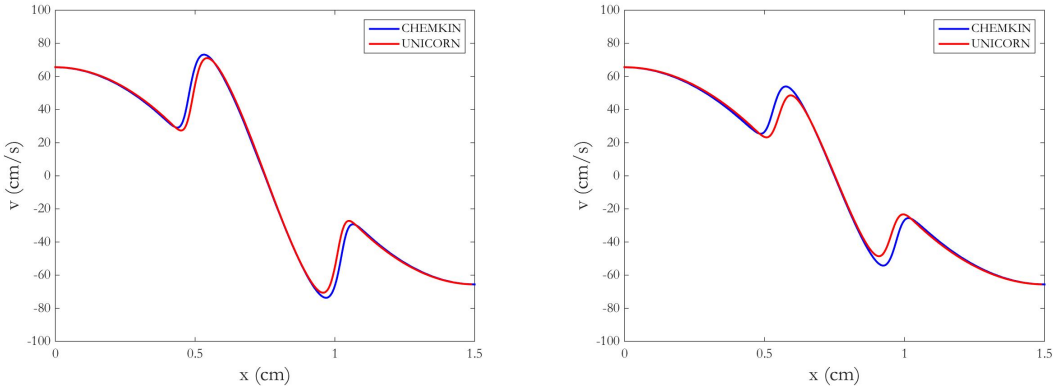

(a) Φ=0.7 (b) Φ=0.6

Figure 47: Axial velocity profile as a function of axial coordinate (50%H_2 and 50%CO syngas, 68% N_2 dilution). CHEMKIN vs UNICORN comparison, for (a) Φ=0.7 and (b) Φ=0.6.

APPENDIX A (Continued)

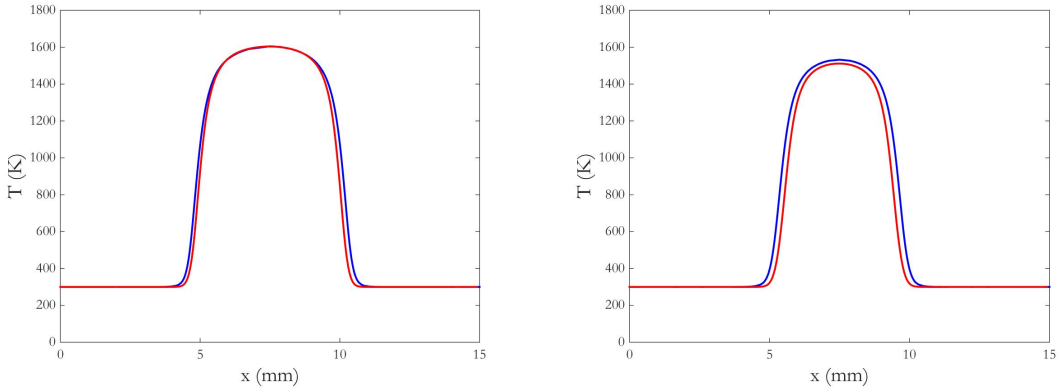

(a) Φ=0.7 (b) Φ=0.6

Figure 48: Temperature profile as a function of axial coordinate (50%H_2 and 50%CO syngas, 68% N_2 dilution). CHEMKIN vs UNICORN comparison, for (a) Φ=0.7 and (b) Φ=0.6.

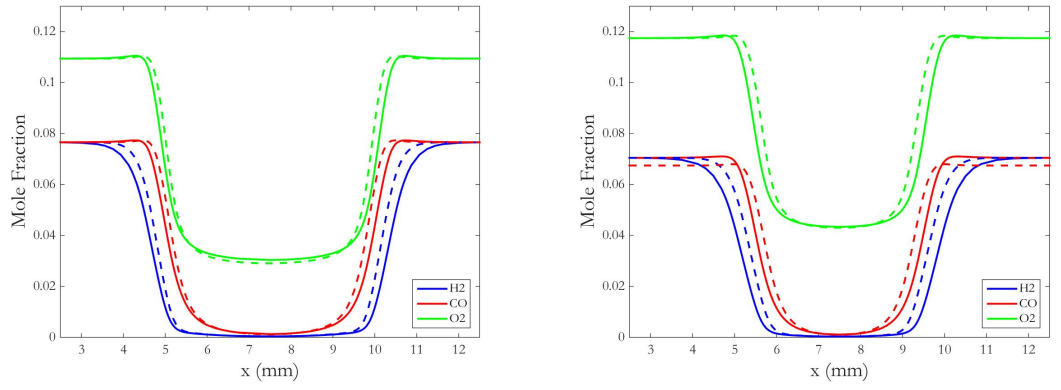

(a) Φ=0.7 (b) Φ=0.6

Figure 49: Reactant species concentration profile profile as a function of axial coordinate (50%H_2 and 50%CO syngas, 68% N_2 dilution). CHEMKIN vs UNICORN comparison, for (a) Φ=0.7 and (b) Φ=0.6.

APPENDIX A (Continued)

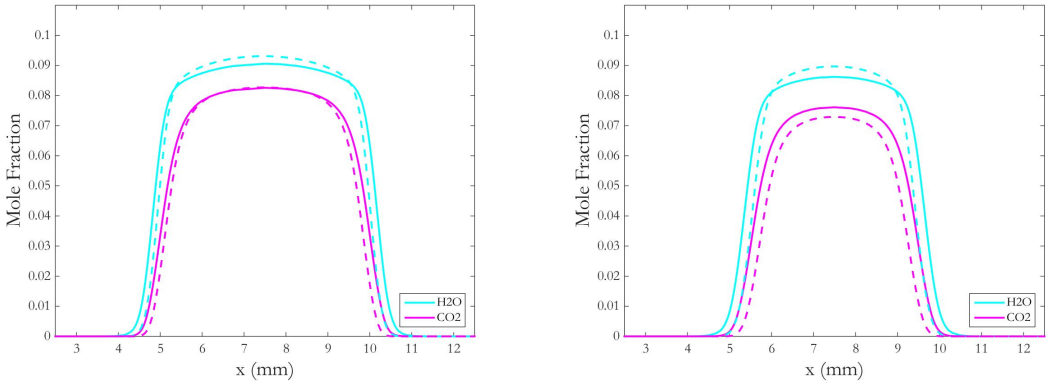

(a) Φ=0.7 (b) Φ=0.6

Figure 50: Product species concentration profile profile as a function of axial coordinate (50%H_2 and 50%CO syngas, 68% N_2 dilution). CHEMKIN vs UNICORN comparison, for (a) Φ=0.7 and (b) Φ=0.6.

Appendix B

RADIATION MODEL ON CHEMKIN PRO

B.1 Radiation model on CHEMKIN PRO

In order to include heat radiation in the calculation, the employed mechanism has been obtained by *modifying the thermodynamic data file of the San Diego mechanism* as reported in figure 51.

```
! [_ AbsorptionCoefficients=" 2 300 2500 -2.3093D-01 -1.1239D+03 9.4153D+06 -2.9988D+09 5.1382D+11 -1.8684D+10 0 " _]
H2O               000000H   2O   1          G       300      5000    1000      1
 3.03399249E+00 2.17691804E-03-1.64072518E-07-9.70419870E-11 1.68200992E-14    2
-3.00042971E+04 4.96677010E+00 4.19864056E+00-2.03643410E-03 6.52040211E-06    3


! [_ AbsorptionCoefficients=" 1 300 750  4.7869D+00 -6.953D-02 2.95775D-04 -4.25732D-07  2.02894D-10 0 0 " _]
! [_ AbsorptionCoefficients=" 1 750 2500 1.0090D+01 -1.183D-02 4.77530D-06 -5.87209D-10 -2.53340D-14 0 0 " _]
CO                000000O   1C   1          G       300      5000    1000      1
 2.71518561E+00 2.06252743E-03-9.98825771E-07 2.30053008E-10-2.03647716E-14    2
-1.41518724E+04 7.81868772E+00 3.57953347E+00-6.10353680E-04 1.01681433E-06    3
 9.07005884E-10-9.04424499E-13-1.43440860E+04 3.50840928E+00                   4

! [_ AbsorptionCoefficients=" 2 300 2500 1.8741D+01 -1.2131D+05 2.735D+08 -1.9405D+11 5.631D+13 -5.8169D+15 0 " _]
CO2               000000O   2C   1          G       300      5000    1000      1
 3.85746029E+00 4.41437026E-03-2.21481404E-06 5.23490188E-10-4.72084164E-14    2
-4.87591660E+04 2.27163806E+00 2.35677352E+00 8.98459677E-03-7.12356269E-06    3
 2.45919022E-09-1.43699548E-13-4.83719697E+04 9.90105222E+00                   4
```

Figure 51: Modified lines of the thermodynamic data file for the San Diego chemical-kinetic mechanism

APPENDIX B (Continued)

Where *Absorption coefficient* means that the set of data is referring to the calculation of the thermal absorption coefficients for the gas species; the first digit 1 or 2 employs the polynomial fitting law 1 or 2 of Equation 7.2 and Equation 7.3; the next two numbers define the temperature range; the following seven numbers are the parameters, c_j, used in curve fitting of Equation 7.2 and Equation 7.3.

CITED LITERATURE

1. Energy Information Agency, U. S.: Annual energy review 2014. DOE/EIA-0384, Retrieved April 2015.

2. Ha, J., Park, J., Kwon, O. B., Lim, I. G., Yun, J. H., Keel, S. I., Park, H. Y., and Kim, T. H.: Flame extinction in interacting co-air and syngas-air premixed flames. Journal of mechanical science and technology, 29(1):419–428, 2015.

3. Reaction Design, R.: Chemkin overview. http://www.reactiondesign.com/products/chemkin, Retrieved April 2015.

4. Kee, R., Rupley, F., and Miller, J.: Chemkin ii: A fortran chemical kinetics package for the analysis of gas phase chemical kinetics. Technical report SAND89-8009B, Sandia National Laboratories, 1993.

5. Kee, R., Dixon-Lewis, G., Warnatz, J., Coltrin, M., and Miller, J.: A fortran computer code package for the evaluation of gas-phase multi-component transport. Sandia National Laboratories report SAND86-8246, 1994.

6. Kee, R., Grcar, J., Smooke, M., Miller, J., and Meeks, E.: A program for modeling steady, laminar, one-dimensional premixed flames. Report SAND85-8240. Sandia National Laboratories, Livermore, CA, 1985.

7. Lutz, A., Kee, R., Grear, J., and Rupley, F.: A fortran program for computing opposed-flow diffusion flames. Sandia National Laboratories report no. SAND96-8243, 1997.

8. San Diego Mechanism web page Mechanical & Aerospace Engineering (combustion research), U. C. S. D.: Chemical-kinetic mechanisms for combustion applications. http://combustion.ucsd.edu, Retrieved April 2015.

9. Reaction Design, R.: Chemkin theory manual.

10. Reynolds, W.: The element potential method for chemical equilibrium analysis: implementation in the interactive program stanjan. Department of mechanical engineering Stanford University, 1986.

CITED LITERATURE (Continued)

11. Katta, V. R., Aggarwal, S. K., and Roquemore, W. M.: Evaluation of chemical-kinetics models for n-heptane combustion using a multidimensional cfd code. Fuel, 93:339–350, 2012.

12. Katta, V. R. and Roquemore, W. M.: Calculation of multidimensional flames using large chemical kinetics. Aiaa Journal, 46(7):1640–1650, 2008.

13. Roquemore, W. and Katta, V.: Role of flow visualization in the development of unicorn. Journal of visualization, 2(3/4):257–272, 2000.

14. Katta, V., Goss, L., and Roquemore, W.: Numerical investigations of transitional h2/n2 jet diffusion flames. AIAA journal, 32(1):84–94, 1994.

15. Katta, V., Meyer, T., Brown, M., Gord, J., and Roquemore, W.: Extinction criterion for unsteady, opposing-jet diffusion flames. Combustion and flame, 137(1):198–221, 2004.

16. Briones, A. M., Aggarwal, S. K., and Katta, V. R.: Effects of h 2 enrichment on the propagation characteristics of ch 4–air triple flames. Combustion and flame, 153(3):367–383, 2008.

17. Tecplot: Master's thesis. from www.tecplot.com, Retrieved April 2015.

18. Turns, S.: An introduction to combustion, concepts and applications - 3rd ed., 2012.

19. Reaction Design, .: Chemkin tutorials manual.

20. Quattrocchi, S., Aggarwal, S. K., and Santarelli, M.: Liftoff and blowout characteristics and structure analysis of syngas diffusion flames. M.S. Thesis, 2014.

21. Law, C.: Dynamics of stretched flames. In Symposium (international) on combustion, volume 22, pages 1381–1402. Elsevier, 1989.

22. Bouvet, N., Halter, F., Chauveau, C., and Yoon, Y.: On the effective lewis number formulations for lean hydrogen/hydrocarbon/air mixtures. International journal of hydrogen energy, 38(14):5949–5960, 2013.

23. Bird, R. B., Stewart, W. E., and Lightfoot, E. N.: Transport phenomena. John Wiley & Sons, 2007.

CITED LITERATURE (Continued)

24. Hawkes, E. R. and Chen, J. H.: Direct numerical simulation of hydrogen-enriched lean premixed methane–air flames. Combustion and Flame, 138(3):242–258, 2004.

25. Karlovitz, B., Denniston, D. W., and Knapschaefer, D. H. ans Wells, F. E.: Fourth symposium (international) on combustion. The combustion institute, page 613, 1953.

26. Lewis, B. and Von Elbe, G.: Combustion, flames and explosion of gases. Academic, NY, 1961.

27. Markstein, G.: Nonsteady flame propagation. MacMillan, NY, 1964.

28. Matalon, M.: Combustion science and technology. 31:169–181, 1983.

29. Naha, S. and Aggarwal, S. K.: Fuel effects on nox emissions in partially premixed flames. Combust. flame, 139:90–105, 2004.

30. Choi, S. K., Cho, E.-S., and Chung, S. H.: Quantification of extinction mechanism in counterflow premixed flames. Journal of mechanical science and technology, 28(9):3863–3871, 2014.

31. Dixon-Lewis, G.: Laminar premixed flame extinction limits. ii combined effects of stretch and radiative loss in the single flame unburnt-to-burnt and the twin-flame unburnt-to-unburnt opposed flow configurations. Proceedings of the royal society A: mathematical, physical and engineering science, 462(2066):349–370, 2006.

32. Law, C. and Sung, C.: Structure, aerodynamics, and geometry of premixed flamelets. Progress in energy and combustion science, 26(4):459–505, 2000.

33. Aung, K., Hassan, M., and Faeth, G.: Effects of pressure and nitrogen dilution on flame/stretch interactions of laminar premixed h 2/o 2/n 2 flames. Combustion and flame, 112(1):1–15, 1998.

34. Clavin, P.: Dynamic behavior of premixed flame fronts in laminar and turbulent flows. Progress in energy and combustion science, 11(1):1–59, 1985.

35. Davis, S., Quinard, J., and Searby, G.: Determination of markstein numbers in counterflow premixed flames. Combustion and flame, 130(1):112–122, 2002.

CITED LITERATURE (Continued)

36. Aggarwal, S. K.: Hydrogen-assisted combustion and emission characteristics of fossil fuels. Handbook of combustion, M. Lackner, F. Winter, and A. K. Agarwal (Eds.), 3, 2010.

37. Bradley, D., Sheppard, C. G. W., Woolley, R., Greenhalgh, D. A., and Lockett, R. D.: The development and structure of flame instabilities and cellularity at low markstein numbers in explosions. Combustion and flame, 122:195–209, 2000.

38. Aggarwal, S. K.: Extinction of laminar partially premixed flames. Progress in energy and combustion science, 35(6):528–570, 2009.

39. Dixon-Lewis, G.: Aspects of laminar premixed flame extinction limits. In Symposium (international) on combustion, volume 25, pages 1325–1332. Elsevier, 1994.

40. Barlow, R., Karpetis, A., Frank, J., and Chen, J.-Y.: Scalar profiles and no formation in laminar opposed-flow partially premixed methane/air flames. Combustion and flame, 127(3):2102–2118, 2001.

41. Prathap, C., Ray, A., and Ravi, M.: Investigation of nitrogen dilution effects on the laminar burning velocity and flame stability of syngas fuel at atmospheric condition. Combustion and flame, 155(1):145–160, 2008.

VITA

NAME: Cesare D'Ippolito

EDUCATION: Master of Science in Mechanical Engineering

University of Illinois at Chicago, USA, 2015

Master of Science in Mechanical Engineering

Politecnico di Torino, Italy, 2015

Bachelor of Science in Automotive Engineering

Politecnico di Torino, Italy, 2013

HONORS: TOP-UIC mobility scholarship for Double Degree program, 2014-2015

SECAC mobility scholarship for Bachelor Exchange program between Politecnico di Torino and Mississippi State University, 2012